

The Compositional Diversity of Extrasolar Terrestrial Planets: I. In–Situ Simulations

Jade C. Bond^{1,3}

Lunar and Planetary Laboratory, University of Arizona, Tucson, AZ 85721

`jbond@psi.edu`

and

David P. O’Brien²

Planetary Science Institute, Tucson, AZ 85719

and

Dante S. Laretta¹

Lunar and Planetary Laboratory, University of Arizona, Tucson, AZ 85721

Received _____; accepted _____

¹Lunar and Planetary Laboratory, University of Arizona, 1629 East University Boulevard, Tucson, AZ 85721-0092.

²Planetary Science Institute, 1700 E. Fort Lowell, Tucson, AZ 85719.

³Now at Planetary Science Institute.

ABSTRACT

Extrasolar planet host stars have been found to be enriched in key planet-building elements. These enrichments have the potential to drastically alter the composition of material available for terrestrial planet formation. Here we report on the combination of dynamical models of late-stage terrestrial planet formation within known extrasolar planetary systems with chemical equilibrium models of the composition of solid material within the disk. This allows us to determine the bulk elemental composition of simulated extrasolar terrestrial planets. A wide variety of resulting planetary compositions are found, ranging from those that are essentially "Earth-like", containing metallic Fe and Mg-silicates, to those that are dominated by graphite and SiC. This shows that a diverse range of terrestrial planets may exist within extrasolar planetary systems.

Subject headings: planets and satellites: composition — planets and satellites: formation — planetary systems

1. Introduction

Extrasolar terrestrial planets are a tantalizing prospect. Given that the number of planets in the galaxy is expected to correlate inversely with planetary mass, it is expected that Earth-sized terrestrial planets are much more common than giant planets (Marcy et al. 2000). Although still undetectable by current exoplanet searches, the possibility of their existence in extrasolar planetary systems has been examined by several authors. Many such studies have focussed on the long term dynamical stability of regions within the planetary system where such planets could exist for geologic timescales (Barnes & Raymond 2004; Raymond & Barnes 2005; Asghari et al. 2004). Several systems have been found to possess such regions (e.g. Barnes & Raymond 2004), indicating that if they are able to form, terrestrial planets may still be present within extrasolar planetary systems. Analyses of this nature are of great interest to future planet search missions as they assist in constraining future planet search targets. However, they provide little insight into the formation mechanism and physical and chemical properties of such planets and do not necessarily indicate the presence of a terrestrial planetary companion.

A few other studies have gone one step further and undertaken detailed N-body simulations of terrestrial planet formation. Raymond et al. (2005) considered terrestrial planet formation in a series of hypothetical ‘hot Jupiter’ simulations and found that terrestrial planets can indeed form in such systems (beyond the orbit of the giant planet) provided the ‘hot Jupiter’ is located within 0.5AU from the host star. Furthermore, such planets may even have water contents comparable to that of the Earth. Terrestrial planets have been found to form even in simulations of systems which have undergone large-scale migration of the giant planet (Raymond et al. 2006b; Mandell et al. 2007). Terrestrial planets were found to form both exterior and interior to the giant planet after migration has occurred and many were located within the habitable zone of the host

star. As many extrasolar planets are believed to have experienced such a migration, it is encouraging that terrestrial planets may still be able to form within these systems. To date, only Raymond et al. (2006a) have undertaken terrestrial planet formation simulations for specific planetary systems. They considered four known planetary systems and found that terrestrial planets could form in one of the systems (55Cnc). Small bodies comparable to asteroid sized objects would be stable in another (HD38529).

An even more intriguing question beyond whether or not terrestrial planets could exist within these systems is their potential chemical composition. Extrasolar planetary host stars are already known to be chemically unusual (Gonzalez 1997, 1998; Butler et al. 2000; Gonzalez & Laws 2000; Gonzalez et al. 1999; Gonzalez & Vanture 1998; Santos et al. 2000, 2001, 2004; Gonzalez et al. 2001; Smith et al. 2001; Reid 2002; Fischer & Valenti 2005; Bond et al. 2006, 2008), displaying systematic enrichments in Fe and smaller, less statistically significant enrichments in other species such as C, Si, Mg and Al (Gonzalez & Vanture 1998; Gonzalez et al. 2001; Santos et al. 2000; Bodaghee et al. 2003; Fischer & Valenti 2005; Beirão et al. 2005; Bond et al. 2006). Given that these enrichments are likely primordial in origin (Santos et al. 2001, 2003a,b, 2005; Fischer & Valenti 2005; Bond et al. 2006), it is thus likely that the planet forming material within these systems will be similarly enriched. Hints of such a correlation between transiting giant planets and stellar metallicity have been observed (Guillot et al. 2006; Burrows et al. 2007). Consequently, it is likely that terrestrial extrasolar planets may have compositions reflecting the enrichments observed in the host stars. Furthermore, several known host stars have been found to have C/O values above 0.8 (Bond et al. 2008). Systems with high C/O ratios will contain large amounts of C phases (such as SiC, TiC and graphite), resulting in any terrestrial planets within these systems being enriched in C and potentially having compositions and mineralogies unlike any body observed within our Solar System.

Despite the likely chemical peculiarities of extrasolar planetary systems and the early successes of extrasolar terrestrial planet formation simulations, no studies of extrasolar terrestrial planet formation completed to date have considered both the dynamics of formation and the detailed chemical compositions of the final terrestrial planets produced. This study addresses this issue by simulating late-stage in-situ terrestrial planet formation within ten extrasolar planetary systems while simultaneously determining the bulk elemental compositions of the planets produced. This is the first such study to consider both the dynamical and chemical nature of potential extrasolar terrestrial planets and it represents a significant step towards understanding the diversity of potential extrasolar terrestrial planets.

2. System Composition

The two most important elemental ratios for determining the mineralogy of extrasolar terrestrial planets are C/O and Mg/Si. Note that throughout this paper, Mg/Si and C/O refers to the elemental number ratios, *not* solar normalized logarithmic values often quoted in stellar spectroscopy (usually shown as $[X/H]$ for the solar normalized logarithmic abundance of element X compared to H). The ratio of C/O controls the distribution of Si among carbide and oxide species. Under the assumption of equilibrium, if the C/O ratio is greater than 0.8 (for a pressure of 10^{-4} bar), Si exists in solid form primarily as SiC. Additionally, a significant amount of solid C is also present as a planet building material. For C/O values below 0.8, Si is present in rock-forming minerals as SiO_4^{4-} (or SiO_2), allowing for the formation of silicates. The silicate mineralogy is controlled by the Mg/Si value. For Mg/Si values less than 1, Mg is in pyroxene (MgSiO_3) and the excess Si is present as other silicate species such as feldspars. For Mg/Si values ranging from 1 to 2, Mg is distributed between olivine (Mg_2SiO_4) and pyroxene. For Mg/Si values extending beyond

2, all available Si is consumed to form olivine with excess Mg available to bond with other elements as MgO or MgS.

Just as stellar C/O values are known to vary within the solar neighborhood (Gustafsson et al. 1999), the C/O values of extrasolar planetary systems also deviate from the solar value. The photospheric C/O vs. Mg/Si values for known extrasolar planetary host stars are shown in Figure 4, based on stellar abundances taken from Gilli et al. (2006) (Si and Mg), Beirão et al. (2005) (Mg), Ecuivillon et al. (2004a) (C) and Ecuivillon et al. (2006) (O). A conservative approach was taken in determining the average error shown in Figure 4. The errors published for each elemental abundance were taken as being the 2σ errors (as the method used to determine them naturally provides the 2σ error range) and were used to determine the maximum and minimum abundance values possible with 2σ confidence for each system. The elemental ratios produced by these extremum abundances were thus taken as the 2σ range in ratio values and are shown as errors in Figure 4.

The mean values of Mg/Si and C/O for all extrasolar planetary systems for which reliable abundances are available are 1.32 and 0.77 respectively, which are above solar values ($\text{Mg/Si}_{\odot} = 1.00$ and $\text{C/O}_{\odot} = 0.54$) (Asplund et al. 2005). This non-solar average and observed variation implies that a wide variety of materials would be available to build terrestrial planets in those systems, and not all planets that form can be expected to be similar to that of Earth. Of the 60 systems shown, 21 have C/O values above 0.8, implying that carbide minerals are important planet building materials in potentially more than 30% of known planetary systems. This implies that a similar fraction of protoplanetary disks should contain high abundances of carbonaceous grains. As comets represent some of the most primitive material within our planetary system, it is likely that a similar mass fraction will apply to the protoplanetary nebula. Furthermore, infrared spectral features at 3.43 and 3.53 μm observed in 4% of protoplanetary disks have been identified as being produced by

nano-diamonds (Acke & van den Ancker 2006). Such high abundances of carbon-rich grains in nascent planetary systems is inconceivable if they have primary mineralogy similar to our Solar System, thus implying that C-rich planetary systems may be more common than previously thought. The idea of C-rich planets is not new (Kuchner & Seager 2005) but the potential prevalence of these bodies has not been previously recognized, nor have specific systems been identified as likely C-rich planetary hosts. These data clearly demonstrate that there are a significant number of systems in which terrestrial planets could have compositions vastly different to any body observed in our Solar System.

Both host and non-host stars¹ display the same distributions in C/O and Mg/Si values (see Figure 5). The mean, median and standard deviation for both the host and non-host stars is shown in Table 2. The values listed in Table 2 are based on the stellar abundances determined in Bond et al. (2008) as Gilli et al. (2006); Beirão et al. (2005); Ecuivillon et al. (2006, 2004a) provide abundances for all four elements for just three non-host stars, thus preventing host and non-host comparisons. It is essential to point out here that the values shown in Figure 5 and Table 2 are based on a different dataset than is used for the simulations presented in this paper and are meant for comparative purposes only. The [Mg/H] values in Bond et al. (2008) are known to be lower than for previously published common stars and the different spectral indicators were used to obtain O abundances (see Bond et al. (2008) for more details). However, as both host and non-host stars were examined in the same way, the use of this data to compare the two populations is still valid. Given the excellent agreement between host and non-host stars, we conclude that known planetary host stars are not preferentially biased towards higher C/O or Mg/Si values compared to stars not known to harbor a planetary companion. This in turn implies

¹Throughout this paper, non-host stars refers to stars observed as part of a planet search program that are not currently known to harbor a planetary companion.

that the prevalence of C-rich planetary systems identified above is not statistically unusual (in terms of stellar composition).

However, a high degree of uncertainty is associated with all stellar C/O and Mg/Si values. The primary source of this error is uncertainty in the stellar elemental abundances themselves. Spectrally determined abundances are sensitive to continuum placement and stellar atmospheric parameters such as stellar effective temperature (T_{eff}), stellar surface gravity ($\log g$), metallicity and microturbulence. These uncertainties result in an average $2\text{-}\sigma$ error of ± 0.04 for [Mg/H], ± 0.07 for [Si/H], ± 0.08 for [C/H] and ± 0.09 for [O/H]². These errors result in considerable percentage uncertainties for the Mg/Si and C/O values of up to 124%. Although large, the errors will not decrease until we are able to reduce the uncertainty on each individual stellar elemental abundance.

Of the four key elements discussed thus far, O is by far the most controversial. Three different spectral lines are available for determining the photospheric O abundance - the forbidden OI lines located at 6300 and 6363 Å, the OI triplet located between 7771 Å and 7775 Å and the OH lines located near 3100 Å (Ecuivillon et al. 2006). Previous studies have found discrepancies between abundances obtained from different spectral lines for the same star of up to 1 dex (Israeli et al. 2004) (A dex is the logarithmic unit for elemental abundances). Each of these lines is subject to interferences from different stellar sources. The forbidden OI lines are weak and blended with Ni, the OI triplet is influenced by non-local thermodynamic equilibrium (non-LTE) effects and the OH lines are influenced by stellar surface features (Ecuivillon et al. 2006). Ecuivillon et al. (2006) undertook a detailed examination of the correlation between these different O indicators for a sample of 96 host and 59 non-host stars. Their study showed that the discrepancies

²[X/H] = $\log(X/H)_{\star} - \log(X/H)_{\odot}$ where X/H is the ratio of the abundance of a given element, X, to H.

in abundances determined by the three different indicators was less than 0.2dex for the majority of stars examined. The forbidden OI and OH lines were found to be in good agreement with each other while abundances obtained from the O triplet lines (with the appropriate NLTE corrections applied to them) were systematically lower. However, all three indicators produced abundances in keeping with the galactic evolutionary trends observed for lower metallicity (and thus younger) stars (Ecuivillon et al. 2006). The C/O ratios shown in Figure 4 (and used throughout this study) are based on the O abundances from Ecuivillon et al. (2006) obtained from the forbidden OI spectral line observed at 6300.3 Å as abundances from this line are in agreement with the abundances obtained from the OH line and produce a marginally better fit to stellar evolutionary models.

The solar O abundance itself has experienced a ‘crisis’ in recent years (Ayres et al. 2006) with several studies suggesting that a downward revision of the solar O value is required (e.g. Ayres et al. 2006; Socas-Navarro & Norton 2007). However, realistic errors for the suggested new O abundance are approximately 0.1 dex (Socas-Navarro & Norton 2007) and the abundances of the present study vary from $[O/H] = 0.38$ (HD 177830) to $[O/H] = -0.10$ (HD 108874), a range of 0.48 dex. As our present study range is almost five times larger than the errors of the revised O abundance, we feel confident in the compositional variations identified here as being caused by variations in the stellar O abundances of specific systems.

Given the errors associated with each individual elemental abundance (and thus also ratio value), it is natural to consider the uncertainty associated with the dispersion seen in Figure 4. The observed dispersion is produced by both dispersion in the actual values and dispersion due to measurement errors. Propagating the errors of the individual abundances leads to a standard deviation of 0.22, slightly reduced from 0.27 without considering errors. Thus it is probable that the real range in elemental ratios is less than is shown in Figure

4 and fewer planetary systems have C/O values above 0.8. Based on the errors described above and shown in Figure 4, only 5 of the 61 planetary systems shown (8% of the sample) can be said with 2σ confidence to have C/O values above 0.8. This increases to just 7 planetary systems (11% of the sample) when we reduce the confidence interval to 1σ . It should also be noted here that the O abundances utilized here are on average higher than those produced by other indicators. As such, the C/O values are lower and should be considered conservative values. Additionally, as the errors are bidirectional, it is also possible that our high C/O sample may be larger. Making the overly-optimistic assumption that all systems lie at the upper bounds of their error range, 47 of the 61 planetary systems (77% of the sample) may have C/O values above 0.8.

Taken together, this suggests that while the number of systems with C/O values larger than 0.8 may be less than indicated in Figure 4, it is likely not as low as the most conservative estimates, and a significant number of planetary systems may have C-rich condensation sequences. Planets that form in these systems would contain significant amounts of carbide phases as major planet building materials, and would differ significantly from the silicate-dominated planets that form in systems with lower C/O values.

3. Simulations

3.1. Extrasolar Planetary Systems

Ten known extrasolar planetary systems spanning the entire compositional spectrum of observed planetary systems were selected for this study. This wide range was purposefully chosen to explore the full diversity of possible extrasolar terrestrial planets. The dynamical and chemical characteristics of each system are shown in Tables 3, (orbital parameters of known planetary companions), 4 (stellar abundances in logarithmic units) and 5 (stellar

abundances normalized to 10^6 Si atoms), while the known giant planet architecture is shown in Figure 6 and the C/O and Mg/Si values were previously shown in Figure 4. Dynamical properties of the known giant planets were taken from the catalog of Butler et al. (2006) [these values were augmented with more recent values from <http://exoplanets.org> when available]. Note that the innermost planet of 55Cnc was neglected in our present simulations due to its location and low mass.

3.2. Chemical Simulations

As in Bond et al. (2009), the chemical composition of material within the disk is assumed to be determined by equilibrium condensation within the primordial stellar nebula. Although the timescales for formation of planetesimals and embryos considered here can be comparable to the timescale for reaction kinetics (eg. less than 1×10^6 yr for the Jovian circumplanetary disk (Mousis & Alibert 2006)), the hot inner mid-plane region (≤ 10 AU from the host star) achieves thermodynamic equilibrium within approximately 100 to 10,000 years (Semenov et al. 2010). Therefore the assumption that the simulated planetesimals form in equilibrium with their surroundings is still valid for this type of study. This approach is further supported by evidence observed within our own Solar System. Primitive chondritic material has been found to be remarkably similar to that predicted by equilibrium condensation studies with a Solar composition (Ebel 2006), with bulk elemental abundances that are also functions of their equilibrium condensation temperature for relevant disk conditions (Davis 2006). Preserved equilibrium compositions can still be seen today in the observed thermal stratification of the asteroid belt (Gradie & Tedesco 1982). Although some uncertainty as to the precise cause of these features still lingers, the fact remains that we can utilize equilibrium condensation temperatures to determine the bulk elemental abundances of solid material within planetary systems.

Equilibrium condensation sequences for an identical list of elements as used in Bond et al. (2009) (H, He, C, N, O, Na, Mg, Al, Si, P, S, Ca, Ti, Cr, Fe and Ni) were obtained using the commercial software package HSC Chemistry (v. 5.1) using the same list of gaseous and solid species as in Bond et al. (2009) (listed here in Table 6). As these elements represent the major solid-forming species, no significant limitations are encountered by neglecting other species from these simulations.

Observed stellar photospheric abundances were adopted as a proxy for the composition of the stellar nebula and were taken from Gilli et al. (2006); Beirão et al. (2005); Ecuivillon et al. (2004b, 2006). It should be noted that all abundances applied here were taken from the same research group and were obtained from the same spectra thus acting to limit any possible systematic differences in abundances due to instrument or methodological differences between various studies. The input values used in HSC Chemistry for each system are shown in Table 7. All species are initially assumed to be in their elemental and gaseous form and no other species or elements are assumed to be present within the system.

Neither N or P abundances have been obtained for extrasolar planetary host stars, primarily due to the difficulty in finding unblended spectral lines to use within the visual spectral range (where most studies have been focussed). For this present study, we overcame this issue by obtaining approximate abundances for both elements based on the well known odd-even effect. Caused by the increased stability of even atomic number nuclei relative to odd-numbered nuclei, this effect produces the observed sawtooth pattern in the Solar elemental abundances. Extrasolar abundances were obtained by fitting a linear trend through the solar abundances for the same elements studied here and then applying this same fit to observed extrasolar host star abundances of Na and Al. This approach assumes that extrasolar host stars will display the same atomic sawtooth pattern, a valid assumption as host stars do not appear to have undergone any form of systematic processing (such as

pollution by a nearby supernova event) to cause a significant deviation (see Bond et al. 2008). The same approach was adopted for those systems without an observed [S/H] value.

As for the Solar System simulations of Bond et al. (2009), “nominal” radial pressure and temperature profiles obtained from the Hersant et al. (2001) protoplanetary disk midplane model were used to correlate chemical compositions with a spatial location within the disk. The stellar mass accretion rate \dot{M} , a primary input to the Hersant model, is known to vary with stellar mass as:

$$\dot{M} \propto M^{3/2} \quad (1)$$

where M is the mass of the star in solar masses (ranging from 0.98 to $1.48M_{\odot}$) and \dot{M} is the mass accretion rate in solar masses per year. The input mass accretion rates were thus scaled for the stellar mass of the host star obtained from the Simbad database³. The resulting stellar accretion rates obtained are shown in Table 8. All other input parameters for the Hersant et al. (2001) models remained unchanged ($\alpha = 0.009$, initial disk radius = 17AU). Minor differences in temperature and pressure profiles were produced for the various systems simulated. For example, the temperature and pressure values at a distance of 1AU from the host star for the systems with the highest and lowest mass accretion rates differed by just 51K and 1.6×10^{-6} bars respectively.

It is quite possible that the mass accretion rate varies throughout the disk itself, potentially producing variations in midplane pressure and temperature values. The Hersant et al. (2001) models assumed a uniform mass accretion rate. However, the

³accessed at <http://simbad.u-strasbg.fr/simbad/>

conditions at 1AU in the system with the highest mass accretion rate (HD177830) occur just 0.09AU closer to the host star in the system with the lowest mass accretion rate (HD72659). This indicates that solid material will still condense out at essentially the same radial location, despite variations in the mass accretion rate of the disk. As such, any modification of midplane conditions from those used here due to a varying mass accretion rate are likely to be small enough as to be neglected for the purposes of this study. It is also important to note that the current approach does not include variations in the midplane conditions produced by different chemical compositions (which would alter parameters such as disk viscosity and opacity), nor does it include the effects of stellar luminosity (which aren't incorporated into the Hersant et al. (2001) model). As such, the scaling applied here is a somewhat simplistic approach to a complex issue but is valid for the current aims of this study.

Midplane pressure and temperature values were determined with an average radial separation of 0.01AU throughout the study region. As in Bond et al. (2009), an ensemble of disk compositions was determined based on Hersant et al. (2001) disk conditions at seven different evolutionary times ($t = 2.5 \times 10^5 \text{yr}$, $5 \times 10^5 \text{yr}$, $1 \times 10^6 \text{yr}$, $1.5 \times 10^6 \text{yr}$, $2 \times 10^6 \text{yr}$, $2.5 \times 10^6 \text{yr}$, $3 \times 10^6 \text{yr}$). However, as we previously found the best fit to known planetary values in the Solar System (specifically the compositions of Venus, Earth and Mars) to occur using disk conditions obtained for $t = 5 \times 10^5 \text{yr}$ (Bond et al. 2009), our discussions will mostly focus on compositions produced by disk conditions at this time. Note that these times only refer to the timing of the thermodynamical conditions under which the planetesimals condensed within the disk.

3.3. Dynamical Simulations

In this study, we build upon our recent success in simulating terrestrial planet formation within the Solar System (Bond et al. 2009) and apply the same methodology here. Terrestrial planet formation in extrasolar planetary systems is a complex problem, especially when giant planet migration is taken into account, and modeling it in detail for even a single system is computationally expensive (Raymond et al. 2006b; Mandell et al. 2007). In the interest of exploring a wide range of systems, we use a more basic approach here which necessarily neglects some of the complexities of planet formation, but still allow us to demonstrate some of the potential implications of varying system compositions on final terrestrial planet compositions. More detailed dynamical simulations will be the subject of future work.

N-body simulations of terrestrial planet accretion in each of the selected extrasolar planetary systems are run using the SyMBA n-body integrator (Duncan et al. 1998). The orbital parameters of the giant planets in each system are taken from the catalog of Butler et al. (2006), and updated with values from exoplanets.org as additional data on these systems were obtained. All values utilized are shown in Table 3. Inclinations of each of the giant planets are assumed to be zero since no such measurements have been obtained for these systems. Due to the computational time required, current simulations only contain an initial population of roughly Lunar- to Mars-mass embryos (i.e. no planetesimal swarm is included). This differs from the Solar System simulations of O’Brien et al. (2006) as used in Bond et al. (2009) as those simulations included a planetesimal swarm. As such, it is possible that differences between the dynamical simulations performed here and those of the Solar System as used in Bond et al. (2009) will occur, most likely in that the dynamical excitation of the resulting systems system will be somewhat larger than they would be if a planetesimal swarm were present.

For each extrasolar planetary system modeled, planetary embryos are distributed in the zone between the star and the giant planet (or in the case where there are one or more giant planets close to the host star such as 55Cnc and Gl777, in the region between the inner and outer giant planets) according to the relations between embryo mass, spacing, and orbital radius given by Kokubo & Ida (2000). No embryos are initially located interior to 0.3 AU. The timestep for the integration was set to at least $20\times$ the orbital period of the innermost planet or planetary embryo, or the orbital period of a body at 0.1 AU, whichever is smaller (this corresponds to a half-day timestep for an inner radius of 0.1 AU), and the simulations are run for 100-250 Myr. Surface mass density profiles that vary as $r^{-3/2}$, normalized to 10 gcm^{-2} at 1 AU, were assumed. For each system, a minimum of 4 accretion simulations were run, using different random number seeds for generating the initial embryo distribution.

Migration of the giant planets is very likely to have occurred in many or all of these systems. However, if migration occurred very early, prior to planetesimal and embryo formation in the terrestrial planet region, then terrestrial planets could have potentially formed after migration, with the giant planets in their current configurations (e.g. Armitage 2003). Our simulations focus on this scenario (termed here “in-situ formation”). If giant planet migration occurred after planetesimals and embryos have formed, then our in-situ assumption does not apply and there is likely to be radial migration of planetary embryos, driven by giant planet migration (eg. Raymond et al. 2006a,b; Mandell et al. 2007). However, as there is currently no clear consensus as to the most common timing of planetary migration, and no evidence for the specific systems that we propose to study, each of our simulations begin with the gas giants already fully formed and located in their current positions. Simulations incorporating giant planet migration will be the focus of the second paper in this series.

3.4. Combining Dynamics and Chemistry

The dynamical and chemical simulations were combined together as outlined in Bond et al. (2009) whereby we assigned each embryo a composition based on its formation location (hence pressure and temperature) and assumed that it then contributed that same composition to the final terrestrial planet. The bulk compositions of the final planets are simply the sum of each object they accrete. Phase changes and outgassing were neglected and all collisions were assumed to result in perfect accretion (i.e. no mass loss occurred).

3.5. Stellar Pollution

The issue of stellar pollution produced by terrestrial planet formation is of great interest in extrasolar planetary systems. Pollution of the stellar photosphere via accretion of a large amount of solid mass during planet formation and migration has been suggested as a possible explanation for the observed metallicity trend for known host stars (Laughlin 2000; Gonzalez et al. 2001; Murray et al. 2001). Thus we determined the amount of material accreted by the host star during the current terrestrial planet simulations and also determined the resulting change in spectroscopic photospheric abundance. As in Bond et al. (2009), any solid material migrating to within 0.1AU from the host star is assumed to have accreted onto the stellar photosphere. This material is then assumed to have been uniformly mixed throughout the stellar photosphere and convective zone. Decreasing convective zone mass with time, granulation within the photosphere and gravitational settling and turbulence within the convective zone are again neglected, resulting in the values determined here being the maximum expected enrichments.

The mass of each element accreted onto the star was determined in the same way as for terrestrial planets, by summing the contributions of the individual embryos it accretes.

As a reminder, the resulting photospheric elemental abundance is given by:

$$[X/H] = \log \left[\frac{f_X}{f_{X,\odot}} \right] \quad (2)$$

where $[X/H]$ is the resulting abundance of element X after accretion of terrestrial planet material, f_X is the mass abundance of element X in the stellar photosphere after accretion and $f_{X,\odot}$ is the mass abundance of element X in the Solar photosphere (from Murray et al. (2001)). Note that $[X/H]$ is still dependant on $f_{X,\odot}$ as by definition it is taken relative to the Solar abundance. Explicitly, f_X is given by:

$$f_X = \left[\frac{m_X}{m_{\text{total}}} \right] \quad (3)$$

where m_X is the mass of element X accreted during the simulation, m_{total} is the total mass of the convective zone. Since the stellar composition is dominated by H, we can make the assumption that $m_{\text{total}} \sim m_H$. Thus:

$$f_X = \left[\frac{m_X}{m_{\text{total}}} \right] \sim \left[\frac{m_X}{m_H} \right] \quad (4)$$

The same holds true for the solar values.

f_X values for the extrasolar planetary host stars were obtained via the stellar abundances of Gilli et al. (2006); Beirão et al. (2005); Ecuillon et al. (2004b, 2006), as these papers represent a comprehensive, internally consistent catalogue of photospheric abundances

for a large number of known planetary host stars. The mass of the convective zone of a star is known to vary with its mass, effective temperature (T_{eff}) and, to some extent, its metallicity. Values for the masses of the convective zone for each of the target stars were thus obtained from Pinsonneault et al. (2001) using the T_{eff} values from Santos et al. (2004). The convective zone masses are shown in Table 9. $f_{X,\odot}$ values were obtained by utilizing the solar abundances of Asplund et al. (2005) and a current solar convective zone mass of $0.03M_{\odot}$ (Murray et al. 2001).

4. Results

4.1. Dynamical

As the current simulations are only preliminary and are designed solely to illustrate potential compositional differences within the final terrestrial planets, a detailed examination of the simulation results is of minimal benefit. However, terrestrial planets were found to form in *all* simulations. 22 of the 40 simulations produced two or more terrestrial planets within one system. The general architecture of the resulting systems is shown in Figures 7 - 11. In several cases, the orbital elements of the giant planets change slightly from the values shown in Fig. 6 due to the ejection of embryos from the system, and mutual perturbations in systems with multiple giant planets.

Several of these planets (e.g. namely those in the simulation for HD4203) are simply embryos that have survived for the duration of the simulation and have not accreted any additional material, but essentially all others are grown from collisions among multiple embryos.

Of the ten planetary systems examined, only one (HD72659) is found to produce terrestrial planets with a median mass comparable to Earth ($1.03 M_{\oplus}$) with six of the 11

planets produced having masses equal to or greater than $1 M_{\oplus}$. All other systems have median planetary masses less than $1 M_{\oplus}$, and, excluding those of HD72659, only four out of 51 terrestrial planets in our simulations have masses equal to or greater than $1 M_{\oplus}$.

With the exception of 55Cancri, terrestrial planets that form in our simulations are located inwards of 1 AU. This is primarily a selection effect as we are currently only simulating terrestrial planet formation interior to the known giant planets, and the majority of systems we study here contain giant planets orbiting within 2AU of their host star. 55Cancri is unusual in that its outermost giant planet has a periapse larger than 5AU, a significant increase over the other systems selected for study. That in turn dictated that the embryos in the 55Cancri simulations initially be located between 1 AU and 5AU, hence the larger semi-major axes of the planets that form there.

The terrestrial planets in these systems generally accrete the vast majority of their mass from their immediately surrounding area without a large amount of radial mixing occurring. As such, the terrestrial planets in the simulations are expected to have compositions reflecting any radial trends within the disk. This amount of radial mixing, however, is likely to increase somewhat in future simulations that include a planetesimal swarm, and may greatly increase in simulations that include the effects of migrating giant planets.

The above results are not a definitive determination of the likely terrestrial planet population in the systems we are studying, as we are currently only considering late stage, in-situ terrestrial planet formation. That is, we are only considering formation that has occurred *after* the known giant planets have formed and migrated to their current orbits. As previously discussed, this is a valid approach as there is no consensus on the timing or extent of migration within these systems and it provides us with a reasonable starting point to consider the chemical compositions of possible terrestrial planets in those systems. However, giant planet migration can have a strong influence on terrestrial planet

formation, in a worst-case scenario preventing terrestrial planets from forming, but it may also accelerate terrestrial planet formation and lead to significant radial mixing of material within the system, especially in systems with close-in giant planets (Raymond et al. 2006b; Mandell et al. 2007). Simulations addressing the formation and chemical/dynamical evolution of terrestrial planets under the influence of giant planet migration are currently running and will be the focus of a future paper.

4.2. Chemical

The condensation sequences and abundances of solid species (normalized to the abundance of the least abundant species) for three representative systems are shown in Figure 12. Plots for all other systems in order of increasing C/O value are available online only (Figures 1 - 3). The 50% condensation temperatures (i.e. temperature at which half of the total amount of a given element has condensed) for each of the systems studied is shown in Table 10. The final elemental abundances for all simulated planets and for times studied are shown in Table 11 (available in full online).

Two very distinct types of condensation sequence are produced for the systems studied here - those resembling the Solar condensation sequence (HD27442, HD72659 and HD213240) and those in which carbide phases are present within the disk (55Cnc, Gl777, HD4203, HD17051, HD19994, HD108874 and HD177830). The C enrichment can further be classified as being low ($0.78 < C/O < 1.0$), in which C and carbide phases are present within a spatially narrow region of the disk at temperatures below ~ 1800 K (55Cnc, Gl777, HD17051 and HD177830), and high ($C/O > 1.0$) where a broader carbide-dominated region is stable for temperatures below ~ 2300 K and thus extends into the innermost reaches of the disk (HD4203, HD19994 and HD108874). The implications of these variations in the distribution of solid material are discussed in Section 5.1. The compositional differences

between these different classes of systems result in significantly different compositions of the terrestrial planets that form in those systems, and the characteristics of those planets will be discussed in the following sections. Unless otherwise stated, all compositions shown are produced by disk conditions at $t = 5 \times 10^5$ years. As previously stated, compositions produced for disk conditions at this time were found by Bond et al. (2009) to produce the best fit to observed Solar System compositions (based on agreeing with the compositions of Venus, Earth and Mars). Compositional changes resulting from disk conditions at different times will be discussed in Section 5.2.

4.2.1. Earth-like Planets

Before we can discuss the results produced by this work, we first need to define in detail what an "Earth-like" planet is. For the purposes of this study, it is taken to be at the most basic level a terrestrial planet whose composition is dominated by O, Fe, Mg and Si, with small amounts of Ca and Al and very little Carbon. Essentially, this refers to a terrestrial planet composed of Mg silicates and metallic Fe with other species present in relatively minor amounts. Water or other hydrous species may or may not be present. At a more detailed level, we have allowed for deviations of $\pm 25\%$ from the elemental abundances for the Earth listed in Kargel & Lewis (1993) for the major elements (O, Fe, Mg, Si). Larger abundances were permitted in the minor elements (with the exception of C) due to their lower relative abundance within the terrestrial planets. Given the variations permitted on the individual abundances, a larger range of variations of 35% was permitted in the geochemical ratios considered here (namely Mg/Si, Al/Si and Ca/Si). It is important to note that these accepted compositional variations span the full range of terrestrial planet compositions observed within the Solar System (i.e. under this taxonomy, both Venus and Mars would be classified based on their elemental composition as being Earth-like).

As such, the definition of Earth-like should not be taken to mean identical to Earth in composition. Rather the classification refers to an elemental composition merely similar to that of the Earth.

Bearing that definition in mind, three systems (HD27442, HD72659 and HD213240) were found to produce condensation sequences (and thus also terrestrial planets) comparable to those of the Solar System. See Figure 12 for the condensation sequence for HD27442. Schematic representations of the abundances (for disk conditions at 5×10^5 years) are shown in Figure 13 while the final elemental abundances for all times studied are shown in Table 11. From these it can be seen that for HD27442, HD72659 and HD213240 the outermost terrestrial planets produced are grossly similar in composition to known terrestrial planets. Their compositions are dominated by O, Fe, Mg and Si with varying amounts of other elements. Upon closer examination, however, large and important differences emerge, primarily due to variations in the compositions of the host star and thus the initial system itself.

Pronounced radial compositional variations can be seen in the simulated terrestrial planets of all three systems. Planets located within ~ 0.5 AU for all three systems contain large amounts of Al, Ca and O, indicating that these planets formed from bodies containing the high-temperature Al and Ca condensates (such as spinel and gehlenite) (see Figure 13). However, beyond ~ 0.5 AU, the refractory composition steadily decreases, producing planets with compositions more closely correlated with that of the Earth, dominated by O, Fe, Mg and Si, in the outer regions of the system. Planets produced within this transition zone between the two planetary types, however, are best described as being refractory-rich, Fe-poor silicate planets.

As expected, this difference is reflected in the planetary geochemical ratios, as the planets located within the inner region have Mg/Si, Al/Si and Ca/Si ratios well above

the Solar System terrestrial planet values. However, for planets located beyond the compositional transitional point, this is not the case. In this region, planetary Mg/Si, Al/Si and Ca/Si values are comparable to Earth values. A steady transition in composition between these two regions is seen for all three systems (see Figure 14). This trend lies well above the observed Earth fractionation line and is a result of the condensation of refractory species in the innermost region and Mg-silicate species further out, with relatively little radial mixing between the two regions during the formation process. It is worth noting that while the Mg/Si values for the planets produced in the system of HD213240 are still just within the upper limits of the accepted Earth-like Mg/Si values, the higher modeled planetary values are a result of the increased Mg/Si value of HD213240 itself ($\text{Mg/Si}_{\odot} = 1.05$, $\text{Mg/Si}_{\text{G1777}} = 1.48$). This results in a system with olivine as the major Mg silicate condensate and little pyroxene present.

The model terrestrial planets in the three systems with condensation sequences comparable to that of the Solar System (HD27442, HD72659 and HD213240) can thus be characterized as being essentially similar in composition to Ca- and Al-rich inclusions (CAI's) (for the innermost planets) and Earth-like (for the outermost planets).

4.2.2. *C-rich Planets*

In systems with C/O values close to or above 0.8, the planets that form can begin to incorporate carbon as a significant planet-building material, in the form of graphite, SiC and TiC, which is a significant difference compared to what occurs in the Solar System. Seven such systems were selected for the current study: four with low carbon enrichment ($0.8 \lesssim \text{C/O} < 1$: 55Cnc, G1777, HD17051 and HD177830) and three with a significantly higher C content ($\text{C/O} > 1$: HD4203, HD19994 and HD108874). The final elemental abundances for all times studied are shown in Table 11.

4.2.3. Low C-enriched Planets

G1777: For disk conditions at $t = 5 \times 10^5$ years, G1777 produces Earth-like terrestrial planets with minor C enrichment. See Figure 12 for the condensation sequence for G1777 and Figure 15 for a schematic of the resulting planetary elemental abundances. The final elemental abundances of the refractory lithophile and siderophile elements are similar to those of Earth with the simulated planets displaying a marginal enrichment in Mg ($\sim 3\text{wt}\%$) and a depletion in Si ($\sim 1\text{wt}\%$) and Fe ($\sim 2\text{wt}\%$) compared to Earth values. The most volatile species (P, Na and S) are enriched over Earth, which is likely a result of the fact that we do not consider volatile loss during accretion, which is expected to be significant as for the Solar System simulations.

The geochemical ratios of Mg/Si and Al/Si are enriched compared to those of the Earth, although they are still in accepted range for an Earth-like planet in this study (see Figure 16). As for HD213240, this increase in the planetary Mg/Si values over that observed for the Earth is due to the slight increase the Mg/Si value of G1777 itself ($\text{Mg}/\text{Si}_{\odot} = 1.05$, $\text{Mg}/\text{Si}_{\text{G1777}} = 1.29$). In turn, this produces a system containing nearly equal amounts of olivine and pyroxene (compared to the pyroxene dominated Solar disk) and results in Mg-enriched planets. Note that we do not see such a large spread in planetary Al/Si values as was observed in Figure 14 as G1777 does not contain any terrestrial planets in the region dominated by Al-rich CAI-like material (i.e. within ~ 0.5 from the host star).

The Ca/Si values, however, are lower than those of Earth ($\text{Ca}/\text{Si}_{\text{G1777}} = 0.07$, $\text{Ca}/\text{Si}_{\oplus} = 0.11$), although once again falling within our accepted range of values. This variation is primarily due the fact that there is relatively less Ca within the system. Ca is one of the least enriched elements within G1777 ($[\text{Ca}/\text{H}] = 0.10$ vs. $[\text{Al}/\text{H}] = 0.34$), resulting in a relative Ca depletion within the solid material. The variation in the abundances of the host star is reflected in the lower Ca/Si value of the final planets produced. This difference is

certainly no larger than that observed for the Solar System simulations previously discussed (Bond et al. 2009).

Although the C/O ratio for G1777 is slightly below 0.8 ($C/O_{G1777}=0.78$), a carbon-rich region is still predicted to occur at lower pressures (10^{-5} bar and below), resulting in the production of a narrow carbide-dominated region (extending from 0.77 to 1.13AU at 5×10^5 years). As a result, the terrestrial planets produced in G1777 are all slightly enriched in C compared to the Earth (containing up to 0.5 wt% C). This enrichment decreases for disk conditions at later times as the C region migrates inwards, interior to the feeding zones of the terrestrial planets.

Given these simulated compositions, the terrestrial planets that could form around G1777 are best characterized as being Earth-like with a minor C-enrichment in their chemical composition. It is also interesting to note G1777 is very close to the average extrasolar planetary host star values of Mg/Si and C/O (1.29 and 0.78 respectively, compared to the average values of 1.32 and 0.77). This result implies that terrestrial planets in an “average” extrasolar planetary system would have compositions comparable to that of our own Solar System but moderately enriched in Mg, and with a potentially minor C-enrichment.

55Cnc: Like G1777, 55Cnc produced terrestrial planets that are C-enriched, containing up to 9.28 wt% C (see Figure 15). They are similar to Earth in that they are expected to be dominated by Mg-silicate species, with metallic Fe also present. However, the planets of 55Cnc are also enriched in both S and Mg beyond our acceptable limits to be called an Earth-like planet. This results in modeled planets with Mg/Si values above that of the Earth and Ca/Si values well below. As for HD213240 and G1777, this high planetary Mg abundance is caused by the fact that 55Cnc is highly enriched in Mg ($[Mg/H] = 0.48$), resulting in olivine becoming the major silicate species present within the disk and thus producing the high Mg/Si value observed.

Although the disk of 55Canceri contains a C-rich zone, producing C-enriched terrestrial planets for disk conditions at $t=5\times 10^5$, for disk conditions at later times, none of the simulated planets are predicted to contain any C because the C-rich region moves interior to the terrestrial planet zone in that system. All of the terrestrial planets in 55Cnc are located between 1.5 and 4AU while the C-rich zone is located between ~ 1375 and 713K, corresponding to a radial distance of 0.46 and 1.48AU (for disk conditions in the Hersant et al. (2001) model at 5×10^5 years). Thus the primary feeding zones for each of the planets are located on the outer edge of the C zone at 5×10^5 years, and well beyond it at later times. Thus for disk conditions at later times, planets best described as Mg-rich Earths are produced. The location of the C zone also implies that the four inner known giant planets of the 55Cnc system (located at 0.038AU, 0.115AU, 0.24AU and 0.781AU) should contain significant amounts of C, both in their solid cores and in their atmospheres *if* they formed at or in close proximity to their current orbital locations and also depending on the exact time of their formation. Given the variation in the location of the C rich zone with time, it is expected that terrestrial planets containing some C would also be produced in the current simulations for disk conditions at later times if a time varying equilibrium composition for the solid material was incorporated into the simulations rather than the “snapshot” approach taken here.

HD17051: Although the disk of HD17051 does contain a C-rich zone, for the disk conditions at $t = 5\times 10^5$ years the simulated terrestrial planets do not contain any C, instead resembling the planets of Solar System-like systems previously discussed (see Figure 15). The innermost planets (within ~ 0.5 AU from the host star) are dominated by Al and Ca, resembling CAI’s, while the outer planets are more Earth-like, consisting of Mg-silicates and metallic Fe. They are still significantly enriched in Fe, mostly due to their primary feeding zone location (and subsequent composition) and the high metallicity of HD17051 itself ($[\text{Fe}/\text{H}] = 0.26$).

However, **for planetesimals initially forming under** disk conditions at later times the planetary composition for all simulated planets changes to more closely resemble a C-enriched Earth-like planet, with planets dominated by O, Fe, Mg and Si and a significant amount of C. Up to 4.37 wt% C is predicted to exist in the planets for the disk conditions at 3×10^6 years. These planets are essentially C-enriched Earths, containing the same major elements in geochemical ratios within limits to be considered Earth-like, but also an enhanced inventory of C, primarily accreted as solid graphite. As for 55Cnc, it is expected that if we were to incorporate time-varying equilibrium compositions into our models that we would see C occurring in the terrestrial planets for all simulation times.

HD177830: HD177830 has the highest Mg/Si (and Al/Si) ratio of any system simulated. This enrichment alters the compositions of major silicate species present within the disk. While the Solar System should have condensed both olivine and pyroxene between 0.35 and 2.5 AU, HD177830 is dominated by olivine beyond 0.3 AU and contains only a small region where pyroxene is predicted to coexist. This unusual composition is reflected in the final planetary abundances as the planets contain large portions of Mg (up to 22.33 wt%) (see Figure 15) and have a mean Mg/Si value of 1.71, well above Earth values ($\text{Mg/Si}_{\oplus} = 1.01$).

Al is also similarly enriched (up to 31.74 wt%), again because of the high Al abundance of the host star and thus the initial system itself. Other refractory and lithophile elemental abundances within the final planets are comparable to that of the Solar System. Of the 10 planets produced in our simulations, five also contain trace amounts of C (up to 2.96 wt%). This increases for disk conditions at later times as the C-rich region migrates inwards from its initial location at 0.63 - 1.66 AU (at $t = 5 \times 10^5$ years), through the primary feeding zone, producing planets with increased C-abundances (up to 9.8 wt%). The planets of HD177830 can best be described as being Mg- and Al-rich silicate planets with some C-enrichment.

Such a Mg dominated planetary composition would undoubtedly alter the interior structure and processes of the planets themselves. Such considerations will be discussed further in Section 5.

4.2.4. High C-enriched Planets

HD19994, HD108874 & HD4203: All three systems all have C/O values above 1.0 (1.26, 1.35 and 1.86 respectively). In all three systems, the inner regions of the disk are completely dominated by refractory species composed of C, SiC and TiC, as opposed to the Ca and Al-rich inclusions characteristic of the earliest solids within our Solar System (see Figure 12 for the condensation sequence for HD4203). Significant amounts of metallic Fe are also present within these systems. As all three systems produced terrestrial planets located within 0.7AU from their host star, these unusual inner disk compositions produced terrestrial planets primarily composed of C, Si and Fe. HD19994 produced terrestrial planets composed almost entirely of SiC and metallic Fe and containing up to 37 wt% Si and between 31 and 63 wt% C, over 100 times more C than is estimated for Earth (see Figure 17, upper left). The outermost terrestrial planet for HD19994 does contain significant amounts of O and Mg, primarily because its feeding zone, although still undoubtedly dominated by C, is also rich in pyroxene. This presence of a Mg silicate species produces a slightly more varied composition for a single simulated planet in one of the four simulations completed.

More extreme deviations occur when we consider the planets formed for HD108874 and HD4203. Both of these systems have considerably wider graphite dominated regions, extending from 1.5AU to within 0.1AU (for disk conditions at 5×10^5 years). As a result, terrestrial planets are found to be composed almost entirely of C, Si and Fe (see Figure 17). Both HD108874 and HD4203 produced terrestrial planets composed almost entirely of C and SiC and containing between 67 and 74 wt% C (for midplane conditions at 5×10^5

years). Only the outermost planet of HD108874 contained less than 50 wt% C (30.54 wt% C), with the remainder of the planet consisting of Fe and Si. For disk conditions at later times, Mg and O are also present in all planets produced for both systems, again due to the incorporation of pyroxene and olivine into the planetary feeding zones. It should be noted that most of the terrestrial planets formed in the HD4203 simulations are single embryos that survived for the duration of the simulation but did not accrete any other solid material. Terrestrial planets within these systems are unlikely to have compositions resembling that of any body we have previously observed. The possible implications of these types of planetary compositions will be discussed in Section 5.

4.3. Stellar Pollution

The average change in stellar photospheric abundances produced by accretion of solids onto the star for disk conditions at 5×10^5 years is shown in Table 12 for each system studied. The majority of systems experienced minimal increases in photospheric abundances as a result of accretion during terrestrial planet formation. The largest elemental enrichments occurred for the most refractory elements (Al, Ca, Ti, Ni and Cr), primarily because refractory material is initially located closest to the star itself. The simulations for HD72659 produced many of the most significant enrichments for all elements examined. This is primarily due to the large amount of mass accreted ($2.640 M_{\oplus}$) and the lower estimated mass of the stellar convective zone ($0.0112 M_{\odot}$). However, as previously discussed, mixing within the stellar radiative zone is not incorporated into the current approach. As such, these values are upper limits for those stars with low mass convective zones and large radiative zones. Furthermore, HD72659 (along with Gl777) has the highest degrees of radial mixing and subsequently also accreted the largest amount of solid material onto their host stars. This resulted in a larger change in the stellar photospheric abundances than for other

systems.

All of the predicted abundance changes are below the errors of current spectroscopic surveys (e.g. ± 0.03 for Fischer & Valenti (2005)), meaning that definitively observable elemental enrichments are not necessarily predicted by our terrestrial planet formation simulations. Of course, inclusion of a swarm of planetesimals within the formation simulations and migration of the giant planets is expected to increase the amount of material accreted by the host star and thus also the predicted stellar abundances. However, these increases are expected to be minor and would thus still result in only marginal increases in the observed elemental abundances

5. Implications and Discussion

5.1. Mass Distribution

Radial midplane mass distributions based on the equilibrium condensation sequence were calculated for each system. As composition is correlated to a specific radial distance within the midplane (via the Hersant et al. (2001) model), the total mass of solid material present interior to a given radial distance within the disk is given by summing the masses contained within each annulus of the disk for which composition is calculated:

$$\text{Mass of solid material} = \sum_{i=0.1\text{AU}}^{i=5.0\text{AU}} 2\pi r_i dr M_{\text{solid}, i} \quad (5)$$

where $M_{\text{solid}, i}$ is the mass of solid material determined by the chemical model to be located in an annulus of width dr at r_i . The mass of solid material possible is determined by using

the minimum mass solar nebula with a gas surface mass density profile varying as $r^{-3/2}$, normalized to 1700 gcm^{-2} at 1 AU. Note that this approach only considers equilibrium driven condensation and neglects other processes that may migrate material and alter the mass distribution.

Based on this calculation, the most carbon-rich systems simulated have significant differences in their mass distributions compared to other systems. The combination of a broad zone of refractory carbon-bearing solids in the inner regions and the relatively small amount of water ice that condenses in the outer regions of these systems suggests that C-rich systems have significantly more solid mass located in the inner regions of the disk than for a Solar-composition disk. This can be seen in Figure 18 which shows the distribution of solid mass within each system normalized to a solar composition disk for disk conditions at $t = 5 \times 10^5$ years.

From Figure 18, the system with the highest C/O value (HD4203) clearly contains significantly more mass in the innermost regions of the disk than a disk of solar composition does. However, the total mass of solid material produced by the current approximations is only $18.4 M_{\oplus}$. As such, it is not clear that a giant planet core composed of refractory C-rich species could be produced within several AU of the host star, allowing for giant planet formation to occur much closer to the host star than previously thought. If significantly more mass were present within the disk than is currently estimated, such a scenario may be possible and would obviously alter the extent and nature of planetary migration required within these systems as it would no longer be required that a planet located at 1-2AU originally formed at 5AU and migrated inwards. Alternatively, if insufficient mass is available for Jovian core formation, production of large terrestrial planets in this region may proceed faster and with greater ease, thus increasing the chance of forming detectable terrestrial planets.

It can be seen from Figure 18 that the planetary system with the most Solar-like composition (HD 72659) has a mass distribution similar to that of the Solar System. The enrichment observed over the solar mass distribution within $\sim 0.5\text{AU}$ from the host star is due to the higher Mg/Si value for HD72659 resulting in the condensation of more Mg silicates. This enhancement is more obvious for the system with the highest Mg/Si value (HD177830). Likewise, the refractory rich system HD27742 also contains more mass in the inner regions of the disk than for a Solar abundance. This is due to the high abundances of several refractory elements ($[\text{Al}/\text{H}]=0.53$, $[\text{Na}/\text{H}]=0.41$, $[\text{Ca}/\text{H}]=0.12$). The variation in mass observed for all systems at $\sim 4.8\text{AU}$ is due to the condensation of hydrous species in various amounts relative to the solar composition disk.

These results imply that the use of an alternative initial mass distribution may be required for planetary systems with high C/O values. Although the planetary formation simulations presented here utilized the classical Solar-System based mass distribution, such an approach is still valid for the illustrative purposes of the current study. The full implications of these results need to be examined in future work by using alternative mass distributions for extrasolar planetary formation simulations for both gas giant planets and smaller terrestrial planets.

5.2. Timing of Formation

Specific planetary compositions have been found to be highly dependent on the time selected for the disk conditions, especially for those systems containing C-dominated regions. This is primarily due to the low degree of radial mixing encountered within the simulations. As a result, as conditions within the area immediately surrounding the planet evolve, the composition of the solid material and thus the final planet itself drastically change. For disk conditions at later times, the simulated planetary compositions evolve to more

closely resemble those of the Solar System. They become dominated by Mg silicate species and metallic Fe. Terrestrial planets in Solar-like systems attain more hydrous material. Variations in composition with disk condition times are most noteworthy for those planets dominated by refractory compositions (such as the inner planets of HD72659 and HD27442). Under later disk conditions, these planets experience a complete shift in their composition, losing the majority of their refractory inventory to be composed primarily of Mg-silicates (olivine and pyroxene). Therefore if solid condensation and initial planetesimal formation occurred significantly later, we would expect to observe predominantly Mg-silicate and metallic Fe planets with enrichments in other elements (such as C) depending on the exact composition of the system. Although disk conditions at 5×10^5 years provide the “best fit” for Solar System simulations (based on fitting the compositions of Venus, Earth and Mars) and are thus utilized here, it remains to be seen whether or not disk conditions at this time provide an accurate description of the conditions under which planetesimals and embryos formed in other planetary systems. Therefore, we require a more detailed understanding of the timing of condensation and planetesimal and embryo formation within protoplanetary disks to be able to further constrain the predicted elemental abundances.

Similarly, as the disk evolves, the various condensation fronts migrate closer to the host star. For example, the water ice line for G1777 migrates from 7.29 AU for midplane conditions at 2.5×10^5 years to 1.48AU for midplane conditions at 3×10^6 years. Similar degrees of migration also occur for the condensation fronts of other species (such as the Mg silicates olivine and pyroxene). In effect, the change in location of the condensation fronts alters the mass distribution within the disk, increasing the mass present in both the very closest regions of the disk ($< 1\text{AU}$) as the refractory species are replaced by the more abundant Mg silicates and in the outer most regions ($> 3\text{AU}$) as water ices appear. The full effects of this change will require formation simulations to be run with alternative mass distributions but it is thought that such conditions will increase the efficiency of forming

close-in terrestrial planets and/or the mass of the resulting planets. Additionally, it will also allow for efficient terrestrial planet growth in the outer regions, possibly to the extent of forming gas giant cores. Given that the average disk lifetime is ~ 3 Myr, not all disks will reach the final chemical compositions modeled here. Thus it remains to be seen not only whether or not sufficient solid mass would be retained during the evolutionary process for Jovian cores to develop but also whether or not core formation can occur before the disk is cleared out.

5.3. Detection of Terrestrial Planets

The results of this study are of great importance for the design of terrestrial planet finding surveys. Our simulations, while preliminary, suggest that terrestrial planets can be stable in a wide range of extrasolar planetary systems. Four distinct classes of planetary composition have been produced by the current simulations: Earth-like, Mg-rich Earth-like, refractory (compositions similar to CAI's) and C-rich. These planetary types are primarily a result of the compositional variations of the host stars and thus the system as a whole. Based on their observed photospheric elemental abundances, the majority of known extrasolar planetary systems are expected to produce terrestrial planets with compositions similar to those within our own Solar System. Therefore, systems with elemental abundances and ratios similar to these (e.g. HD72659) are ideal places to focus future “Earth-like” planet searches.

Based on our dynamical simulations, the masses of the terrestrial planets produced are too low to be detected by current radial velocity surveys. However, many of the simulated planets are in orbits (assuming the simulated inclinations are correct) that would place them within the prime target space for detection by the Kepler mission. Designed to detect extrasolar planets via transit studies, Kepler is the first mission that has the potential of

detecting Earth-mass (and lower) extrasolar planets located within the habitable zone of a planetary system. It has the sensitivity to detect the transit of an Earth mass body within 2AU from the host star and a Mars mass body (0.1Me) within 0.4AU. Single transit events may not be sufficient to positively identify the presence of a planet, although planets at 1 AU should transit 3-4 times during the lifetime of the kepler mission, thus reducing the likelihood of contamination in the data. The vast majority of the terrestrial planets formed here (with the exception of the lowest mass, highest semimajor axis planets) are well within this range and thus may be detectable if they are indeed present within these systems (assuming the system is aligned such that transits can be observed from orbit). Only HD4203 produces no potentially detectable planets, based on their predicted masses. Thus it is likely that we will have an independent check of extrasolar terrestrial planet formation simulations within the next 5 years (but not necessarily for these systems, only for a range of systems which may be similar to these). Such information will be vital for further refinement of planetary formation models for both giant and terrestrial planets. Obtaining compositional information about such terrestrial planets, however, will be more difficult as the size and location of the predicted planets will prohibit direct spectroscopic studies. It is also unlikely that the terrestrial planets will contain atmospheres large enough to be detected and characterized by transit surveys. As such, detailed extrasolar terrestrial planetary chemical compositions will remain unknown for the foreseeable future.

In addition to detection via transit surveys, attempts are also being made to obtain direct images of extrasolar planetary systems. One such example is Darwin, a proposed ESA space based mission that would utilize nulling interferometry in the infrared to directly search for terrestrial extrasolar planets. The compositional variations outlined here are likely to influence our ability to successfully detect these planets. Carbon-rich asteroids are known to be highly non-reflective. For example, 624 Hektor (D-type asteroid) has a geometric albedo of 0.025 while 10 Hygiea (C-type asteroid) has a geometric albedo of

0.0717 (compared to a geometric albedo of 0.367 for the Earth and 0.113 for the moon). As both of these asteroids are assumed to be carbon-rich, it is likely that the carbon-rich planets identified here are similarly dark. Thus it is expected that searches for these planets in the visible spectrum will be difficult due to the small amount of light reflected by these bodies. However, a lower albedo results in greater thermal emission from a body, suggesting that the infrared signature from these planets would extend to shorter wavelengths than corresponding silicate planets. As a result, infrared searches (such as that of Darwin) are ideally suited to detect carbon-rich terrestrial planets and thus should be focused on stellar systems with compositions similar to that of the C-rich stars identified here to maximize results. Of course, this conclusion neglects any possible effects of a planetary atmosphere.

5.4. Hydrous Species

As one would intuitively expect, hydrous material (water and serpentine in the current simulations) is primarily located in the outer, colder regions of the disks. This corresponds to beyond ~ 7.3 AU for disk conditions at 2.5×10^5 years and beyond ~ 1.4 AU for disk conditions at 3×10^6 years for all compositions examined. As a result of this distribution, terrestrial planets forming in the inner regions of a given planetary system are unlikely to directly accrete significant amounts of hydrated material. In the current in-situ simulations, none of the simulated terrestrial planets directly accrete any hydrous species for disk conditions at 5×10^5 years. As the composition of the planetesimals is dictated by the thermodynamic conditions of the disk at the time of condensation only, if any of the simulated planetesimals were to condense/form at later times, they would be more likely to

be water-rich given that the ‘snow line’⁴ migrates inwards as the disk cools, producing a greater overlap between their feeding zones and the water-rich region of the disk.

However, a far greater effect is expected to be produced by migration of giant planets within the system (Raymond et al. 2006b; Mandell et al. 2007). Migration of a giant planet has been shown to be capable of driving a large amount of material from the outer regions of a disk inwards. In the case of hydrous material, this has been found to result in water-rich terrestrial planets being formed both interior and exterior to the giant planet (Raymond et al. 2006b; Mandell et al. 2007). The full extent of this increase in water content will be examined by a suite of simulations incorporating giant migration that are currently running and will be the focus of future work.

In the Solar System, it has been hypothesized that the Earth’s water could have originated from hydrated material in the region where the asteroid belt now lies, or from comets beyond the orbit of Jupiter. While belts of debris resembling the asteroid belt could exist interior to the giant planets in several of the extrasolar systems and may be incorporated into the terrestrial planets, as noted above, none of that material is expected to be hydrated at early times in the disk. We can not address the issue of cometary delivery of water in these simulations, as bodies beyond the orbits of the giant planets are not presently included in our dynamical models.

Water can also potentially be incorporated into a planetary body via adsorption onto solid grains within the disk (Drake 2005). While this process has not been considered in our current simulations, it is possible that there will be some water delivered during the formation process to the terrestrial planets produced in the Earth-like systems (HD27442,

⁴Note that here ‘snow line’ refers to the location within the disk where the thermodynamic conditions are such that water ice condenses (i.e. where $T = 150\text{K}$).

HD72659 and HD213240) as the solid grains are bathed in water vapor over the entire span of the disk. This same process will likely not be as effective at delivering water to the C-rich systems (55Cnc, Gl777, HD4203, HD17051, HD19994, HD108874 and HD177830) as they only have water vapor present at temperatures below ~ 800 K. This temperature range corresponds to beyond a radial distance of ~ 1.2 AU for Hersant et al. (2001) midplane conditions at 2.5×10^5 years and ~ 0.2 AU for midplane conditions at 3×10^6 years. As few terrestrial planets in our simulations accrete material from beyond 1.2 AU, it is expected that C-rich planets forming early in the lifetime of the disk will remain dry without additional water being incorporated into the planets via adsorption. Thus it appears that terrestrial planets are likely to obtain some amount of water (through giant planet migration mixing the disk, variations in composition with time i.e. heterogeneous accretion, adsorption and exogenous delivery), while those within Solar-like systems may receive more water and other hydrous species than terrestrial planets within C-rich systems.

5.5. Planetary Interiors and Processes

Given the wide variety of predicted planetary compositions, a similarly diverse range of planetary interiors structures is also expected. To better quantify this, we examined three specific cases: a $1.03M_{\oplus}$ Earth-like planet located at 0.95 AU (HD72659), a $1.22M_{\oplus}$ Mg-rich Earth-like planet located at 0.43 AU (HD177830) and a $0.47M_{\oplus}$ C-rich planet located at 0.38 AU (HD108874). Approximate interior structures for each were calculated using equilibrium mineralogy for a global magma ocean with $P = 20$ GPa and $T = 2000^{\circ}\text{C}$. Equilibrium compositions at these conditions have been found to produce the best agreement between predicted and observed siderophile abundances within the primitive upper mantle of the Earth (Drake 2000). Elemental abundances were taken from the results discussed in Section 4.2. Resulting mineral assemblages were sorted by density to define

the compositional layers. Note that this assumes that a planet undergoes complete melting and differentiation. Approximate planetary radii were obtained from Sotin et al. (2007) based on planetary mass. These planetary radii are based on silicate planetary equations of state and as such are unlikely to completely describe the C-rich planets modeled here. However, no studies have considered such assemblages, forcing us to assume a silicate based approximate radius. Density variations at high pressures were not considered in defining the depths of various layers. Although important for planetary evolution processes such as mantle stripping, the effects of large impacts (such as the moon forming impact) are also neglected. The resulting interior structures (shown to scale) can be seen in Figure 19.

The interior mineralogy and structure of one of our model planets orbiting HD72659 is similar to Earth. It contains a pyroxene and feldspathic dominated crust (~ 133 km deep) overlying an olivine mantle (~ 985 km deep) with an Fe-Ni-S core (radius ~ 4930 km). The crust is thicker than seen on Earth as we are currently neglecting density and phase changes. Given its structure and comparable mineralogy, we would expect to observe planetary processes similar to those seen on Earth. The planets location within the habitable zone of the host star suggests that a liquid water ocean is feasible, provided sufficient hydrous material can be delivered. Melting conditions and magma compositions are expected to be comparable and it is feasible that a liquid core would develop, resulting in the production of a magnetic dynamo. In general, based on their mass and composition, the terrestrial planets of HD72659 are likely to have structures and mineral assemblages similar to those observed in our system.

The simulated planet for HD177830 (the system with the highest Mg/Si value) is depleted in Si, relative to the Earth, resulting in high spinel and olivine content in the mantle (resembling that of type I kimberlites) and a thicker mellite and calcium dominated crust than found for HD72659 (~ 309 km deep). The core would produce a considerable

amount of heat via potential energy release during differentiation, potentially producing melts with compositions similar to komatiite (dominated by olivine with trace amounts of pyroxene and plagioclase). Volcanic eruptions would be comparable to basaltic flows observed on Earth due to the low silica content of the melt. However, given the thickness of the crust, extrusive volcanism and plate tectonics are unlikely to occur as high stress levels would be required to fracture the crust. Producing and sustaining such stresses would be challenging. Therefore, it is questionable whether or not a planet with this composition and structure would be tectonically active for long periods of time. Given the similar composition and size of the core compared to Earth, a magnetic dynamo is still expected to be produced within the core.

Finally, carbide planets are expected to form around HD108874. The resulting composition and structure is unlike any known planet. Its small size, refractory composition and possible lack of radioactive elements (due to the potential absence of phosphate species, common hosts for U and Th, and possible lack of feldspar and carbonates, the common host of K) will inhibit long-term geologic activity due to the difficulty of melting the mantle. Only large amounts of heat due to core formation and/or tidal heating would be able to provide the required mantle heating. Once all the primordial heat has been removed, it is unlikely that the mantle would remain molten on geologic timescales. Until that time, given the buoyancy of molten carbon, volcanic eruptions would be expected to be highly enriched in C. The core is also expected to be molten, thus making it likely that a magnetic dynamo would be produced (Gaidos & Selsis 2007). Note that this assumes that sufficient heat is initially available to melt the body and allow for differentiation and core formation to occur in the first place. In essence, although initially molten and probably active, old carbide planets of this type would be geologically dead.

Incomplete mixing of material accreted at later times is likely to result in deviations

from the equilibrium picture presented here. For example, accretion of oxidized and water-rich material late in the formation process may result in a stratified redox state and water-rich crust as observed for the Earth. Unfortunately, it is not possible to determine these effects with current models as it requires a level of understanding of the impact and accretion process (e.g. mantle mixing, fragmentation) on small planetary bodies that we currently do not have.

These results are also key for super Earth studies such as that of Valencia et al. (2007) and O’Neill et al. (2007). Previous simulations have assumed Earth-based compositions and structures. Based on the present simulations, a wide variety of both are possible and will need to be considered.

5.6. Planet Habitability

The habitable zone of a planetary system is defined as being the range of orbital radii for which water may be present on the surface of a planet. For the stars considered here, that corresponds to radii from $\sim 0.7\text{AU}$ to $\sim 1.45\text{AU}$. The vast majority of the planets produced by the current simulations orbit interior to this region (exterior in the case of 55Cnc) and thus are unlikely to be habitable in the classical sense. 10 planets are produced within the classical habitable zone, existing in orbits extending from 0.70AU to 1.19AU . Seven of these planets are formed in Solar-like systems (HD24772 and HD72659) and have compositions loosely comparable to that of Earth. As such, we feel that these systems (and others similar to them) are the ideal place to focus future astrobiological searches as they may not only contain planets with compositions similar to that of Earth but also exist in the biologically favorable region of the planetary system.

Of the seven C-rich systems, only two produced planets within the habitable zone.

Gl777 formed two terrestrial planets within the habitable zone while HD19994 formed a terrestrial planet at 0.70AU, just at the inner edge of the habitable zone. All other planets are located well inside the required radii. Both of the habitable planets around Gl777 are C-enriched Earth-like planets, making them potential sites for the development of life. The single habitable planet produced by the HD19994 simulations is dominated by C, along with O, Fe, Si and Mg. It is unclear whether such a composition would be favorable to life. Additionally, the low planet mass ($0.06M_{\oplus}$) further makes it unlikely that this particular simulated planet could ever actually host life. As such, under the current definition of habitable, we conclude that of the seven C-rich systems currently simulated, Gl777 has the best chance of supporting life, but this is by no means guaranteed.

5.7. Biologically Important Elements

In addition to water, complex life (as we know it) also requires several key elements to exist. The six essential elements are H, C, N, O, P and S. As was the case for the Solar System simulations discussed in Bond et al. (2009) none of the planets accreted any N and are also lacking in H. The terrestrial planets formed in the Solar-like systems contained various amounts of O and P but some were deficient in S and all were lacking C, as for the Solar System simulations. The most C-rich systems, on the other hand, were lacking in O, P and S.

Thus it is clear that for life as we know it to develop on any of the terrestrial planets formed in the current simulations, significant amounts of several elements must be supplied from exogenous sources within the system. All elements may be supplied from the outer, cooler regions of the disk. Thus it is possible that migration or the radial mixing of cometary-type material into the terrestrial planet region may produce planets with the necessary elements for life to develop. As for the Solar System simulations, all biologically

required elements would be introduced in a form that could potentially be utilized by early life. This is especially intriguing for those planets located within the habitable zone. On the other hand, alternative pathways could potentially develop for the formation of an alternative biologic cycle without requiring the same six elements.

5.8. Host Star Enrichment

As previously discussed, stellar photospheric pollution has been suggested as a possible explanation for the observed high metallicity of extrasolar planetary host stars (Laughlin 2000; Gonzalez et al. 2001; Murray et al. 2001). The current simulations, though, do not support this hypothesis. Enrichments are produced primarily in Al, Ca and Ti, not Fe as is required by the pollution theory. Furthermore, relatively small masses of solid material are accreted by the host stars during planet formation, suggesting that insufficient material is accreted to produce the observed enrichments. Thus unless migration of the giant planets can systematically result in accretion of giant planets by the host star, our results agree with previous authors (e.g Santos et al. 2001, 2003a,b, 2005; Fischer & Valenti 2005) in finding that the observed host star enrichment is primordial in origin.

Our simulations also imply that enrichments due to stellar pollution are most likely to be observed for the refractory elements in high mass stars with low convective zone masses. This suggests that surveys for pollution effects caused by terrestrial planet formation should focus on Ti, Al and Ca abundances in A-type and high mass F-type stars as they are expected to have the lowest convective zone masses. However, more detailed simulations of the fate of material accreted into radiative zones need to be undertaken to support this hypothesis.

6. Summary

Terrestrial planet formation simulations have been undertaken for ten different extrasolar planetary systems. Terrestrial planets were found to form in all systems studied, with half of the simulations producing multiple terrestrial planets. The simulated planets are possibly detectable by Kepler (if the system orientation is favorable), thus potentially allowing for future independent verification of formation simulations.

The compositions of these planets are found to vary greatly, from those comparable to Earth and CAIs to other planets highly enriched in carbide phases. These compositional variations are produced by variations in the elemental abundances of the host star and thus the system as a whole, with the Mg/Si and C/O ratios being the most important for determining the final planetary compositions. Based on this, it is expected that C-rich planets will comprise a sizeable portion of extrasolar terrestrial planets and need to be considered in significantly more detail. These compositions are highly dependant on the disk conditions selected for study, requiring us to develop a more detailed understanding of the timing of planetary formation within these systems.

Given the wide variety of compositions predicted, it is also likely that planetary mineralogies and processes within these planets will be different from those of our own Solar System. Compositions range from planets dominated by Fe and Mg-silicate species to those composed almost entirely of Fe and C. These compositional variations are likely to generate differences in detectability with C-rich planets being easier to detect via infrared surveys such as the Darwin mission due to their lower albedo and hence larger IR emission.

The most habitable planets are expected to be those forming in systems with compositions similar to Solar. The simulated compositions make these planets ideal targets for future astrobiological surveys and studies. Planets in the C-rich systems that we model are likely to be lacking water and generally located interior to the habitable zone, making

such planets unfavorable for the development of life as we know it.

Finally, pollution of the host star by the planetary formation process appears to be negligible for the majority of systems. Enrichments are produced only for those stars with the least massive convective zones and even then only in the most refractory elements (Ti, Al and Ca). Therefore, it is unlikely that pollution by accreted terrestrial material is a viable explanation for the currently observed host star metallicity trend. This also implies that pollution studies should be undertaken for A-type and massive F-type stars as they are more likely to display the preferential enrichment in Ti, Al and Ca that appears to be indicative of terrestrial planet formation.

J. C. Bond and D. P. O’Brien were funded by grant NNX09AB91G from NASA’s Origins of Solar Systems Program. J. C. Bond and D. S. Laretta were funded by grant NNX07AF96G from NASA’s Cosmochemistry Program. Thanks to the anonymous reviewer for their helpful comments in the production of this paper.

A. Online Material: Tables

Table 1. Predicted bulk elemental abundances for all simulated extrasolar terrestrial planets. All values are in wt% of the final predicted planet for all seven sets of disk conditions examined. Planet number increases with increasing distance from the host star.

System	H	Mg	O	S	Fe	Al	Ca	Na	Ni	Cr	P	Ti	Si	C	
55Cnc															
t=2.5×10 ⁵ years															
55Cnc 1-4	0.00	16.59	26.02	2.58	20.92	1.40	0.65	0.51	1.27	0.24	0.16	0.06	11.54	0.00	18.06
55Cnc 2-4	0.00	16.50	25.88	2.93	20.79	1.39	0.65	0.51	1.26	0.24	0.16	0.06	11.47	0.00	18.18
55Cnc 3-4	0.00	16.80	26.21	2.20	21.14	1.41	0.71	0.52	1.28	0.24	0.16	0.06	11.73	0.00	17.53
55Cnc 3-5	3.71	12.59	53.11	3.09	15.88	1.06	0.50	0.00	0.96	0.18	0.12	0.05	8.76	0.00	0.00
55Cnc 4-4	1.79	15.74	43.90	3.87	19.87	1.32	0.62	0.31	1.20	0.23	0.15	0.06	10.95	0.00	0.00
t=5×10 ⁵ years															
55Cnc 1-4	0.00	19.43	30.61	4.75	24.49	1.63	0.77	0.62	1.48	0.28	0.18	0.07	13.51	0.00	2.18
55Cnc 2-4	0.00	19.85	31.29	4.87	25.03	1.67	0.78	0.63	1.51	0.29	0.19	0.08	13.81	0.00	0.00
55Cnc 3-4	0.00	19.06	31.26	4.63	24.04	1.60	0.75	0.60	1.45	0.28	0.18	0.07	13.26	0.00	2.83
55Cnc 3-5	0.00	18.67	35.33	4.58	23.58	1.57	0.74	0.60	1.42	0.27	0.18	0.07	12.99	0.00	0.00
55Cnc 4-4	0.00	17.57	30.44	3.78	22.18	1.48	0.69	0.55	1.34	0.25	0.17	0.07	12.21	0.00	9.28

Table 1—Continued

System	H	Mg	O	S	Fe	Al	Ca	Na	Ni	Cr	P	Ti	Si	C	
$t=1\times 10^6$ years															
55Cnc 1-4	0.00	18.68	35.30	4.59	23.59	1.57	0.74	0.60	1.42	0.27	0.18	0.07	12.99	0.00	0.00
55Cnc 2-4	0.00	18.68	35.33	4.59	23.57	1.57	0.74	0.60	1.42	0.27	0.18	0.07	12.99	0.00	0.00
55Cnc 3-4	0.00	18.71	35.25	4.59	23.58	1.57	0.74	0.60	1.43	0.27	0.18	0.07	13.01	0.00	0.00
55Cnc 3-5	0.71	17.64	38.81	4.33	22.24	1.48	0.70	0.00	1.34	0.25	0.17	0.07	12.27	0.00	0.00
55Cnc 4-4	0.03	19.23	33.40	4.72	24.26	1.62	0.76	0.61	1.47	0.28	0.18	0.07	13.37	0.00	0.00
$t=1.5\times 10^6$ years															
55Cnc 1-4	0.00	18.70	35.33	4.59	23.62	1.54	0.71	0.59	1.43	0.27	0.18	0.07	12.97	0.00	0.00
55Cnc 2-4	0.00	18.67	35.33	4.58	23.58	1.57	0.74	0.60	1.42	0.27	0.18	0.07	12.99	0.00	0.00
55Cnc 3-4	0.21	18.36	36.37	4.51	23.18	1.54	0.72	0.42	1.40	0.27	0.17	0.07	12.77	0.00	0.00
55Cnc 3-5	3.71	12.59	53.11	3.09	15.88	1.06	0.50	0.00	0.96	0.18	0.12	0.05	8.76	0.00	0.00
55Cnc 4-4	1.79	15.77	43.83	3.87	19.87	1.33	0.62	0.31	1.20	0.23	0.15	0.06	10.97	0.00	0.00
$t=2\times 10^6$ years															

Table 1—Continued

System	H	Mg	O	S	Fe	Al	Ca	Na	Ni	Cr	P	Ti	Si	C	
55Cnc 1-4	1.24	16.70	41.35	4.10	21.06	1.40	0.66	0.13	1.27	0.24	0.16	0.06	11.61	0.00	0.00
55Cnc 2-4	0.49	17.96	37.72	4.41	22.66	1.51	0.71	0.19	1.37	0.26	0.17	0.07	12.49	0.00	0.00
55Cnc 3-4	1.11	16.86	40.64	4.14	21.28	1.42	0.66	0.42	1.28	0.24	0.16	0.06	11.72	0.00	0.00
55Cnc 3-5	0.00	19.85	31.28	4.87	25.03	1.67	0.78	0.64	1.51	0.29	0.19	0.08	13.81	0.00	0.00
55Cnc 4-4	0.00	18.36	28.22	3.15	23.20	1.54	0.72	0.31	1.40	0.27	0.17	0.07	12.76	0.01	9.82
$t=2.5 \times 10^6$ years															
55Cnc 1-4	2.71	14.23	48.35	3.50	17.95	1.20	0.56	0.13	1.08	0.21	0.13	0.05	9.90	0.00	0.00
55Cnc 2-4	2.73	14.23	48.48	3.50	17.94	1.20	0.56	0.00	1.08	0.21	0.13	0.05	9.89	0.00	0.00
55Cnc 3-4	1.45	16.35	42.35	4.02	20.62	1.37	0.64	0.13	1.25	0.24	0.15	0.06	11.37	0.00	0.00
55Cnc 3-5	3.71	12.59	53.11	3.09	15.88	1.06	0.50	0.00	0.96	0.18	0.12	0.05	8.76	0.00	0.00
55Cnc 4-4	1.79	15.74	43.90	3.87	19.87	1.32	0.62	0.31	1.20	0.23	0.15	0.06	10.95	0.00	0.00
$t=3 \times 10^6$ years															
55Cnc 1-4	3.05	13.70	49.98	3.37	17.27	1.15	0.54	0.00	1.04	0.20	0.13	0.05	9.53	0.00	0.00

Table 1—Continued

System	H	Mg	O	S	Fe	Al	Ca	Na	Ni	Cr	P	Ti	Si	C	
55Cnc 2-4	3.70	12.60	53.09	3.10	15.89	1.06	0.50	0.00	0.96	0.18	0.12	0.05	8.76	0.00	0.00
55Cnc 3-4	2.93	13.90	49.40	3.42	17.53	1.17	0.55	0.00	1.06	0.20	0.13	0.05	9.67	0.00	0.00
55Cnc 3-5	3.71	12.59	53.11	3.09	15.88	1.06	0.50	0.00	0.96	0.18	0.12	0.05	8.76	0.00	0.00
55Cnc 4-4	1.79	15.76	43.89	3.87	19.89	1.31	0.62	0.30	1.20	0.23	0.15	0.06	10.93	0.00	0.00
G1777															
$t=2.5\times 10^5$ years															
G1777 1-4	0.00	16.61	33.23	1.58	22.48	5.64	3.79	0.27	1.46	0.28	0.15	0.30	13.96	0.01	0.24
G1777 2-4	0.00	15.09	34.73	0.30	19.48	9.98	6.69	0.00	1.41	0.19	0.12	0.55	11.46	0.01	0.00
G1777 2-5	0.00	12.90	36.83	0.48	13.81	13.74	9.30	0.12	1.00	0.15	0.08	0.76	10.62	0.00	0.20
G1777 3-4	0.00	11.92	37.57	0.76	11.59	15.79	10.62	0.00	0.75	0.15	0.08	0.88	9.89	0.01	0.00
G1777 3-5	0.00	16.15	33.83	0.76	21.45	7.32	4.96	0.08	1.54	0.23	0.13	0.40	13.00	0.01	0.13
G1777 4-4	0.00	13.97	35.90	0.43	16.43	11.77	7.94	0.11	1.09	0.19	0.11	0.65	11.21	0.01	0.18
$t=5\times 10^5$ years															

Table 1—Continued

System	H	Mg	O	S	Fe	Al	Ca	Na	Ni	Cr	P	Ti	Si	C	
GI777 1-4	0.00	18.02	32.19	2.08	26.24	1.60	1.09	0.67	1.70	0.33	0.18	0.08	15.47	0.00	0.34
GI777 2-4	0.00	18.62	31.84	0.62	27.28	1.67	1.13	0.37	1.77	0.34	0.19	0.07	15.61	0.01	0.50
GI777 2-5	0.00	18.38	31.43	2.39	26.68	1.62	1.10	0.29	1.73	0.33	0.18	0.09	15.65	0.02	0.10
GI777 3-4	0.00	18.65	31.78	0.95	27.32	1.67	1.13	0.35	1.77	0.34	0.19	0.08	15.49	0.00	0.29
GI777 3-5	0.00	18.17	31.59	2.38	26.35	1.60	1.09	0.46	1.71	0.33	0.18	0.08	15.77	0.01	0.27
GI777 4-4	0.00	18.45	31.82	1.50	26.84	1.64	1.11	0.41	1.74	0.33	0.18	0.08	15.68	0.01	0.19
$t=1\times 10^6$ years															
GI777 1-4	0.00	17.21	32.61	4.69	24.89	1.52	1.03	0.77	1.61	0.31	0.17	0.08	15.05	0.00	0.04
GI777 2-4	0.00	17.68	31.66	3.51	25.63	1.56	1.13	0.79	1.66	0.32	0.21	0.08	15.51	0.00	0.25
GI777 2-5	0.00	17.61	32.47	3.24	25.49	1.55	1.05	0.80	1.65	0.32	0.17	0.08	15.41	0.00	0.16
GI777 3-4	0.00	17.72	32.10	2.96	25.69	1.56	1.06	0.80	1.66	0.32	0.18	0.08	15.54	0.00	0.33
GI777 3-5	0.00	17.40	32.09	4.39	25.20	1.54	1.07	0.79	1.63	0.32	0.19	0.09	15.24	0.00	0.06
GI777 4-4	0.00	17.57	32.32	3.57	25.44	1.55	1.05	0.79	1.65	0.32	0.17	0.08	15.38	0.00	0.10

Table 1—Continued

System	H	Mg	O	S	Fe	Al	Ca	Na	Ni	Cr	P	Ti	Si	C	
$t=1.5 \times 10^6$ years															
GI777 1-4	0.00	16.94	33.13	5.23	24.50	1.49	1.01	0.76	1.58	0.31	0.17	0.08	14.78	0.00	0.02
GI777 2-4	0.00	17.21	32.33	4.87	24.97	1.52	1.03	0.78	1.62	0.31	0.17	0.09	15.10	0.00	0.00
GI777 2-5	0.00	17.15	32.42	5.23	24.76	1.51	1.02	0.77	1.60	0.31	0.17	0.08	14.98	0.00	0.00
GI777 3-4	0.00	17.30	31.95	4.79	25.22	1.53	1.04	0.78	1.62	0.32	0.17	0.09	15.17	0.00	0.03
GI777 3-5	0.00	16.98	32.86	5.43	24.49	1.49	1.01	0.76	1.59	0.31	0.17	0.08	14.82	0.00	0.00
GI777 4-4	0.00	17.13	32.36	5.18	24.85	1.51	1.02	0.77	1.60	0.31	0.17	0.08	14.99	0.00	0.01
$t=2 \times 10^6$ years															
GI777 1-4	0.14	17.00	34.99	5.20	23.10	1.41	0.95	0.69	1.50	0.29	0.16	0.08	14.50	0.00	0.00
GI777 2-4	0.00	17.07	32.64	5.43	24.57	1.50	1.01	0.77	1.59	0.31	0.17	0.08	14.86	0.00	0.00
GI777 2-5	0.07	16.79	33.37	5.48	24.26	1.48	1.00	0.76	1.57	0.30	0.17	0.08	14.67	0.00	0.00
GI777 3-4	0.00	17.01	32.87	5.40	24.49	1.49	1.01	0.76	1.59	0.31	0.17	0.08	14.82	0.00	0.00
GI777 3-5	0.00	16.85	33.47	5.51	24.19	1.47	1.00	0.76	1.57	0.30	0.17	0.08	14.64	0.00	0.00

Table 1—Continued

System	H	Mg	O	S	Fe	Al	Ca	Na	Ni	Cr	P	Ti	Si	C	
GI777 4-4	0.06	16.83	33.41	5.45	24.23	1.48	1.00	0.76	1.57	0.30	0.17	0.08	14.66	0.00	0.00
$t=2.5 \times 10^6$ years															
GI777 1-4	0.62	15.73	37.22	5.15	22.62	1.38	0.93	0.68	1.46	0.28	0.15	0.08	13.68	0.00	0.00
GI777 2-4	0.00	16.80	33.60	5.48	24.15	1.47	1.00	0.75	1.56	0.30	0.17	0.08	14.62	0.00	0.00
GI777 2-5	0.10	16.98	34.25	5.36	23.51	1.43	0.97	0.71	1.52	0.30	0.16	0.08	14.62	0.00	0.00
GI777 3-4	0.00	16.88	33.24	5.52	24.29	1.48	1.00	0.76	1.57	0.31	0.17	0.08	14.70	0.00	0.00
GI777 3-5	0.05	16.62	34.31	5.45	23.86	1.45	0.99	0.74	1.54	0.30	0.16	0.08	14.44	0.00	0.00
GI777 4-4	0.07	16.42	33.79	5.57	24.46	1.52	0.92	0.76	1.58	0.31	0.17	0.08	14.33	0.00	0.00
$t=3 \times 10^6$ years															
GI777 1-4	1.12	14.96	39.74	4.91	21.52	1.31	0.89	0.65	1.39	0.27	0.15	0.07	13.01	0.00	0.00
GI777 2-4	0.00	16.76	33.90	5.48	24.02	1.46	0.99	0.75	1.56	0.30	0.16	0.08	14.54	0.00	0.00
GI777 2-5	0.12	16.51	34.53	5.43	23.79	1.45	0.98	0.72	1.54	0.30	0.16	0.08	14.39	0.00	0.00
GI777 3-4	0.00	16.81	33.69	5.50	24.09	1.47	1.00	0.75	1.56	0.30	0.16	0.08	14.58	0.00	0.00
GI777 3-5	0.11	16.22	34.71	5.49	24.05	1.49	0.92	0.75	1.56	0.30	0.16	0.08	14.15	0.00	0.00

Table 1—Continued

System	H	Mg	O	S	Fe	Al	Ca	Na	Ni	Cr	P	Ti	Si	C	
Gl777 4-4	0.39	16.13	35.87	5.29	23.19	1.41	0.96	0.70	1.50	0.29	0.16	0.08	14.03	0.00	0.00
HD4203															
$t=2.5 \times 10^5$ years															
HD4203 1-3	0.00	0.00	0.00	0.00	0.00	0.00	0.00	0.00	0.00	0.00	0.00	0.16	26.18	0.00	73.66
HD4203 2-3	0.00	0.00	0.00	0.00	0.00	0.00	0.00	0.00	0.00	0.00	0.00	0.16	26.13	0.00	73.71
HD4203 3-3	0.00	0.00	0.00	0.00	0.00	0.00	0.00	0.00	0.00	0.00	0.00	0.16	26.20	0.00	73.64
HD4203 4-3	0.00	0.00	0.00	0.00	0.00	0.00	0.00	0.00	0.00	0.00	0.00	0.16	26.23	0.00	73.61
$t=5 \times 10^5$ years															
HD4203 1-3	0.00	0.00	0.00	0.00	0.63	0.00	0.00	0.00	0.00	0.00	0.12	0.16	26.07	0.00	73.02
HD4203 2-3	0.00	0.00	0.00	0.00	0.00	0.00	0.00	0.00	0.00	0.00	0.00	0.16	26.26	0.00	73.58
HD4203 3-3	0.00	0.00	0.00	0.00	0.74	0.00	0.00	0.00	0.00	0.00	0.14	0.16	26.03	0.00	72.93
HD4203 4-3	0.00	0.00	0.00	0.00	7.95	0.00	0.00	0.00	0.78	0.02	0.30	0.14	23.90	0.00	66.89

Table 1—Continued

System	H	Mg	O	S	Fe	Al	Ca	Na	Ni	Cr	P	Ti	Si	C	
$t=1\times 10^6$ years															
HD4203 1-3	0.00	0.00	0.00	0.77	31.36	1.95	0.96	0.00	2.13	0.35	0.23	0.09	16.58	1.01	44.56
HD4203 2-3	0.00	0.00	0.00	0.16	30.45	1.83	0.20	0.00	2.16	0.26	0.24	0.10	16.83	0.95	46.81
HD4203 3-3	0.00	0.00	0.00	0.98	31.73	1.99	1.23	0.00	2.12	0.38	0.22	0.09	16.48	1.03	43.75
HD4203 4-3	0.00	0.09	0.00	1.10	31.84	1.98	1.23	0.00	2.11	0.40	0.22	0.09	16.51	1.03	43.40
$t=1.5\times 10^6$ years															
HD4203 1-3	0.00	11.43	18.62	2.13	16.94	1.06	0.65	0.00	1.12	0.21	0.12	0.05	10.61	0.01	37.03
HD4203 2-3	0.00	12.48	16.02	1.67	18.51	1.15	0.71	0.00	1.23	0.23	0.13	0.05	10.57	0.00	37.23
HD4203 3-3	0.00	11.09	19.41	2.38	16.43	1.02	0.63	0.00	1.09	0.21	0.11	0.05	10.65	0.01	36.91
HD4203 4-3	0.00	11.03	20.08	1.36	16.34	1.02	0.63	0.00	1.08	0.21	0.11	0.05	10.83	0.01	37.23
$t=2\times 10^6$ years															
HD4203 1-3	0.00	11.00	20.63	0.46	16.29	1.01	0.63	0.44	1.08	0.20	0.11	0.04	10.80	0.01	37.28

Table 1—Continued

System	H	Mg	O	S	Fe	Al	Ca	Na	Ni	Cr	P	Ti	Si	C	
HD4203 2-3	0.00	11.00	20.43	0.74	16.29	1.01	0.63	0.29	1.08	0.20	0.11	0.05	10.80	0.01	37.35
HD4203 3-3	0.00	11.00	20.59	0.55	16.27	1.01	0.63	0.49	1.08	0.20	0.11	0.05	10.80	0.01	37.21
HD4203 4-3	0.00	11.06	21.00	0.00	16.36	1.02	0.63	0.51	1.09	0.21	0.11	0.03	10.85	0.00	37.13
$t=2.5\times 10^6$ years															
HD4203 1-3	0.00	11.05	21.06	0.66	16.35	1.02	0.63	0.51	1.09	0.21	0.11	0.04	10.84	0.00	36.43
HD4203 2-3	0.00	11.06	21.01	0.00	16.37	1.02	0.63	0.51	1.09	0.21	0.11	0.03	10.86	0.00	37.10
HD4203 3-3	0.00	11.02	21.05	0.78	16.31	1.02	0.63	0.51	1.08	0.20	0.11	0.05	10.82	0.00	36.41
HD4203 4-3	0.00	11.10	21.22	1.90	16.43	1.02	0.63	0.51	1.09	0.21	0.11	0.05	10.90	0.00	34.82
$t=3\times 10^6$ years															
HD4203 1-3	0.00	11.21	21.44	2.12	16.60	1.03	0.64	0.52	1.10	0.21	0.12	0.05	11.01	0.00	33.95
HD4203 2-3	0.00	11.06	21.14	1.66	16.37	1.02	0.63	0.51	1.09	0.21	0.11	0.05	10.86	0.00	35.30
HD4203 3-3	0.00	11.19	21.40	2.19	16.57	1.03	0.64	0.52	1.10	0.21	0.12	0.05	10.99	0.00	34.00

Table 1—Continued

System	H	Mg	O	S	Fe	Al	Ca	Na	Ni	Cr	P	Ti	Si	C	
HD4203 4-3	0.00	11.72	22.61	2.79	17.21	1.07	0.66	0.54	1.14	0.22	0.12	0.05	11.70	0.00	30.18
HD17051															
$t=2.5 \times 10^5$ years															
HD17051 1-3	0.00	3.00	41.33	0.00	0.00	22.04	24.11	0.00	0.00	0.00	0.00	1.51	8.01	0.00	0.00
HD17051 1-4	0.00	0.00	42.22	0.00	0.00	25.66	22.86	0.00	0.00	0.00	0.00	1.77	7.49	0.00	0.00
HD17051 2-3	0.00	0.00	47.02	0.00	0.00	46.02	3.52	0.00	0.00	0.00	0.00	3.13	0.32	0.00	0.00
HD17051 2-4	0.00	0.00	42.34	0.00	0.00	26.16	22.39	0.00	0.00	0.00	0.00	1.80	7.32	0.00	0.00
HD17051 3-3	0.00	0.00	46.00	0.00	0.00	41.69	7.62	0.00	0.00	0.00	0.00	2.84	1.84	0.00	0.00
HD17051 4-3	0.00	0.00	44.45	0.00	0.00	35.12	13.87	0.00	0.00	0.00	0.00	2.40	4.16	0.00	0.00
HD17051 4-4	0.00	0.00	42.11	0.00	0.00	25.20	23.30	0.00	0.00	0.00	0.00	1.74	7.65	0.00	0.00
$t=5 \times 10^5$ years															
HD17051 1-3	0.00	0.00	40.61	0.00	0.00	18.85	29.24	0.00	0.00	0.00	0.00	1.49	9.81	0.00	0.00
HD17051 1-4	0.00	11.52	22.22	0.00	48.02	1.98	2.18	0.00	2.59	0.56	0.22	0.14	10.53	0.04	0.00
HD17051 2-3	0.00	0.00	41.80	0.00	0.00	23.70	24.71	0.00	0.00	0.00	0.00	1.49	8.30	0.00	0.00

Table 1—Continued

System	H	Mg	O	S	Fe	Al	Ca	Na	Ni	Cr	P	Ti	Si	C	
HD17051 2-4	0.00	0.00	41.76	0.00	0.00	23.55	24.85	0.00	0.00	0.00	0.00	1.50	8.34	0.00	0.00
HD17051 3-3	0.00	0.00	41.83	0.00	0.00	23.62	24.77	0.00	0.00	0.00	0.00	1.33	8.45	0.00	0.00
HD17051 4-3	0.00	0.00	41.85	0.00	0.00	23.78	24.62	0.00	0.00	0.00	0.00	1.42	8.33	0.00	0.00
HD17051 4-4	0.00	10.43	20.09	0.00	51.86	2.37	2.60	0.00	2.95	0.48	0.25	0.13	8.81	0.02	0.00
$t=1\times 10^6$ years															
HD17051 1-3	0.00	16.98	22.80	1.72	35.78	1.47	1.62	0.00	1.92	0.42	0.17	0.10	14.56	0.00	2.46
HD17051 1-4	0.00	14.01	28.38	0.00	29.37	1.21	1.33	0.83	1.58	0.34	0.14	0.05	15.12	0.00	7.64
HD17051 2-3	0.00	10.46	19.86	0.00	52.27	2.40	2.64	0.00	2.98	0.48	0.25	0.12	8.53	0.01	0.00
HD17051 2-4	0.00	13.66	25.62	1.73	33.97	1.40	1.54	0.00	1.83	0.40	0.16	0.10	13.72	0.02	5.86
HD17051 3-3	0.00	10.86	20.68	0.00	50.78	2.25	2.48	0.00	2.85	0.50	0.24	0.13	9.21	0.02	0.00
HD17051 4-3	0.00	12.43	22.34	0.81	43.61	1.93	2.36	0.00	2.44	0.45	0.20	0.12	11.35	0.02	1.95
HD17051 4-4	0.00	13.93	27.87	0.56	29.22	1.20	1.32	0.65	1.57	0.34	0.13	0.07	15.04	0.01	8.08
$t=1.5\times 10^6$ years															
HD17051 1-3	0.00	13.92	28.19	0.00	29.20	1.20	1.32	0.81	1.57	0.34	0.13	0.05	15.02	0.00	8.24

Table 1—Continued

System	H	Mg	O	S	Fe	Al	Ca	Na	Ni	Cr	P	Ti	Si	C	
HD17051 1-4	0.00	13.50	27.57	3.15	28.29	1.16	1.28	0.81	1.52	0.33	0.13	0.08	14.57	0.00	7.60
HD17051 2-3	0.00	14.68	26.11	2.13	30.78	1.27	1.39	0.00	1.66	0.36	0.14	0.09	14.48	0.01	6.90
HD17051 2-4	0.00	14.02	28.22	0.35	29.42	1.21	1.33	0.65	1.58	0.34	0.14	0.08	15.13	0.01	7.52
HD17051 3-3	0.00	14.43	26.49	1.93	30.27	1.25	1.37	0.00	1.63	0.35	0.14	0.09	14.69	0.01	7.35
HD17051 4-3	0.00	14.35	27.02	1.14	30.09	1.24	1.36	0.30	1.62	0.35	0.14	0.08	14.82	0.01	7.49
HD17051 4-4	0.00	14.59	29.78	2.04	30.53	1.26	1.38	0.87	1.64	0.36	0.14	0.09	15.74	0.00	1.59
$t=2\times 10^6$ years															
HD17051 1-3	0.00	14.43	29.48	0.66	30.27	1.24	1.37	0.86	1.63	0.35	0.14	0.09	15.58	0.00	3.90
HD17051 1-4	0.00	14.03	28.84	4.75	29.41	1.21	1.33	0.84	1.58	0.34	0.14	0.08	15.15	0.00	2.30
HD17051 2-3	0.00	13.84	27.68	0.82	29.01	1.19	1.64	0.65	1.56	0.34	0.13	0.07	14.93	0.01	8.12
HD17051 2-4	0.00	14.51	29.59	1.78	30.39	1.25	1.38	0.87	1.64	0.36	0.14	0.09	15.66	0.00	2.35
HD17051 3-3	0.00	13.90	27.94	0.53	29.15	1.20	1.53	0.71	1.57	0.34	0.13	0.07	15.00	0.01	7.91
HD17051 4-3	0.00	14.14	28.61	0.54	29.64	1.22	1.34	0.75	1.60	0.35	0.14	0.07	15.26	0.00	6.34

Table 1—Continued

System	H	Mg	O	S	Fe	Al	Ca	Na	Ni	Cr	P	Ti	Si	C	
HD17051 4-4	0.00	13.71	28.08	4.23	28.71	1.18	1.30	0.82	1.54	0.34	0.13	0.08	14.79	0.00	5.10
$t=2.5 \times 10^6$ years															
HD17051 1-3	0.00	14.51	29.90	3.57	30.40	1.25	1.65	0.87	1.63	0.36	0.14	0.09	15.64	0.00	0.00
HD17051 1-4	0.00	13.85	31.78	4.99	29.00	1.19	1.31	0.83	1.56	0.34	0.13	0.08	14.94	0.00	0.00
HD17051 2-3	0.00	14.19	28.92	0.00	29.75	1.22	1.35	0.85	1.60	0.35	0.14	0.08	15.32	0.00	6.24
HD17051 2-4	0.00	14.31	29.41	3.59	29.80	1.23	1.50	0.85	1.61	0.35	0.14	0.09	15.44	0.00	1.68
HD17051 3-3	0.00	14.29	29.16	0.41	29.98	1.23	1.36	0.85	1.61	0.35	0.14	0.09	15.44	0.00	5.08
HD17051 4-3	0.00	14.43	29.47	1.62	30.24	1.24	1.37	0.86	1.63	0.35	0.14	0.09	15.57	0.00	2.99
HD17051 4-4	0.00	14.08	30.66	4.97	29.50	1.21	1.34	0.84	1.59	0.35	0.14	0.08	15.20	0.00	0.05
$t=3 \times 10^6$ years															
HD17051 1-3	0.00	13.70	28.24	4.38	28.76	1.18	1.56	0.82	1.54	0.34	0.13	0.08	14.77	0.00	4.50
HD17051 1-4	0.00	13.84	31.77	5.02	28.99	1.19	1.31	0.83	1.56	0.34	0.13	0.08	14.93	0.00	0.00
HD17051 2-3	0.00	14.64	29.89	1.99	30.65	1.26	1.39	0.87	1.65	0.36	0.14	0.09	15.80	0.00	1.28
HD17051 2-4	0.00	14.19	29.18	4.57	29.76	1.22	1.35	0.85	1.60	0.35	0.14	0.08	15.31	0.00	1.40

Table 1—Continued

System	H	Mg	O	S	Fe	Al	Ca	Na	Ni	Cr	P	Ti	Si	C	
HD17051 3-3	0.00	14.62	29.88	2.51	30.62	1.26	1.39	0.87	1.65	0.36	0.14	0.09	15.77	0.00	0.83
HD17051 4-3	0.00	14.40	29.49	3.28	30.19	1.24	1.37	0.86	1.62	0.35	0.14	0.09	15.54	0.00	1.43
HD17051 4-4	0.00	13.85	31.78	5.00	28.99	1.19	1.31	0.83	1.56	0.34	0.13	0.08	14.93	0.00	0.00
HD19994															
$t=2.5\times 10^5$ years															
HD19994 1-3	0.00	0.00	0.00	0.00	0.00	0.00	0.00	0.00	0.00	0.00	0.00	0.21	36.61	0.00	63.18
HD19994 2-3	0.00	0.00	0.00	0.00	0.00	0.00	0.00	0.00	0.00	0.00	0.00	0.21	36.62	0.00	63.17
HD19994 3-3	0.00	0.00	0.00	0.00	0.00	0.00	0.00	0.00	0.00	0.00	0.00	0.21	36.64	0.00	63.15
HD19994 3-4	0.00	0.00	0.00	0.00	0.00	0.00	0.00	0.00	0.00	0.00	0.00	0.21	36.59	0.00	63.20
HD19994 3-5	0.00	0.00	0.00	0.00	0.00	0.00	0.00	0.00	0.00	0.00	0.00	0.21	36.67	0.00	63.13
HD19994 4-3	0.00	0.00	0.00	0.00	0.00	0.00	0.00	0.00	0.00	0.00	0.00	0.21	36.52	0.00	63.27
HD19994 4-4	0.00	0.00	0.00	0.00	0.00	0.00	0.00	0.00	0.00	0.00	0.00	0.21	36.68	0.00	63.11
$t=5\times 10^5$ years															
HD19994 1-3	0.00	0.00	0.00	0.00	3.49	0.00	0.00	0.00	0.27	0.02	0.11	0.20	35.25	0.00	60.66

Table 1—Continued

System	H	Mg	O	S	Fe	Al	Ca	Na	Ni	Cr	P	Ti	Si	C	
HD19994 2-3	0.00	0.00	0.00	0.00	4.05	0.00	0.00	0.00	0.36	0.02	0.11	0.20	35.00	0.00	60.27
HD19994 3-3	0.00	0.00	0.00	0.00	0.00	0.00	0.00	0.00	0.00	0.00	0.00	0.21	36.68	0.00	63.11
HD19994 3-4	0.00	0.00	0.00	0.88	22.83	1.34	1.10	0.00	1.57	0.28	0.15	0.14	26.50	0.70	44.50
HD19994 3-5	0.00	10.85	20.26	1.81	20.82	1.21	0.99	0.00	1.41	0.28	0.14	0.05	11.02	0.00	31.16
HD19994 4-3	0.00	0.00	0.00	0.00	0.00	0.00	0.00	0.00	0.00	0.00	0.00	0.21	36.68	0.00	63.11
HD19994 4-4	0.00	0.00	0.00	0.41	15.58	0.55	0.51	0.00	1.08	0.18	0.13	0.17	29.93	0.29	51.17
$t=1\times 10^6$ years															
HD19994 1-3	0.00	4.06	7.42	1.11	29.28	1.48	1.17	0.01	2.07	0.35	0.21	0.09	18.10	0.36	34.29
HD19994 2-3	0.00	4.52	8.92	1.05	25.31	1.31	1.02	0.03	1.81	0.30	0.23	0.10	18.81	0.33	36.25
HD19994 3-3	0.00	4.78	7.26	1.47	29.66	1.65	1.33	0.00	2.08	0.37	0.23	0.09	18.57	0.43	32.08
HD19994 3-4	0.00	6.06	12.79	0.63	28.18	1.64	1.34	0.57	1.92	0.38	0.18	0.07	14.84	0.51	30.89
HD19994 3-5	0.00	10.72	22.87	0.14	20.53	1.19	0.97	1.02	1.39	0.28	0.13	0.05	12.12	0.00	28.59
HD19994 4-3	0.00	0.26	0.41	0.78	28.40	1.06	0.81	0.00	2.16	0.28	0.31	0.13	24.22	0.37	40.81
HD19994 4-4	0.00	9.05	16.44	1.04	24.60	1.51	1.17	0.33	1.67	0.33	0.16	0.06	14.02	0.23	29.39

Table 1—Continued

System	H	Mg	O	S	Fe	Al	Ca	Na	Ni	Cr	P	Ti	Si	C	
$t=1.5 \times 10^6$ years															
HD19994 1-3	0.00	9.89	20.15	0.79	21.49	1.30	0.93	0.40	1.46	0.29	0.14	0.05	12.02	0.01	31.09
HD19994 2-3	0.00	10.21	19.89	0.87	21.55	1.36	1.02	0.51	1.46	0.29	0.14	0.05	12.24	0.00	30.40
HD19994 3-3	0.00	10.53	20.77	0.79	20.53	1.51	0.83	0.56	1.39	0.28	0.13	0.05	11.56	0.01	31.05
HD19994 3-4	0.00	10.75	22.60	1.11	20.49	1.25	0.97	0.66	1.39	0.28	0.13	0.05	12.16	0.01	28.16
HD19994 3-5	0.00	10.42	22.21	2.81	19.89	1.16	0.94	0.99	1.35	0.27	0.13	0.05	11.76	0.00	28.03
HD19994 4-3	0.00	9.72	17.77	1.65	22.90	1.53	1.09	0.17	1.55	0.31	0.15	0.06	12.47	0.01	30.63
HD19994 4-4	0.00	10.34	21.79	0.81	20.04	1.30	0.85	0.82	1.36	0.27	0.13	0.05	11.62	0.00	30.62
$t=2 \times 10^6$ years															
HD19994 1-3	0.00	10.55	22.27	0.60	20.09	1.27	0.95	0.89	1.36	0.27	0.13	0.05	11.86	0.00	29.71
HD19994 2-3	0.00	10.67	22.49	0.92	20.37	1.25	0.97	0.82	1.38	0.27	0.13	0.05	12.02	0.00	28.65
HD19994 3-3	0.00	10.56	22.34	0.22	20.20	1.19	0.96	0.90	1.37	0.27	0.13	0.05	11.93	0.00	29.89
HD19994 3-4	0.00	10.40	22.10	1.60	19.89	1.16	0.94	0.99	1.35	0.27	0.13	0.04	11.75	0.00	29.39
HD19994 3-5	0.00	14.06	32.41	4.29	26.79	1.56	1.27	1.33	1.82	0.36	0.17	0.07	15.87	0.00	0.00

Table 1—Continued

System	H	Mg	O	S	Fe	Al	Ca	Na	Ni	Cr	P	Ti	Si	C	
HD19994 4-3	0.00	10.50	21.89	0.52	19.89	1.38	0.94	0.64	1.35	0.27	0.13	0.05	11.75	0.01	30.69
HD19994 4-4	0.00	10.61	22.63	1.31	20.35	1.18	0.96	1.01	1.38	0.27	0.13	0.05	11.97	0.00	28.13
$t=2.5\times 10^6$ years															
HD19994 1-3	0.00	10.80	23.00	1.16	20.70	1.20	0.98	1.03	1.40	0.28	0.13	0.05	12.19	0.00	27.06
HD19994 2-3	0.00	10.66	22.69	1.30	20.42	1.19	0.97	1.01	1.39	0.27	0.13	0.05	12.03	0.00	27.89
HD19994 3-3	0.00	11.07	23.59	1.13	21.18	1.23	1.00	1.05	1.44	0.29	0.14	0.05	12.51	0.00	25.34
HD19994 3-4	0.00	11.73	25.18	2.22	22.41	1.30	1.06	1.11	1.52	0.30	0.15	0.06	13.25	0.00	19.71
HD19994 3-5	0.00	14.05	32.40	4.32	26.78	1.56	1.27	1.33	1.82	0.36	0.17	0.07	15.86	0.00	0.00
HD19994 4-3	0.00	10.59	22.48	0.25	20.26	1.18	0.96	1.00	1.37	0.27	0.13	0.05	11.96	0.00	29.49
HD19994 4-4	0.00	11.86	25.96	2.58	22.67	1.32	1.08	1.12	1.54	0.31	0.15	0.06	13.39	0.00	17.99
$t=3\times 10^6$ years															
HD19994 1-3	0.00	11.33	24.41	2.14	21.74	1.26	1.03	1.08	1.48	0.29	0.14	0.05	12.75	0.00	22.29
HD19994 2-3	0.00	11.50	24.80	2.19	22.05	1.28	1.05	1.09	1.50	0.30	0.14	0.05	12.97	0.00	21.06

Table 1—Continued

System	H	Mg	O	S	Fe	Al	Ca	Na	Ni	Cr	P	Ti	Si	C	
HD19994 3-3	0.00	11.00	23.49	2.12	21.09	1.23	1.00	1.04	1.43	0.28	0.14	0.05	12.41	0.00	24.72
HD19994 3-4	0.00	12.91	28.96	3.36	24.69	1.43	1.17	1.22	1.67	0.33	0.16	0.06	14.59	0.00	9.44
HD19994 3-5	0.00	14.04	32.37	4.35	26.81	1.56	1.27	1.33	1.82	0.36	0.17	0.07	15.85	0.00	0.00
HD19994 4-3	0.00	11.13	23.78	0.98	21.31	1.24	1.01	1.06	1.45	0.29	0.14	0.05	12.58	0.00	25.00
HD19994 4-4	0.00	12.05	26.65	3.30	23.08	1.34	1.10	1.14	1.57	0.31	0.15	0.06	13.57	0.00	15.68
HD27442															
$t=2.5\times 10^5$ years															
HD27442 1-3	0.00	9.56	42.97	0.00	0.00	29.22	12.88	0.00	0.00	0.00	0.00	1.21	4.16	0.00	0.00
HD27442 1-4	0.00	9.02	43.25	0.00	0.00	29.02	12.66	0.00	0.00	0.00	0.00	1.23	4.82	0.00	0.00
HD27442 1-5	0.00	9.46	42.94	0.00	0.00	29.10	13.05	0.00	0.00	0.00	0.00	1.24	4.21	0.00	0.00
HD27442 2-3	0.00	13.86	43.62	0.00	0.00	23.36	10.33	0.00	0.00	0.00	0.00	0.97	7.85	0.00	0.00
HD27442 2-4	0.00	9.89	43.08	0.00	0.00	28.32	12.66	0.00	0.00	0.00	0.00	1.20	4.86	0.00	0.00
HD27442 3-3	0.00	7.64	43.34	0.00	0.00	30.69	12.90	0.00	0.00	0.00	0.00	1.29	4.14	0.00	0.00
HD27442 3-4	0.00	8.89	43.40	0.00	0.00	28.84	12.44	0.00	0.00	0.00	0.00	1.22	5.21	0.00	0.00
HD27442 3-5	0.00	28.40	45.18	0.00	0.00	6.02	2.70	0.00	0.00	0.00	0.00	0.26	17.45	0.00	0.00

Table 1—Continued

System	H	Mg	O	S	Fe	Al	Ca	Na	Ni	Cr	P	Ti	Si	C	
HD27442 4-3	0.00	9.54	42.96	0.00	0.00	29.19	12.92	0.00	0.00	0.00	0.00	1.22	4.17	0.00	0.00
HD27442 4-4	0.00	9.46	42.94	0.00	0.00	29.10	13.05	0.00	0.00	0.00	0.00	1.24	4.21	0.00	0.00
HD27442 4-5	0.00	9.61	42.78	0.00	2.66	25.78	10.68	0.00	0.16	0.03	0.02	1.10	7.19	0.00	0.00
$t=5\times 10^5$ years															
HD27442 1-3	0.00	12.21	43.57	0.00	0.00	24.67	11.06	0.00	0.00	0.00	0.00	1.05	7.44	0.00	0.00
HD27442 1-4	0.00	19.05	39.82	0.00	11.17	9.63	4.32	0.00	0.79	0.08	0.05	0.41	14.67	0.00	0.00
HD27442 1-5	0.00	18.78	34.93	0.00	23.78	1.76	0.79	0.00	1.49	0.17	0.12	0.08	18.10	0.00	0.00
HD27442 2-3	0.00	16.19	40.29	0.00	9.30	14.18	6.36	0.00	0.60	0.08	0.06	0.60	12.33	0.00	0.00
HD27442 2-4	0.00	17.39	40.30	0.00	9.62	12.48	5.60	0.00	0.66	0.07	0.04	0.53	13.30	0.00	0.00
HD27442 3-3	0.00	14.57	40.66	0.00	7.53	17.67	7.93	0.00	0.54	0.05	0.04	0.75	10.26	0.00	0.00
HD27442 3-4	0.00	19.05	39.48	0.00	12.60	8.06	3.61	0.00	0.82	0.10	0.07	0.34	15.89	0.00	0.00
HD27442 3-5	0.00	18.29	34.56	0.00	24.75	1.65	0.74	0.00	1.46	0.24	0.19	0.07	18.05	0.00	0.00
HD27442 4-3	0.00	13.27	43.43	0.00	0.63	23.00	10.31	0.00	0.07	0.00	0.00	0.98	8.31	0.00	0.00
HD27442 4-4	0.00	18.32	34.47	0.00	24.77	1.65	0.74	0.00	1.46	0.24	0.19	0.07	18.08	0.00	0.00
HD27442 4-5	0.00	19.15	37.54	0.00	17.22	5.38	2.41	0.08	1.08	0.14	0.10	0.23	16.65	0.00	0.00
$t=1\times 10^6$ years															

Table 1—Continued

System	H	Mg	O	S	Fe	Al	Ca	Na	Ni	Cr	P	Ti	Si	C	
HD27442 1-3	0.00	19.47	35.20	0.00	22.91	1.90	0.85	0.00	1.47	0.19	0.13	0.08	17.80	0.00	0.00
HD27442 1-4	0.00	18.16	34.40	0.26	24.56	1.64	0.74	0.39	1.45	0.24	0.18	0.07	17.91	0.00	0.00
HD27442 1-5	0.00	18.10	34.47	0.00	24.51	1.63	0.73	0.76	1.45	0.24	0.18	0.07	17.86	0.00	0.00
HD27442 2-3	0.00	18.34	34.39	1.24	23.65	1.71	0.77	0.25	1.46	0.20	0.14	0.07	17.78	0.00	0.00
HD27442 2-4	0.00	18.06	34.22	0.90	24.38	1.63	0.73	0.35	1.44	0.24	0.18	0.07	17.81	0.00	0.00
HD27442 3-3	0.00	18.55	34.76	0.00	24.05	1.73	0.77	0.22	1.47	0.21	0.15	0.07	18.02	0.00	0.00
HD27442 3-4	0.00	18.02	34.20	0.92	24.37	1.63	0.73	0.44	1.44	0.24	0.18	0.07	17.77	0.00	0.00
HD27442 3-5	0.00	16.90	32.40	6.47	22.84	1.52	0.68	0.71	1.35	0.22	0.17	0.06	16.67	0.00	0.00
HD27442 4-3	0.00	18.56	34.72	0.00	24.22	1.72	0.77	0.00	1.48	0.21	0.15	0.07	18.08	0.00	0.00
HD27442 4-4	0.00	17.23	33.04	4.60	23.30	1.56	0.70	0.73	1.38	0.23	0.17	0.07	17.00	0.00	0.00
HD27442 4-5	0.00	17.86	34.00	1.50	24.16	1.61	0.72	0.61	1.43	0.24	0.18	0.07	17.62	0.00	0.00
$t=1.5 \times 10^6$ years															
HD27442 1-3	0.00	18.24	34.51	0.00	24.67	1.65	0.74	0.25	1.46	0.24	0.18	0.07	17.99	0.00	0.00
HD27442 1-4	0.00	17.49	33.41	3.28	23.67	1.58	0.71	0.74	1.40	0.23	0.18	0.07	17.26	0.00	0.00
HD27442 1-5	0.00	17.01	32.63	5.77	23.03	1.54	0.69	0.72	1.36	0.23	0.17	0.07	16.79	0.00	0.00

Table 1—Continued

System	H	Mg	O	S	Fe	Al	Ca	Na	Ni	Cr	P	Ti	Si	C	
HD27442 2-3	0.00	17.74	33.71	2.45	23.99	1.60	0.72	0.40	1.42	0.23	0.18	0.07	17.50	0.00	0.00
HD27442 2-4	0.00	17.56	33.50	3.02	23.75	1.58	0.71	0.68	1.40	0.23	0.18	0.07	17.32	0.00	0.00
HD27442 3-3	0.00	17.85	33.93	1.74	24.14	1.61	0.72	0.49	1.43	0.24	0.18	0.07	17.61	0.00	0.00
HD27442 3-4	0.00	17.39	33.22	3.88	23.53	1.57	0.70	0.70	1.39	0.23	0.18	0.07	17.15	0.00	0.00
HD27442 3-5	0.00	16.65	31.95	7.82	22.51	1.50	0.67	0.70	1.33	0.22	0.17	0.06	16.42	0.00	0.00
HD27442 4-3	0.00	18.16	34.44	0.19	24.58	1.64	0.74	0.39	1.45	0.24	0.18	0.07	17.92	0.00	0.00
HD27442 4-4	0.00	16.71	32.05	7.46	22.62	1.51	0.68	0.71	1.34	0.22	0.17	0.06	16.48	0.00	0.00
HD27442 4-5	0.00	17.08	32.90	5.27	23.10	1.54	0.69	0.72	1.36	0.23	0.17	0.07	16.85	0.00	0.00
$t=2\times 10^6$ years															
HD27442 1-3	0.00	17.93	34.17	0.95	24.25	1.62	0.73	0.75	1.43	0.24	0.18	0.07	17.69	0.00	0.00
HD27442 1-4	0.00	16.94	32.47	6.21	22.92	1.53	0.69	0.72	1.35	0.22	0.17	0.07	16.71	0.00	0.00
HD27442 1-5	0.00	16.72	32.07	7.39	22.63	1.51	0.68	0.71	1.34	0.22	0.17	0.06	16.50	0.00	0.00
HD27442 2-3	0.00	17.47	33.73	3.06	23.62	1.58	0.71	0.73	1.40	0.23	0.18	0.07	17.23	0.00	0.00
HD27442 2-4	0.00	17.01	32.71	5.74	23.00	1.53	0.69	0.72	1.36	0.22	0.17	0.07	16.77	0.00	0.00
HD27442 3-3	0.00	17.42	33.29	3.68	23.56	1.57	0.70	0.73	1.39	0.23	0.18	0.07	17.18	0.00	0.00

Table 1—Continued

System	H	Mg	O	S	Fe	Al	Ca	Na	Ni	Cr	P	Ti	Si	C	
HD27442 3-4	0.00	16.95	32.57	6.08	22.93	1.53	0.69	0.72	1.35	0.22	0.17	0.07	16.72	0.00	0.00
HD27442 3-5	0.00	16.29	33.27	7.79	22.02	1.47	0.66	0.69	1.30	0.22	0.17	0.06	16.07	0.00	0.00
HD27442 4-3	0.00	17.74	33.85	1.94	23.99	1.60	0.72	0.75	1.42	0.23	0.18	0.07	17.50	0.00	0.00
HD27442 4-4	0.00	16.58	32.10	7.89	22.43	1.50	0.67	0.70	1.32	0.22	0.17	0.06	16.35	0.00	0.00
HD27442 4-5	0.00	16.68	32.40	7.23	22.56	1.51	0.67	0.71	1.33	0.22	0.17	0.06	16.45	0.00	0.00
$t=2.5\times 10^6$ years															
HD27442 1-3	0.00	17.35	33.17	4.02	23.48	1.57	0.70	0.73	1.39	0.23	0.18	0.07	17.12	0.00	0.00
HD27442 1-4	0.00	16.68	32.25	7.37	22.57	1.51	0.67	0.71	1.33	0.22	0.17	0.06	16.46	0.00	0.00
HD27442 1-5	0.00	16.63	31.95	7.85	22.50	1.50	0.67	0.70	1.33	0.22	0.17	0.06	16.40	0.00	0.00
HD27442 2-3	0.00	17.04	33.07	5.25	23.05	1.54	0.69	0.72	1.36	0.23	0.17	0.07	16.81	0.00	0.00
HD27442 2-4	0.00	16.71	32.42	7.11	22.60	1.51	0.68	0.71	1.34	0.22	0.17	0.06	16.48	0.00	0.00
HD27442 3-3	0.00	17.03	32.70	5.66	23.04	1.54	0.69	0.72	1.36	0.22	0.17	0.07	16.80	0.00	0.00
HD27442 3-4	0.00	16.65	32.43	7.31	22.52	1.50	0.67	0.70	1.33	0.22	0.17	0.06	16.42	0.00	0.00
HD27442 3-5	0.00	16.23	33.45	7.78	21.98	1.47	0.66	0.69	1.30	0.21	0.16	0.06	16.01	0.00	0.00
HD27442 4-3	0.00	17.17	32.84	5.02	23.22	1.55	0.69	0.73	1.37	0.23	0.17	0.07	16.94	0.00	0.00

Table 1—Continued

System	H	Mg	O	S	Fe	Al	Ca	Na	Ni	Cr	P	Ti	Si	C	
HD27442 4-4	0.00	16.28	33.36	7.79	21.96	1.47	0.66	0.69	1.30	0.22	0.16	0.06	16.05	0.00	0.00
HD27442 4-5	0.00	16.54	32.41	7.72	22.38	1.49	0.67	0.70	1.32	0.22	0.17	0.06	16.32	0.00	0.00
$t=3\times 10^6$ years															
HD27442 1-3	0.00	16.93	32.46	6.29	22.88	1.53	0.68	0.72	1.35	0.22	0.17	0.07	16.70	0.00	0.00
HD27442 1-4	0.00	16.55	32.42	7.70	22.38	1.49	0.67	0.70	1.32	0.22	0.17	0.06	16.32	0.00	0.00
HD27442 1-5	0.00	16.38	32.87	7.84	22.17	1.48	0.66	0.69	1.31	0.22	0.17	0.06	16.15	0.00	0.00
HD27442 2-3	0.00	16.70	32.77	6.78	22.59	1.51	0.68	0.71	1.34	0.22	0.17	0.06	16.48	0.00	0.00
HD27442 2-4	0.00	16.58	32.41	7.60	22.42	1.50	0.67	0.70	1.32	0.22	0.17	0.06	16.35	0.00	0.00
HD27442 3-3	0.00	16.72	32.52	6.98	22.60	1.51	0.68	0.71	1.34	0.22	0.17	0.06	16.49	0.00	0.00
HD27442 3-4	0.00	16.51	32.58	7.66	22.34	1.49	0.67	0.70	1.32	0.22	0.17	0.06	16.29	0.00	0.00
HD27442 3-5	0.00	16.24	33.48	7.78	21.94	1.47	0.66	0.69	1.30	0.21	0.16	0.06	16.01	0.00	0.00
HD27442 4-3	0.00	16.84	32.31	6.73	22.78	1.52	0.68	0.71	1.35	0.22	0.17	0.06	16.62	0.00	0.00
HD27442 4-4	0.00	16.24	33.46	7.78	21.95	1.46	0.66	0.69	1.30	0.21	0.16	0.06	16.02	0.00	0.00
HD27442 4-5	0.00	16.41	32.81	7.81	22.19	1.48	0.66	0.69	1.31	0.22	0.17	0.06	16.19	0.00	0.00
HD72659															
$t=2.5\times 10^5$ years															

Table 1—Continued

System	H	Mg	O	S	Fe	Al	Ca	Na	Ni	Cr	P	Ti	Si	C	
HD72659 1-3	0.00	5.36	41.06	0.00	4.61	20.79	16.65	0.07	0.30	0.06	0.02	1.28	9.81	0.00	0.00
HD72659 1-4	0.00	17.89	35.13	0.09	22.28	2.79	2.43	0.37	1.36	0.29	0.13	0.16	17.07	0.00	0.00
HD726592-3	0.00	1.76	42.51	0.00	0.00	26.96	20.40	0.00	0.00	0.00	0.00	1.73	6.64	0.00	0.00
HD726592-4	0.00	9.32	41.28	0.00	5.46	15.86	13.67	0.04	0.36	0.06	0.03	0.90	13.01	0.00	0.00
HD726592-5	0.00	16.68	33.80	0.73	24.46	2.79	2.44	0.55	1.48	0.33	0.15	0.14	16.46	0.00	0.00
HD72659 3-3	0.00	6.11	40.13	0.24	7.11	19.61	14.79	0.13	0.43	0.10	0.04	1.23	10.08	0.00	0.00
HD72659 3-4	0.00	12.68	39.74	0.00	10.00	11.45	9.97	0.00	0.65	0.11	0.05	0.64	14.70	0.00	0.00
HD72659 3-5	0.00	13.57	35.93	0.00	20.08	6.62	5.43	0.29	1.22	0.27	0.12	0.28	16.20	0.00	0.00
HD72659 4-3	0.00	7.09	41.67	0.00	3.73	18.49	15.98	0.00	0.23	0.05	0.02	1.07	11.67	0.00	0.00
HD72659 4-4	0.00	0.91	43.14	0.00	0.00	27.83	19.03	0.00	0.00	0.00	0.00	1.75	7.34	0.00	0.00
HD72659 4-5	0.00	18.10	33.51	0.00	26.03	1.43	1.31	0.44	1.61	0.33	0.15	0.10	16.99	0.00	0.00
$t=5\times 10^5$ years															
HD72659 1-3	0.00	11.47	38.56	0.35	11.80	11.96	10.39	0.16	0.74	0.15	0.07	0.69	13.66	0.00	0.00
HD72659 1-4	0.00	17.56	32.99	1.40	25.99	1.38	1.27	0.76	1.57	0.35	0.16	0.09	16.48	0.00	0.00
HD726592-3	0.00	5.46	42.61	0.00	0.00	21.14	19.43	0.00	0.00	0.00	0.00	1.31	10.05	0.00	0.00

Table 1—Continued

System	H	Mg	O	S	Fe	Al	Ca	Na	Ni	Cr	P	Ti	Si	C	
HD726592-4	0.00	15.82	35.73	0.04	20.59	5.34	4.02	0.25	1.29	0.26	0.12	0.26	16.28	0.00	0.00
HD726592-5	0.00	17.19	33.38	2.40	25.47	1.29	1.24	0.77	1.54	0.34	0.15	0.09	16.13	0.00	0.00
HD72659 3-3	0.00	9.63	39.34	0.54	9.73	14.04	12.14	0.23	0.59	0.13	0.06	0.81	12.76	0.00	0.00
HD72659 3-4	0.00	18.39	33.81	0.00	25.33	1.47	1.35	0.41	1.57	0.33	0.15	0.10	17.10	0.00	0.00
HD72659 3-5	0.00	17.80	33.12	0.50	26.34	1.40	1.28	0.65	1.60	0.36	0.16	0.09	16.71	0.00	0.00
HD72659 4-3	0.00	14.10	37.45	0.00	15.99	8.11	6.91	0.16	0.99	0.21	0.09	0.41	15.56	0.00	0.00
HD72659 4-4	0.00	7.63	39.39	0.00	7.58	17.73	15.94	0.00	0.46	0.10	0.04	1.19	9.94	0.00	0.00
HD72659 4-5	0.00	17.48	32.68	1.85	25.91	1.38	1.26	0.85	1.57	0.35	0.15	0.09	16.43	0.00	0.00
$t=1\times 10^6$ years															
HD72659 1-3	0.00	18.19	34.52	0.70	23.59	2.14	1.64	0.44	1.48	0.30	0.13	0.13	16.74	0.00	0.00
HD72659 1-4	0.00	16.87	33.37	3.48	25.03	1.29	1.22	0.82	1.51	0.34	0.15	0.09	15.84	0.00	0.00
HD726592-3	0.00	17.68	36.48	0.00	19.04	4.28	3.71	0.06	1.23	0.23	0.10	0.21	16.97	0.00	0.00
HD726592-4	0.00	17.69	33.16	0.89	26.10	1.39	1.28	0.71	1.58	0.35	0.15	0.09	16.60	0.00	0.00
HD726592-5	0.10	16.36	34.87	3.82	24.28	1.20	1.18	0.79	1.47	0.33	0.14	0.09	15.38	0.00	0.00
HD72659 3-3	0.00	17.29	34.76	1.13	23.08	2.81	2.10	0.35	1.45	0.29	0.13	0.15	16.49	0.00	0.00

Table 1—Continued

System	H	Mg	O	S	Fe	Al	Ca	Na	Ni	Cr	P	Ti	Si	C	
HD72659 3-4	0.00	17.57	32.85	1.40	26.01	1.38	1.27	0.85	1.58	0.35	0.16	0.09	16.51	0.00	0.00
HD72659 3-5	0.00	17.07	33.00	3.13	25.27	1.34	1.23	0.83	1.53	0.34	0.15	0.09	16.02	0.00	0.00
HD72659 4-3	0.00	17.80	33.10	0.68	26.24	1.40	1.28	0.58	1.59	0.35	0.16	0.09	16.72	0.00	0.00
HD72659 4-4	0.00	17.56	37.58	0.00	16.76	5.59	3.78	0.25	1.12	0.19	0.08	0.25	16.84	0.00	0.00
HD72659 4-5	0.00	16.70	33.73	3.77	24.80	1.25	1.20	0.81	1.50	0.33	0.15	0.09	15.67	0.00	0.00
$t=1.5 \times 10^6$ years															
HD72659 1-3	0.00	17.44	33.17	1.15	26.46	1.34	1.26	0.65	1.56	0.35	0.15	0.09	16.37	0.00	0.00
HD72659 1-4	0.00	16.51	34.22	4.06	24.49	1.18	1.19	0.80	1.48	0.33	0.15	0.09	15.50	0.00	0.00
HD726592-3	0.00	17.96	33.24	0.00	26.58	1.41	1.29	0.43	1.61	0.36	0.16	0.10	16.86	0.00	0.00
HD726592-4	0.00	17.26	33.14	2.28	25.57	1.36	1.24	0.80	1.55	0.35	0.15	0.09	16.20	0.00	0.00
HD726592-5	0.14	16.04	35.26	4.07	24.38	1.14	1.15	0.78	1.44	0.32	0.14	0.09	15.05	0.00	0.00
HD72659 3-3	0.07	17.30	34.00	1.43	25.61	1.36	1.25	0.60	1.55	0.35	0.15	0.09	16.24	0.00	0.00
HD72659 3-4	0.00	17.12	32.95	2.99	25.37	1.33	1.23	0.83	1.54	0.34	0.15	0.09	16.07	0.00	0.00
HD72659 3-5	0.00	16.66	34.13	3.66	24.67	1.17	1.20	0.81	1.49	0.33	0.15	0.09	15.64	0.00	0.00
HD72659 4-3	0.00	17.46	32.97	1.76	25.85	1.37	1.26	0.78	1.57	0.35	0.15	0.09	16.38	0.00	0.00

Table 1—Continued

System	H	Mg	O	S	Fe	Al	Ca	Na	Ni	Cr	P	Ti	Si	C	
HD72659 4-4	0.00	17.88	33.10	0.46	26.49	1.41	1.29	0.37	1.60	0.36	0.16	0.09	16.79	0.00	0.00
HD72659 4-5	0.00	16.18	34.08	4.14	25.39	1.07	1.17	0.78	1.45	0.32	0.14	0.09	15.18	0.00	0.00
$t=2\times 10^6$ years															
HD72659 1-3	0.05	17.22	33.62	1.91	25.53	1.33	1.24	0.79	1.55	0.34	0.15	0.09	16.18	0.00	0.00
HD72659 1-4	0.09	16.17	35.41	4.13	23.94	1.14	1.17	0.78	1.45	0.32	0.14	0.09	15.17	0.00	0.00
HD726592-3	0.00	16.97	33.26	3.27	25.14	1.30	1.22	0.82	1.52	0.34	0.15	0.09	15.92	0.00	0.00
HD726592-4	0.00	16.97	33.26	3.27	25.14	1.30	1.22	0.82	1.52	0.34	0.15	0.09	15.92	0.00	0.00
HD726592-5	1.26	14.29	41.61	3.68	21.20	1.02	1.03	0.69	1.28	0.29	0.13	0.08	13.43	0.00	0.00
HD72659 3-3	0.09	17.12	34.32	1.66	25.34	1.29	1.23	0.75	1.53	0.34	0.15	0.09	16.07	0.00	0.00
HD72659 3-4	0.00	16.75	33.36	3.93	24.84	1.32	1.21	0.81	1.50	0.33	0.15	0.09	15.71	0.00	0.00
HD72659 3-5	0.00	16.45	34.63	4.12	24.33	1.02	1.18	0.80	1.47	0.33	0.15	0.09	15.43	0.00	0.00
HD72659 4-3	0.00	17.12	33.41	2.60	25.34	1.30	1.23	0.83	1.53	0.34	0.15	0.09	16.06	0.00	0.00
HD72659 4-4	0.00	17.67	32.92	1.09	26.17	1.39	1.27	0.70	1.58	0.35	0.16	0.09	16.60	0.00	0.00
HD72659 4-5	0.10	16.08	35.49	4.14	23.96	1.16	1.16	0.78	1.45	0.32	0.14	0.09	15.12	0.00	0.00
$t=2.5\times 10^6$ years															
HD72659 1-3	0.07	16.99	33.78	2.49	25.26	1.31	1.22	0.82	1.52	0.34	0.15	0.09	15.95	0.00	0.00

Table 1—Continued

System	H	Mg	O	S	Fe	Al	Ca	Na	Ni	Cr	P	Ti	Si	C	
HD72659 1-4	0.19	15.91	36.33	4.08	23.58	1.08	1.15	0.77	1.43	0.32	0.14	0.08	14.93	0.00	0.00
HD726592-3	0.00	17.72	33.10	0.64	26.21	1.39	1.28	0.86	1.59	0.35	0.16	0.09	16.62	0.00	0.00
HD726592-4	0.00	16.73	33.58	3.82	24.82	1.26	1.21	0.81	1.50	0.33	0.15	0.09	15.71	0.00	0.00
HD726592-5	1.39	14.12	42.28	3.63	20.92	0.98	1.02	0.68	1.27	0.28	0.12	0.07	13.25	0.00	0.00
HD72659 3-3	0.72	16.09	37.20	1.95	23.80	1.21	1.16	0.78	1.44	0.32	0.14	0.09	15.11	0.00	0.00
HD72659 3-4	0.00	16.53	34.03	4.17	24.54	1.18	1.19	0.80	1.48	0.33	0.15	0.09	15.51	0.00	0.00
HD72659 3-5	0.00	16.32	35.07	4.18	24.14	1.02	1.17	0.79	1.46	0.33	0.14	0.09	15.31	0.00	0.00
HD72659 4-3	0.00	16.93	33.34	3.30	25.12	1.28	1.22	0.82	1.52	0.34	0.15	0.09	15.88	0.00	0.00
HD72659 4-4	0.00	17.43	33.29	1.18	26.11	1.37	1.25	0.84	1.56	0.35	0.15	0.09	16.38	0.00	0.00
HD72659 4-5	0.25	15.74	36.95	4.04	23.31	1.10	1.13	0.76	1.41	0.31	0.14	0.08	14.77	0.00	0.00
$t=3\times 10^6$ years															
HD72659 1-3	0.07	16.85	33.87	3.00	24.99	1.29	1.21	0.82	1.51	0.34	0.15	0.09	15.82	0.00	0.00
HD72659 1-4	0.91	14.85	39.97	3.81	21.99	0.99	1.03	0.72	1.33	0.30	0.13	0.08	13.91	0.00	0.00
HD726592-3	0.00	17.53	32.81	1.59	25.96	1.38	1.26	0.85	1.57	0.35	0.15	0.09	16.45	0.00	0.00
HD726592-4	0.00	16.72	34.20	4.04	24.06	1.22	1.20	0.81	1.50	0.33	0.15	0.09	15.69	0.00	0.00

Table 1—Continued

System	H	Mg	O	S	Fe	Al	Ca	Na	Ni	Cr	P	Ti	Si	C	
HD726592-5	2.21	12.91	46.29	3.31	19.10	0.92	0.93	0.62	1.16	0.26	0.11	0.07	12.11	0.00	0.00
HD72659 3-3	0.74	16.07	37.23	2.55	23.17	1.24	1.16	0.78	1.44	0.32	0.14	0.09	15.08	0.00	0.00
HD72659 3-4	0.00	16.37	34.76	4.19	24.23	1.09	1.18	0.79	1.47	0.33	0.14	0.09	15.36	0.00	0.00
HD72659 3-5	0.23	15.87	36.32	4.08	23.61	1.13	1.14	0.77	1.42	0.32	0.14	0.08	14.89	0.00	0.00
HD72659 4-3	0.00	16.74	33.69	3.75	24.81	1.23	1.21	0.81	1.50	0.33	0.15	0.09	15.71	0.00	0.00
HD72659 4-4	0.00	17.39	33.27	1.57	25.82	1.37	1.25	0.84	1.56	0.35	0.15	0.09	16.32	0.00	0.00
HD72659 4-5	0.38	15.55	37.64	3.99	23.00	1.05	1.12	0.75	1.39	0.31	0.14	0.08	14.59	0.00	0.00
HD108874															
$t=2.5 \times 10^5$ years															
HD108874 1-4	0.00	0.00	0.00	0.00	0.00	0.00	0.00	0.00	0.00	0.00	0.00	0.30	28.73	0.00	70.98
HD108874 2-4	0.00	0.00	0.00	0.00	0.00	0.00	0.00	0.00	0.00	0.00	0.00	0.30	28.77	0.00	70.93
HD108874 3-4	0.00	0.00	0.00	0.00	0.00	0.00	0.00	0.00	0.00	0.00	0.00	0.30	28.69	0.00	71.01
HD108874 4-4	0.00	0.00	0.00	0.00	0.00	0.00	0.00	0.00	0.00	0.00	0.00	0.30	28.74	0.00	70.96
HD108874 4-5	0.00	0.00	0.00	0.00	0.00	0.00	0.00	0.00	0.00	0.00	0.00	0.29	28.77	0.00	70.94

Table 1—Continued

System	H	Mg	O	S	Fe	Al	Ca	Na	Ni	Cr	P	Ti	Si	C	
$t=5\times 10^5$ years															
HD108874 1-4	0.00	0.00	0.00	0.00	0.65	0.00	0.00	0.00	0.00	0.00	0.12	0.29	28.62	0.00	70.32
HD108874 2-4	0.00	0.00	0.00	0.00	6.03	0.05	0.00	0.00	0.40	0.03	0.12	0.27	26.90	0.02	66.18
HD108874 3-4	0.00	0.00	0.00	0.00	0.46	0.00	0.00	0.00	0.00	0.00	0.09	0.29	28.66	0.00	70.50
HD108874 4-4	0.00	0.00	0.00	0.00	0.22	0.00	0.00	0.00	0.00	0.00	0.04	0.29	28.77	0.00	70.68
HD108874 4-5	0.00	0.01	0.00	1.19	45.78	2.61	1.47	0.00	2.62	0.52	0.30	0.12	13.48	1.36	30.54
$t=1\times 10^6$ years															
HD108874 1-4	0.00	4.65	5.98	1.74	38.67	2.20	1.29	0.00	2.19	0.46	0.25	0.10	11.90	0.74	29.82
HD108874 2-4	0.00	10.38	14.20	2.88	27.92	1.59	0.94	0.00	1.58	0.34	0.18	0.07	10.85	0.31	28.78
HD108874 3-4	0.00	3.26	3.20	2.28	40.73	2.29	1.18	0.00	2.34	0.46	0.27	0.11	13.15	0.97	29.76
HD108874 4-4	0.00	7.41	10.08	2.43	33.15	1.87	1.02	0.00	1.89	0.39	0.22	0.09	11.32	0.62	29.52
HD108874 4-5	0.00	13.03	21.80	0.33	21.20	1.20	0.71	0.44	1.20	0.26	0.14	0.03	10.42	0.01	29.24
$t=1.5\times 10^6$ years															

Table 1—Continued

System	H	Mg	O	S	Fe	Al	Ca	Na	Ni	Cr	P	Ti	Si	C	
HD108874 1-4	0.00	13.01	20.64	2.24	21.17	1.20	0.71	0.15	1.19	0.26	0.13	0.05	10.35	0.01	28.88
HD108874 2-4	0.00	13.06	21.50	1.26	21.26	1.21	0.71	0.38	1.20	0.26	0.14	0.04	10.44	0.01	28.53
HD108874 3-4	0.00	13.22	20.29	2.30	21.51	1.22	0.72	0.11	1.21	0.26	0.14	0.06	9.94	0.01	29.00
HD108874 4-4	0.00	13.14	20.97	1.54	21.38	1.21	0.72	0.27	1.21	0.26	0.14	0.03	10.21	0.01	28.92
HD108874 4-5	0.00	12.93	22.00	3.37	21.03	1.20	0.71	0.50	1.19	0.26	0.13	0.06	10.34	0.00	26.30
$t=2\times 10^6$ years															
HD108874 1-4	0.00	13.11	22.00	0.88	21.43	1.22	0.71	0.50	1.21	0.26	0.14	0.04	10.40	0.00	28.10
HD108874 2-4	0.00	13.61	23.01	2.56	22.22	1.26	0.75	0.52	1.25	0.27	0.14	0.05	10.81	0.00	23.52
HD108874 3-4	0.00	13.05	21.72	0.63	21.41	1.22	0.71	0.46	1.21	0.26	0.14	0.04	10.27	0.01	28.86
HD108874 4-4	0.00	13.23	22.26	1.70	21.61	1.23	0.72	0.49	1.22	0.27	0.14	0.04	10.50	0.00	26.58
HD108874 4-5	0.00	13.01	22.24	4.98	21.15	1.20	0.71	0.50	1.19	0.26	0.13	0.06	10.41	0.00	24.15
$t=2.5\times 10^6$ years															
HD108874 1-4	0.00	13.75	23.40	2.84	22.35	1.27	0.75	0.53	1.26	0.27	0.14	0.06	11.00	0.00	22.36

Table 1—Continued

System	H	Mg	O	S	Fe	Al	Ca	Na	Ni	Cr	P	Ti	Si	C	
HD108874 2-4	0.00	13.59	23.16	4.09	22.10	1.26	0.74	0.52	1.25	0.27	0.14	0.06	10.87	0.00	21.96
HD108874 3-4	0.00	13.43	22.81	2.11	21.85	1.24	0.73	0.52	1.23	0.27	0.14	0.06	10.74	0.00	24.88
HD108874 4-4	0.00	13.97	23.79	3.41	22.71	1.29	0.76	0.54	1.28	0.28	0.14	0.06	11.17	0.00	20.60
HD108874 4-5	0.00	16.43	28.23	6.77	24.64	1.52	0.89	0.63	1.51	0.33	0.17	0.07	13.14	0.00	5.68
$t=3\times 10^6$ years															
HD108874 1-4	0.00	13.87	23.69	4.51	22.55	1.28	0.75	0.53	1.27	0.28	0.14	0.06	11.09	0.00	19.97
HD108874 2-4	0.00	14.85	25.44	5.55	23.55	1.37	0.81	0.57	1.36	0.30	0.15	0.06	11.87	0.00	14.12
HD108874 3-4	0.00	14.81	25.28	4.51	24.08	1.37	0.81	0.57	1.36	0.30	0.15	0.06	11.85	0.00	14.85
HD108874 4-4	0.00	13.64	23.31	4.65	22.17	1.26	0.74	0.52	1.25	0.27	0.14	0.06	10.91	0.00	21.07
HD108874 4-5	0.00	17.36	30.33	7.15	25.97	1.59	0.94	0.66	1.58	0.34	0.18	0.07	13.84	0.00	0.00
HD177830															
$t=2.5\times 10^5$ years															
HD177830 1-3	0.00	10.03	44.23	0.00	0.00	34.53	7.69	0.00	0.00	0.00	0.00	1.19	2.35	0.00	0.00

Table 1—Continued

System	H	Mg	O	S	Fe	Al	Ca	Na	Ni	Cr	P	Ti	Si	C	
HD177830 1-4	0.00	6.45	45.25	0.00	0.00	38.68	6.44	0.00	0.00	0.00	0.00	1.31	1.87	0.00	0.00
HD177830 2-3	0.00	1.56	47.00	0.00	0.00	45.84	3.33	0.00	0.00	0.00	0.00	1.55	0.71	0.00	0.00
HD177830 2-4	0.00	9.38	44.20	0.00	0.00	34.39	8.29	0.00	0.00	0.00	0.00	1.18	2.56	0.00	0.00
HD177830 2-5	0.00	18.06	35.12	1.20	17.14	14.42	4.00	0.00	1.24	0.16	0.15	0.50	7.99	0.01	0.00
HD177830 3-3	0.00	11.90	43.55	0.00	0.00	31.78	8.88	0.00	0.00	0.00	0.00	1.10	2.79	0.00	0.00
HD177830 3-4	0.00	8.55	43.96	0.00	1.83	34.92	6.66	0.00	0.16	0.01	0.01	1.19	2.71	0.00	0.00
HD177830 4-3	0.00	2.23	46.60	0.00	0.00	44.18	4.38	0.00	0.00	0.00	0.00	1.50	1.10	0.00	0.00
HD177830 4-4	0.00	5.39	45.59	0.00	0.00	40.06	5.93	0.00	0.00	0.00	0.00	1.36	1.68	0.00	0.00
HD177830 4-5	0.00	10.43	43.94	0.00	0.00	33.33	8.51	0.00	0.00	0.00	0.00	1.15	2.65	0.00	0.00
$t=5\times 10^5$ years															
HD177830 1-3	0.00	15.70	37.27	0.23	13.62	18.03	5.94	0.00	1.05	0.10	0.12	0.81	7.12	0.01	0.00
HD177830 1-4	0.00	14.61	39.62	0.46	7.93	23.36	6.58	0.00	0.70	0.06	0.06	0.81	5.52	0.00	0.30
HD177830 2-3	0.00	11.59	43.46	0.00	0.00	31.39	9.41	0.00	0.00	0.00	0.00	1.21	2.94	0.00	0.00
HD177830 2-4	0.00	16.18	36.74	0.67	14.00	17.80	5.03	0.00	1.14	0.10	0.11	0.61	7.18	0.00	0.44
HD177830 2-5	0.00	21.96	30.76	0.62	25.79	2.02	0.57	0.16	1.88	0.24	0.23	0.07	12.73	0.01	2.96

Table 1—Continued

System	H	Mg	O	S	Fe	Al	Ca	Na	Ni	Cr	P	Ti	Si	C	
HD177830 3-3	0.00	22.33	29.23	2.03	29.10	2.28	0.65	0.00	2.11	0.27	0.26	0.08	11.64	0.02	0.00
HD177830 3-4	0.00	15.95	37.75	0.39	12.20	19.08	5.54	0.00	1.00	0.09	0.09	0.69	6.85	0.00	0.35
HD177830 4-3	0.00	11.86	43.55	0.00	0.00	31.74	8.94	0.00	0.00	0.00	0.00	1.10	2.81	0.00	0.00
HD177830 4-4	0.00	14.72	38.29	0.54	10.68	21.50	6.62	0.00	0.86	0.09	0.08	0.87	5.74	0.00	0.00
HD177830 4-5	0.00	14.57	40.46	0.00	7.15	23.83	6.73	0.00	0.70	0.04	0.04	0.82	5.65	0.00	0.00
$t=1\times 10^6$ years															
HD177830 1-3	0.00	22.02	30.02	1.96	24.55	1.99	0.58	0.13	1.82	0.21	0.21	0.07	12.68	0.00	3.75
HD177830 1-4	0.00	20.86	31.14	1.81	23.47	4.95	1.43	0.06	1.77	0.20	0.20	0.16	11.51	0.01	2.42
HD177830 2-3	0.00	20.46	32.53	0.74	23.63	6.70	1.98	0.00	2.05	0.16	0.17	0.22	11.02	0.00	0.33
HD177830 2-4	0.00	21.97	29.87	2.44	24.45	1.92	0.54	0.11	1.78	0.23	0.21	0.06	12.72	0.01	3.69
HD177830 2-5	0.00	21.16	30.56	3.85	22.22	1.74	0.49	0.26	1.62	0.21	0.20	0.06	12.83	0.00	4.80
HD177830 3-3	0.00	22.00	31.47	0.38	23.13	1.81	0.51	0.28	1.68	0.22	0.20	0.06	13.35	0.00	4.92
HD177830 3-4	0.00	21.30	31.06	1.89	23.25	3.98	1.13	0.10	1.75	0.20	0.20	0.13	12.01	0.01	3.00
HD177830 4-3	0.00	21.36	29.63	1.07	29.57	2.83	0.80	0.00	2.35	0.22	0.24	0.07	11.78	0.00	0.07

Table 1—Continued

System	H	Mg	O	S	Fe	Al	Ca	Na	Ni	Cr	P	Ti	Si	C	
HD177830 4-4	0.00	21.07	31.98	1.38	22.59	5.63	1.60	0.09	1.78	0.19	0.18	0.19	11.36	0.00	1.96
HD177830 4-5	0.00	22.12	29.67	2.71	24.00	1.88	0.53	0.04	1.75	0.22	0.21	0.07	12.78	0.01	4.00
$t=1.5\times 10^6$ years															
HD177830 1-3	0.00	21.78	30.60	2.84	22.89	1.79	0.51	0.20	1.67	0.21	0.20	0.06	12.86	0.00	4.39
HD177830 1-4	0.00	21.88	30.39	2.79	23.59	1.85	0.52	0.18	1.72	0.22	0.21	0.06	12.86	0.01	3.71
HD177830 2-3	0.00	22.68	29.02	3.57	24.82	1.78	0.55	0.04	1.81	0.23	0.22	0.06	12.34	0.00	2.89
HD177830 2-4	0.00	21.59	31.18	2.60	22.85	1.79	0.51	0.26	1.66	0.21	0.20	0.06	13.19	0.01	3.89
HD177830 2-5	0.00	21.22	30.77	6.16	22.31	1.75	0.49	0.21	1.62	0.21	0.20	0.06	12.87	0.00	2.13
HD177830 3-3	0.00	20.76	29.94	5.46	21.85	1.71	0.48	0.15	1.59	0.20	0.19	0.06	12.59	0.00	5.01
HD177830 3-4	0.00	21.81	30.56	3.11	23.36	1.81	0.52	0.19	1.70	0.22	0.21	0.06	12.89	0.00	3.56
HD177830 4-3	0.00	22.36	29.51	3.08	23.50	1.84	0.52	0.05	1.71	0.22	0.21	0.06	12.69	0.01	4.22
HD177830 4-4	0.00	21.90	30.12	3.11	24.02	1.80	0.53	0.20	1.75	0.22	0.21	0.06	12.69	0.00	3.38
HD177830 4-5	0.00	21.86	31.33	1.47	22.96	1.80	0.51	0.24	1.67	0.21	0.20	0.06	13.25	0.00	4.43
$t=2\times 10^6$ years															
HD177830 1-3	0.00	21.26	30.74	4.50	22.33	1.75	0.50	0.27	1.63	0.21	0.20	0.06	12.89	0.00	3.68
HD177830 1-4	0.00	21.67	31.09	3.30	22.76	1.78	0.50	0.23	1.66	0.21	0.20	0.06	13.12	0.00	3.41

Table 1—Continued

System	H	Mg	O	S	Fe	Al	Ca	Na	Ni	Cr	P	Ti	Si	C	
HD177830 2-3	0.00	21.87	31.10	0.96	22.97	1.80	0.51	0.19	1.67	0.21	0.20	0.05	13.24	0.01	5.22
HD177830 2-4	0.00	21.41	30.98	4.53	22.50	1.76	0.50	0.24	1.64	0.21	0.20	0.06	12.98	0.00	2.99
HD177830 2-5	0.00	20.69	32.33	6.44	21.72	1.70	0.48	0.25	1.58	0.20	0.19	0.06	12.55	0.00	1.81
HD177830 3-3	0.00	20.41	29.71	6.28	21.43	1.68	0.48	0.24	1.56	0.20	0.19	0.06	12.38	0.00	5.40
HD177830 3-4	0.00	21.36	30.79	3.93	22.44	1.76	0.50	0.22	1.63	0.21	0.20	0.06	12.95	0.00	3.95
HD177830 4-3	0.00	21.90	31.17	0.88	22.99	1.80	0.51	0.26	1.67	0.21	0.20	0.04	13.20	0.01	5.15
HD177830 4-4	0.00	21.35	30.65	2.97	22.42	1.76	0.50	0.21	1.63	0.21	0.20	0.06	12.95	0.01	5.09
HD177830 4-5	0.00	21.65	31.39	4.56	22.74	1.78	0.50	0.25	1.66	0.21	0.20	0.06	13.13	0.00	1.88
$t=2.5 \times 10^6$ years															
HD177830 1-3	0.00	21.46	31.11	5.42	22.54	1.77	0.50	0.24	1.64	0.21	0.20	0.06	13.02	0.00	1.84
HD177830 1-4	0.00	21.31	30.84	4.36	22.37	1.75	0.50	0.26	1.63	0.21	0.20	0.06	12.93	0.00	3.60
HD177830 2-3	0.00	21.84	31.39	1.94	22.93	1.80	0.51	0.27	1.67	0.21	0.20	0.06	13.25	0.00	3.92
HD177830 2-4	0.00	21.06	30.64	5.87	22.11	1.73	0.50	0.25	1.61	0.21	0.19	0.06	12.78	0.00	3.00
HD177830 2-5	0.00	21.03	32.92	6.65	22.10	1.73	0.49	0.26	1.61	0.21	0.19	0.06	12.75	0.00	0.00

Table 1—Continued

System	H	Mg	O	S	Fe	Al	Ca	Na	Ni	Cr	P	Ti	Si	C	
HD177830 3-3	0.00	21.54	31.35	6.79	22.62	1.77	0.50	0.26	1.65	0.21	0.20	0.06	13.06	0.00	0.00
HD177830 3-4	0.00	21.31	31.14	5.00	22.37	1.75	0.50	0.26	1.63	0.21	0.20	0.06	12.93	0.00	2.65
HD177830 4-3	0.00	21.80	31.42	2.65	22.88	1.79	0.52	0.28	1.67	0.21	0.20	0.06	13.23	0.00	3.28
HD177830 4-4	0.00	21.48	31.10	4.17	22.56	1.77	0.50	0.27	1.64	0.21	0.20	0.06	13.03	0.00	3.02
HD177830 4-5	0.00	21.00	30.52	5.81	22.05	1.73	0.49	0.24	1.61	0.20	0.19	0.06	12.74	0.00	3.36
$t=3\times 10^6$ years															
HD177830 1-3	0.00	21.20	30.86	6.18	22.27	1.74	0.49	0.26	1.62	0.21	0.20	0.06	12.86	0.00	2.05
HD177830 1-4	0.00	21.22	31.17	5.45	22.29	1.75	0.50	0.26	1.62	0.21	0.20	0.06	12.87	0.00	2.40
HD177830 2-3	0.00	21.59	31.29	4.26	22.69	1.78	0.51	0.27	1.65	0.21	0.20	0.06	13.10	0.00	2.39
HD177830 2-4	0.00	21.20	31.28	6.40	22.25	1.74	0.49	0.26	1.62	0.21	0.20	0.06	12.86	0.00	1.44
HD177830 2-5	0.00	21.03	32.92	6.66	22.10	1.73	0.49	0.26	1.61	0.21	0.19	0.06	12.75	0.00	0.00
HD177830 3-3	0.00	21.53	31.34	6.81	22.61	1.77	0.50	0.26	1.65	0.21	0.20	0.06	13.06	0.00	0.00
HD177830 3-4	0.00	21.26	31.15	5.85	22.33	1.75	0.50	0.26	1.63	0.21	0.20	0.06	12.90	0.00	1.91
HD177830 4-3	0.00	21.74	31.64	4.95	22.83	1.79	0.51	0.27	1.66	0.21	0.20	0.06	13.19	0.00	0.94
HD177830 4-4	0.00	21.52	31.24	5.40	22.60	1.77	0.50	0.26	1.65	0.21	0.20	0.06	13.05	0.00	1.54

Table 1—Continued

System	H	Mg	O	S	Fe	Al	Ca	Na	Ni	Cr	P	Ti	Si	C	
HD177830 4-5	0.00	20.66	30.07	6.25	21.68	1.70	0.48	0.25	1.58	0.20	0.19	0.06	12.53	0.00	4.37
HD177830															
$t=2.5 \times 10^5$ years															
HD213240 1-3	0.00	4.57	42.18	0.00	0.00	25.65	19.79	0.00	0.00	0.00	0.00	1.24	6.57	0.00	0.00
HD213240 2-3	0.00	4.11	42.25	0.00	0.00	25.94	19.85	0.00	0.00	0.00	0.00	1.26	6.59	0.00	0.00
HD213240 3-3	0.00	3.92	42.29	0.00	0.00	26.07	19.87	0.00	0.00	0.00	0.00	1.26	6.59	0.00	0.00
HD213240 4-3	0.00	3.64	42.33	0.00	0.00	26.26	19.89	0.00	0.00	0.00	0.00	1.27	6.60	0.00	0.00
HD213240 4-4	0.00	5.51	41.99	0.00	0.00	24.89	19.81	0.00	0.00	0.00	0.00	1.21	6.59	0.00	0.00
$t=5 \times 10^5$ years															
HD213240 1-3	0.00	13.00	43.08	0.00	0.00	19.89	13.62	0.00	0.00	0.00	0.00	0.97	9.44	0.00	0.00
HD213240 2-3	0.00	14.37	39.87	0.00	7.87	13.81	11.25	0.00	0.48	0.07	0.04	0.67	11.57	0.00	0.00
HD213240 3-3	0.00	13.68	42.59	0.00	1.43	18.03	12.89	0.00	0.12	0.01	0.00	0.88	10.37	0.00	0.00
HD213240 4-3	0.00	13.04	42.42	0.00	1.68	18.70	13.16	0.00	0.14	0.01	0.00	0.91	9.95	0.00	0.00

Table 1—Continued

System	H	Mg	O	S	Fe	Al	Ca	Na	Ni	Cr	P	Ti	Si	C	
HD213240 4-4	0.00	19.02	31.55	0.00	29.53	1.53	1.22	0.00	1.71	0.33	0.17	0.07	14.86	0.00	0.00
$t=1\times 10^6$ years															
HD213240 1-3	0.00	19.89	32.68	0.00	27.02	1.67	1.33	0.09	1.56	0.30	0.16	0.08	15.22	0.00	0.00
HD213240 2-3	0.00	19.47	32.25	0.00	27.89	1.58	1.26	0.30	1.67	0.29	0.14	0.08	15.07	0.00	0.00
HD213240 3-3	0.00	19.43	32.18	0.00	28.05	1.58	1.26	0.18	1.68	0.29	0.15	0.08	15.12	0.00	0.00
HD213240 4-3	0.00	19.56	32.26	0.00	27.88	1.59	1.26	0.15	1.67	0.28	0.14	0.08	15.13	0.00	0.00
HD213240 4-4	0.00	18.77	31.65	0.00	29.10	1.51	1.20	0.85	1.68	0.33	0.17	0.07	14.67	0.00	0.00
$t=1.5\times 10^6$ years															
HD213240 1-3	0.00	18.80	31.61	0.00	29.19	1.51	1.21	0.74	1.69	0.33	0.17	0.07	14.69	0.00	0.00
HD213240 2-3	0.00	18.78	31.53	0.29	29.14	1.51	1.20	0.63	1.68	0.33	0.17	0.07	14.67	0.00	0.00
HD213240 3-3	0.00	18.83	31.61	0.00	29.23	1.51	1.21	0.63	1.69	0.33	0.17	0.07	14.72	0.00	0.00
HD213240 4-3	0.00	18.85	31.60	0.00	29.26	1.51	1.21	0.59	1.69	0.33	0.17	0.07	14.73	0.00	0.00
HD213240 4-4	0.00	18.04	30.43	3.86	27.98	1.45	1.16	0.82	1.62	0.31	0.16	0.07	14.10	0.00	0.00

Table 1—Continued

System	H	Mg	O	S	Fe	Al	Ca	Na	Ni	Cr	P	Ti	Si	C	
$t=2\times 10^6$ years															
HD213240 1-3	0.00	18.69	31.50	0.41	29.00	1.50	1.20	0.84	1.67	0.32	0.17	0.07	14.61	0.00	0.00
HD213240 2-3	0.00	18.52	31.23	1.33	28.73	1.49	1.19	0.84	1.66	0.32	0.17	0.07	14.47	0.00	0.00
HD213240 3-3	0.00	18.62	31.40	0.79	28.88	1.50	1.19	0.84	1.67	0.32	0.17	0.07	14.55	0.00	0.00
HD213240 4-3	0.00	18.65	31.46	0.60	28.93	1.50	1.20	0.84	1.67	0.32	0.17	0.07	14.58	0.00	0.00
HD213240 4-4	0.00	17.87	30.16	4.63	27.75	1.44	1.15	0.88	1.60	0.31	0.16	0.07	13.97	0.00	0.00
$t=2.5\times 10^6$ years															
HD213240 1-3	0.00	18.42	31.07	1.82	28.59	1.48	1.18	0.83	1.65	0.32	0.17	0.07	14.40	0.00	0.00
HD213240 2-3	0.00	18.31	30.89	2.37	28.42	1.47	1.17	0.85	1.64	0.32	0.17	0.07	14.31	0.00	0.00
HD213240 3-3	0.00	18.40	31.03	1.95	28.55	1.48	1.18	0.83	1.65	0.32	0.17	0.07	14.38	0.00	0.00
HD213240 4-3	0.00	18.45	31.12	1.66	28.63	1.48	1.18	0.83	1.65	0.32	0.17	0.07	14.42	0.00	0.00
HD213240 4-4	0.00	17.85	30.12	4.70	27.78	1.43	1.14	0.88	1.60	0.31	0.16	0.07	13.95	0.00	0.00
$t=3\times 10^6$ years															

Table 1—Continued

System	H	Mg	O	S	Fe	Al	Ca	Na	Ni	Cr	P	Ti	Si	C	
HD213240 1-3	0.00	18.15	30.61	3.25	28.18	1.46	1.16	0.83	1.63	0.31	0.16	0.07	14.19	0.00	0.00
HD213240 2-3	0.00	18.15	30.62	3.22	28.18	1.46	1.16	0.85	1.63	0.31	0.16	0.07	14.19	0.00	0.00
HD213240 3-3	0.00	18.19	30.69	3.01	28.24	1.46	1.17	0.84	1.63	0.32	0.16	0.07	14.22	0.00	0.00
HD213240 4-3	0.00	18.23	30.75	2.83	28.29	1.47	1.17	0.84	1.63	0.32	0.16	0.07	14.25	0.00	0.00
HD213240 4-4	0.00	16.72	34.55	4.41	26.00	1.34	1.07	0.83	1.50	0.29	0.15	0.07	13.07	0.00	0.00

B. Online Material: Chemical Condensation Sequence Plots

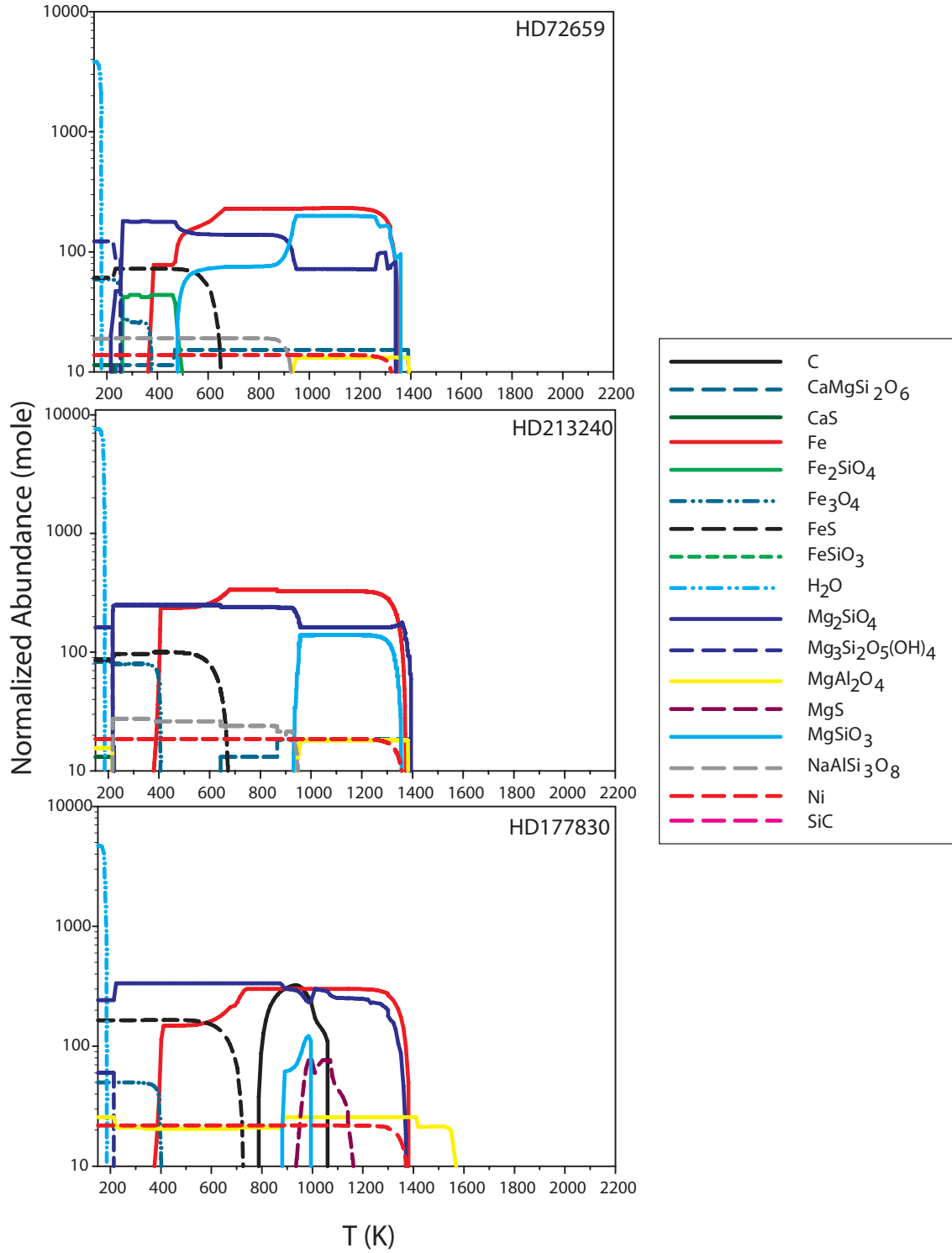


Fig. 1.— Schematic of the output obtained from HSC Chemistry for HD72659 (top), HD213240 (middle) and HD177830 (bottom) at a pressure of 10^{-4} bar. Only solid species present within the system are shown. All abundances are normalized to the least abundant species present. Input elemental abundances are shown in Table 7.

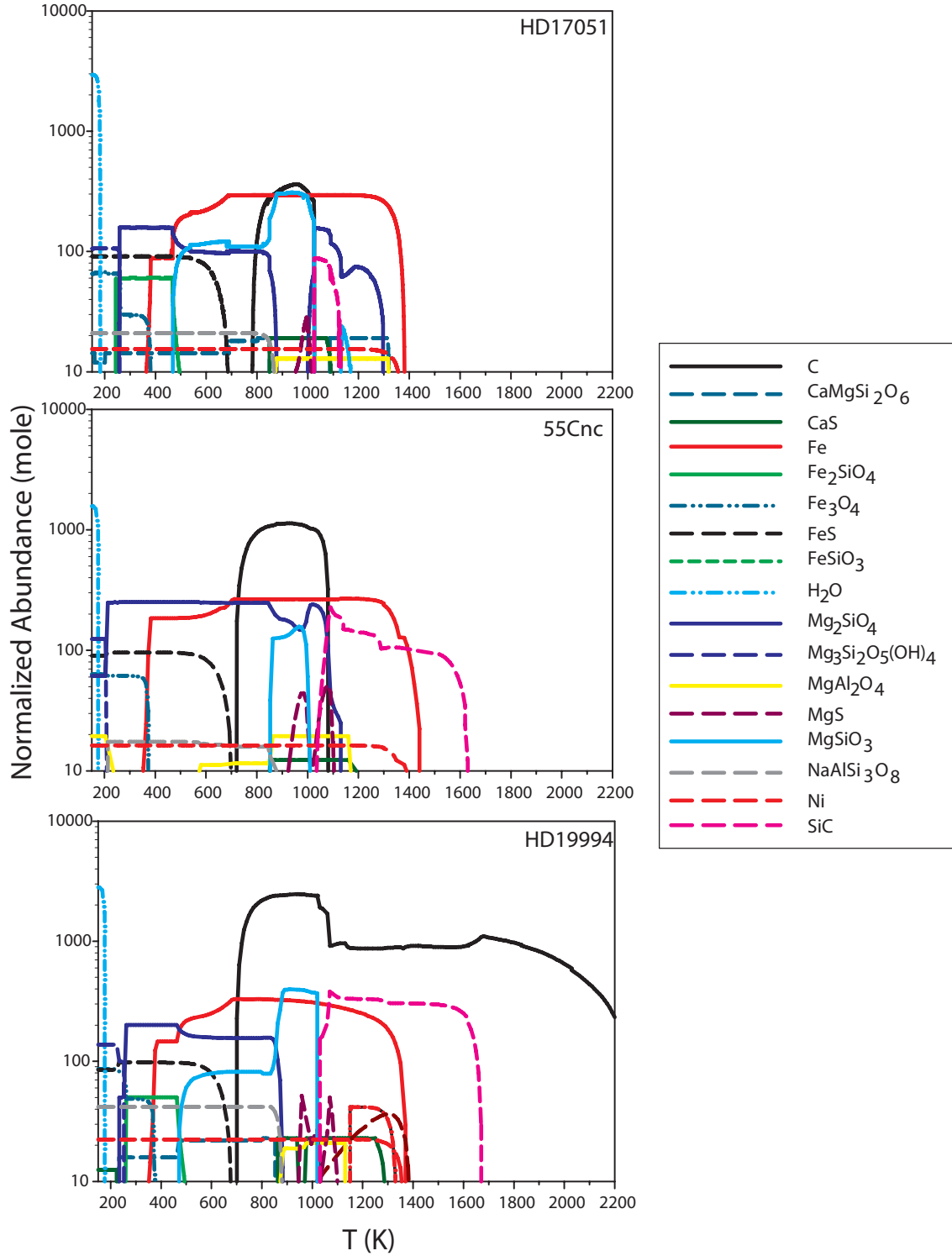


Fig. 2.— Schematic of the output obtained from HSC Chemistry for HD17051 (top), HD55Cnc (middle) and HD19994 (bottom) at a pressure of 10^{-4} bar. Only solid species present within the system are shown. All abundances are normalized to the least abundant species present. Input elemental abundances are shown in Table 7.

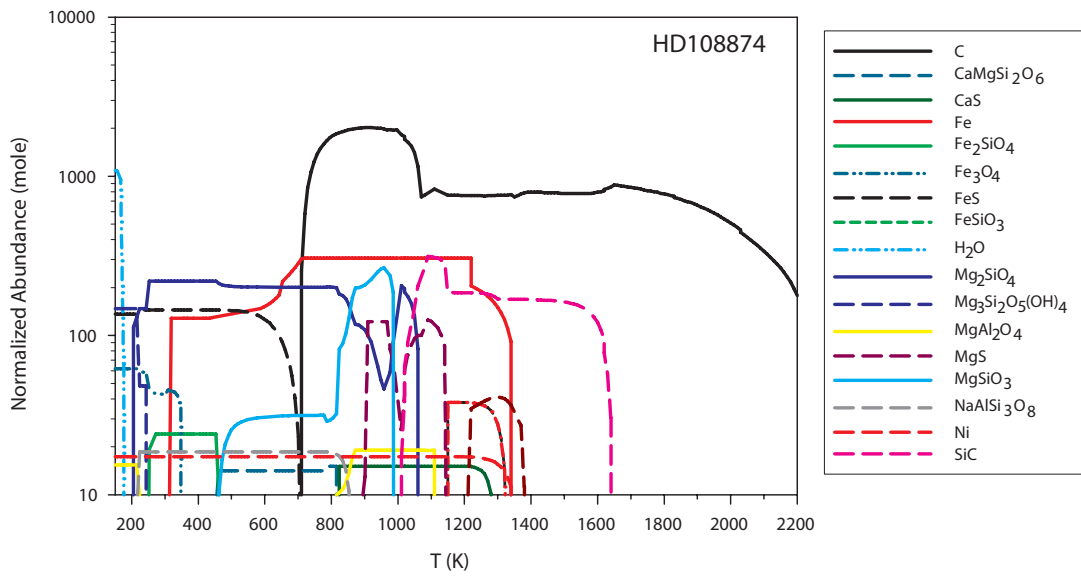


Fig. 3.— Schematic of the output obtained from HSC Chemistry for HD108874 at a pressure of 10^{-4} bar. Only solid species present within the system are shown. All abundances are normalized to the least abundant species present. Input elemental abundances are shown in Table 7.

REFERENCES

- Acke, B., & van den Ancker, M. E. 2006, *Astronomy & Astrophysics*, 457, 171
- Armitage, P. J. 2003, *Astrophysical Journal Letters*, 582, L47
- Asghari, N., et al. 2004, *Astronomy & Astrophysics*, 426, 353
- Asplund, M., Grevesse, N., & Sauval, A. J. 2005, in *Astronomical Society of the Pacific Conference Series*, Vol. 336, *Cosmic Abundances as Records of Stellar Evolution and Nucleosynthesis*, ed. T. G. Barnes, III & F. N. Bash, 25–38
- Ayres, T. R., Plymate, C., & Keller, C. U. 2006, *Astrophysical Journal Supplemental Series*, 165, 618
- Barnes, R., & Raymond, S. N. 2004, *Astrophysical Journal*, 617, 569
- Beirão, P., Santos, N. C., Israelian, G., & Mayor, M. 2005, *Astronomy & Astrophysics*, 438, 251
- Bodaghee, A., Santos, N. C., Israelian, G., & Mayor, M. 2003, *Astronomy & Astrophysics*, 404, 715
- Bond, J. C., Lauretta, D. S., & O'Brien, D. P. 2009, *Icarus*
- Bond, J. C., Tinney, C. G., Butler, R. P., Jones, H. R. A., Marcy, G. W., Penny, A. J., & Carter, B. D. 2006, *Monthly Notices of the Royal Astronomical Society*, 370, 163
- Bond, J. C., et al. 2008, *Astrophysical Journal*, 682, 1234
- Burrows, A., Hubeny, I., Budaj, J., & Hubbard, W. B. 2007, *Astrophysical Journal*, 661, 502

- Butler, R. P., Vogt, S. S., Marcy, G. W., Fischer, D. A., Henry, G. W., & Apps, K. 2000, *Astrophysical Journal*, 545, 504
- Butler, R. P., et al. 2006, *Astrophysical Journal*, 646, 505
- Davis, A. M. 2006, in *Meteorites and the Early Solar System II*, ed. D. S. Lauretta & H. Y. McSween Jr. (Tucson, AZ USA: University of Arizona Press), 295–307
- Drake, M. J. 2000, *Geochimica et Cosmochimica Acta*, 64, 2363
- . 2005, *Meteoritics and Planetary Science*, 40, 519
- Duncan, M. J., Levison, H. F., & Lee, M. H. 1998, *Astronomical Journal*, 116, 2067
- Ebel, D. S. 2006, in *Meteorites and the Early Solar System II*, ed. D. S. Lauretta & H. Y. McSween Jr. (Tucson, AZ USA: University of Arizona Press), 253–277
- Ecuvillon, A., Israelian, G., Santos, N. C., Mayor, M., Villar, V., & Bihain, G. 2004a, *Astronomy & Astrophysics*, 426, 619
- . 2004b, *Astronomy & Astrophysics*, 426, 619
- Ecuvillon, A., Israelian, G., Santos, N. C., Shchukina, N. G., Mayor, M., & Rebolo, R. 2006, *Astronomy & Astrophysics*, 445, 633
- Fischer, D. A., & Valenti, J. 2005, *Astrophysical Journal*, 622, 1102
- Gaidos, E., & Selsis, F. 2007, in *Protostars and Planets V*, ed. B. Reipurth, D. Jewitt, & K. Keil (Tucson, AZ USA: University of Arizona Press), 929–944
- Gilli, G., Israelian, G., Ecuvillon, A., Santos, N. C., & Mayor, M. 2006, *Astronomy & Astrophysics*, 449, 723
- Gonzalez, G. 1997, *Monthly Notices of the Royal Astronomical Society*, 285, 403

- . 1998, *Astronomy & Astrophysics*, 334, 221
- Gonzalez, G., & Laws, C. 2000, *Astrophysical Journal*, 119, 390
- Gonzalez, G., Laws, C., Tyagi, S., & Reddy, B. E. 2001, *Astronomical Journal*, 121, 432
- Gonzalez, G., & Vanture, A. D. 1998, *Astronomy & Astrophysics*, 339, L29
- Gonzalez, G., Wallerstein, G., & Saar, S. H. 1999, *Astrophysical Journal*, 511, L111
- Gradie, J., & Tedesco, E. 1982, *Science*, 216, 1405
- Guillot, T., Santos, N. C., Pont, F., Iro, N., Melo, C., & Ribas, I. 2006, *Astronomy & Astrophysics*, 453, L21
- Gustafsson, B., Karlsson, T., Olsson, E., Edvardsson, B., & Ryde, N. 1999, *A&A*, 342, 426
- Hersant, F., Gautier, D., & Huré, J.-M. 2001, *Astrophysical Journal*, 554, 391
- Israelian, G., Shchukina, N., Rebolo, R., Basri, G., González Hernández, J. I., & Kajino, T. 2004, *Astronomy & Astrophysics*, 419, 1095
- Kargel, J. S., & Lewis, J. S. 1993, *Icarus*, 105, 1
- Kokubo, E., & Ida, S. 2000, *Icarus*, 143, 15
- Kuchner, M. J., & Seager, S. 2005, *ArXiv Astrophysics e-prints*
- Laughlin, G. 2000, *Astrophysical Journal*, 545, 1064
- Lodders, K., & Fegley, B. 1997, *Icarus*, 126, 373
- Mandell, A. M., Raymond, S. N., & Sigurdsson, S. 2007, *Astrophysical Journal*, 660, 823

- Marcy, G., Butler, P. R., Fischer, D. A., & Vogt, S. S. 2000, in *Astronomical Society of the Pacific Conference Series*, Vol. 213, *Bioastronomy* 99, ed. G. Lemarchand & K. Meech, 85–94
- McDonough, W. F., & Sun, S. 1995, *Chemical Geology*, 120, 223
- Morgan, J. W., & Anders, E. 1980, *Proceedings of the National Academy of Science*, 77, 6973
- Mousis, O., & Alibert, Y. 2006, *A&A*, 448, 771
- Murray, N., Chaboyer, B., Arras, P., Hansen, B., & Noyes, R. W. 2001, *Astrophysical Journal*, 555, 801
- O’Brien, D. P., Morbidelli, A., & Levison, H. F. 2006, *Icarus*, 184, 39
- O’Neill, C., Jellinek, A. M., & Lenardic, A. 2007, *Earth and Planetary Science Letters*, 261, 20
- Pinsonneault, M. H., DePoy, D. L., & Coffee, M. 2001, *Astrophysical Journal Letters*, 556, L59
- Raymond, S. N., & Barnes, R. 2005, *Astrophysical Journal*, 619, 549
- Raymond, S. N., Barnes, R., & Kaib, N. A. 2006a, *Astrophysical Journal*, 644, 1223
- Raymond, S. N., Mandell, A. M., & Sigurdsson, S. 2006b, *Science*, 313, 1413
- Raymond, S. N., Quinn, T., & Lunine, J. I. 2005, *Icarus*, 177, 256
- Reid, I. N. 2002, *Publications of the Astronomical Society of the Pacific*, 114, 306
- Santos, N. C., Israelian, G., & Mayor, M. 2000, *Astronomy & Astrophysics*, 363, 228
- . 2001, *Astronomy & Astrophysics*, 373, 1019

- . 2004, *Astronomy & Astrophysics*, 415, 1153
- Santos, N. C., Israelian, G., Mayor, M., Bento, J. P., Almeida, P. C., Sousa, S. G., & Ecuivillon, A. 2005, *Astronomy & Astrophysics*, 437, 1127
- Santos, N. C., Israelian, G., Mayor, M., Rebolo, R., & Udry, S. 2003a, *Astronomy & Astrophysics*, 398, 363
- . 2003b, *Astronomy & Astrophysics*, 398, 363
- Semenov, D., Chakraborty, S., & Thiemens, M. 2010, in *Protoplanetary Dust*, ed. D. Apai & D. S. Lauretta (New York, NY USA: Cambridge; New York: Cambridge University Press, c2010), 97–127
- Smith, V. V., Cunha, K., & Lazzaro, D. 2001, *Astronomical Journal*, 121, 3207
- Socas-Navarro, H., & Norton, A. A. 2007, *Astrophysical Journal Letters*, 660, L153
- Sotin, C., Grasset, O., & Mocquet, A. 2007, *Icarus*, 191, 337
- Valencia, D., O’Connell, R. J., & Sasselov, D. D. 2007, *Astrophysical Journal Letters*, 670, L45

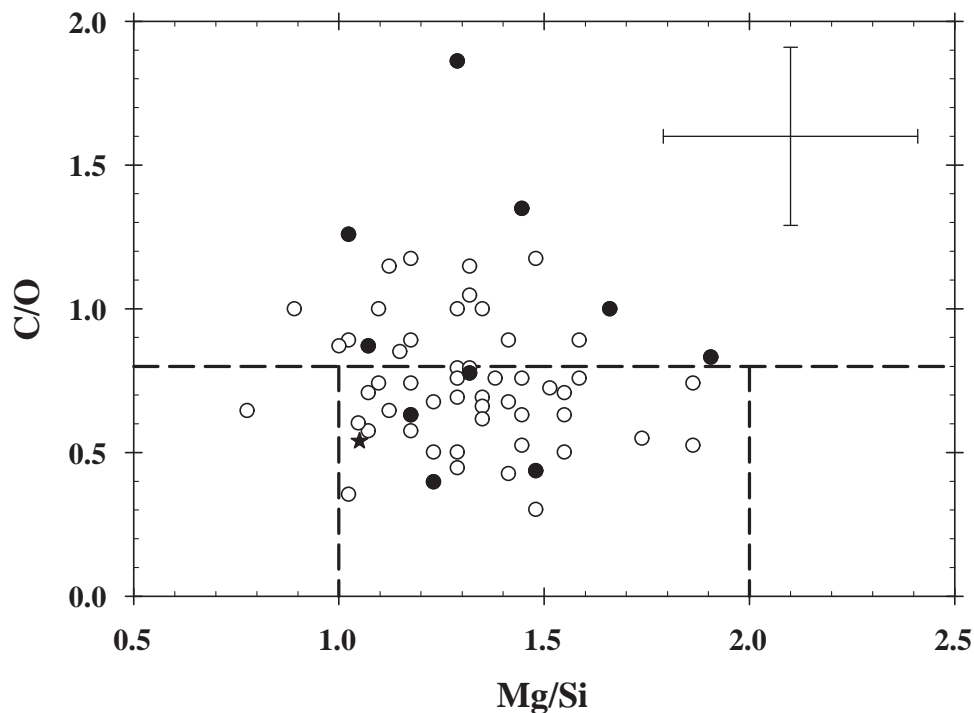


Fig. 4.— Mg/Si vs. C/O for known planetary host stars with reliable stellar abundances. Filled circles represent those systems selected for this study. Stellar photospheric values were taken from Gilli et al. (2006) (Si, Mg), Beirão et al. (2005) (Mg), Ecuivillon et al. (2004a) (C) and Ecuivillon et al. (2006) (O). Solar values are shown by the black star and were taken from Asplund et al. (2005). The dashed line indicates a C/O value of 0.8 and marks the transitions between a silicate-dominated composition and a carbide-dominated composition at 10^{-4} bar. Average $2\text{-}\sigma$ error bars shown in upper right. All ratios are elemental number ratios, *not* solar normalized logarithmic values.

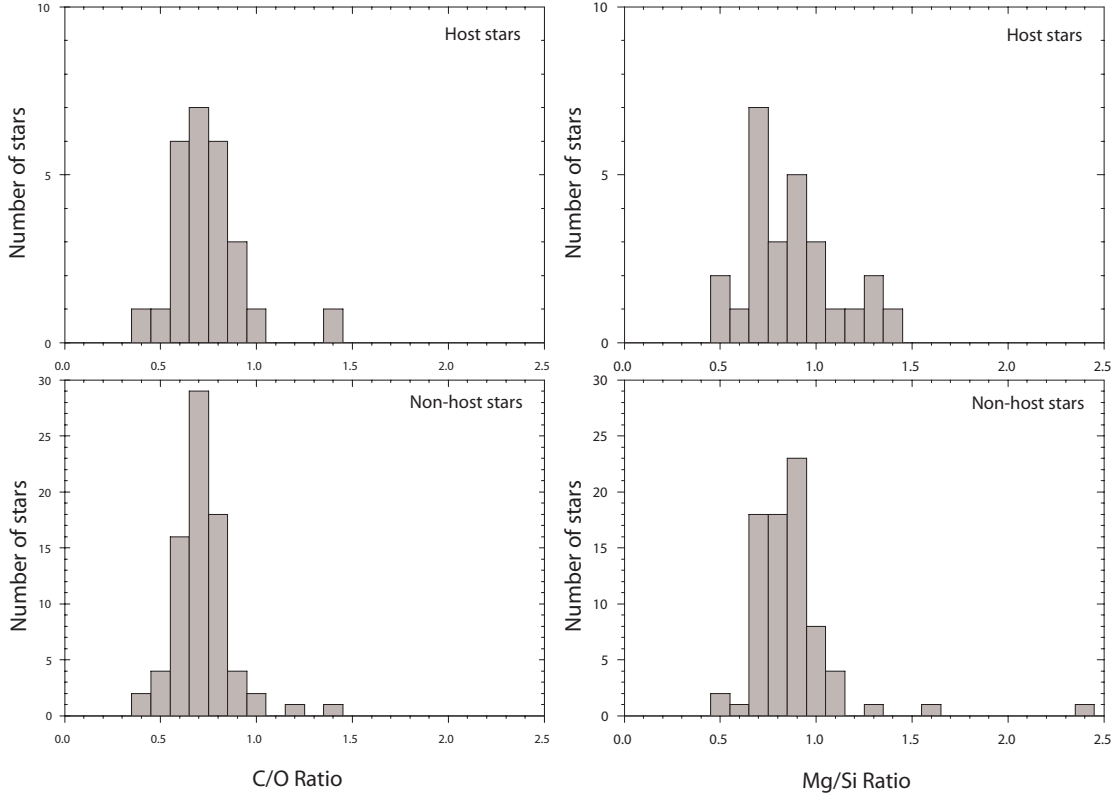


Fig. 5.— C/O and Mg/Si distributions for host and non-host stars based on the abundances determined in Bond et al. (2008). *Left:* C/O distributions for host (top) and non-host (bottom) stars. *Right:* Mg/Si distributions for host (top) and non-host (bottom) stars. All ratios are elemental number ratios, *not* solar normalized logarithmic values. Note that these values are for a different dataset to that shown in Figure 4 and utilized in this work.

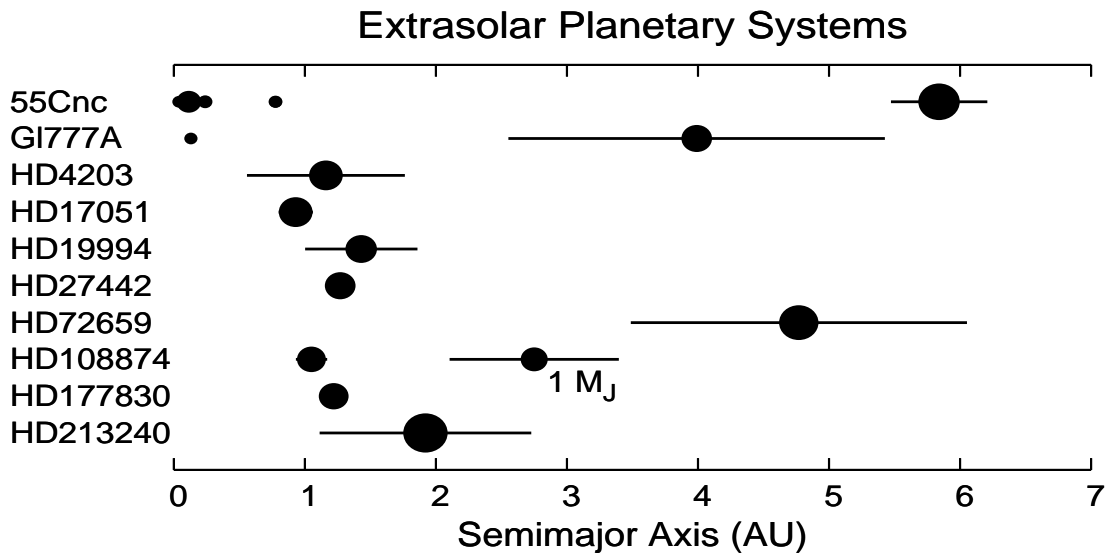


Fig. 6.— Location of known giant planets in the systems selected for study. The horizontal lines indicate the variation from periastron and apastron. The size of the circles scales with the planetary $M \sin i$ value. All planets are assumed to have zero inclination. All values taken from the Butler et al. (2006) catalog.

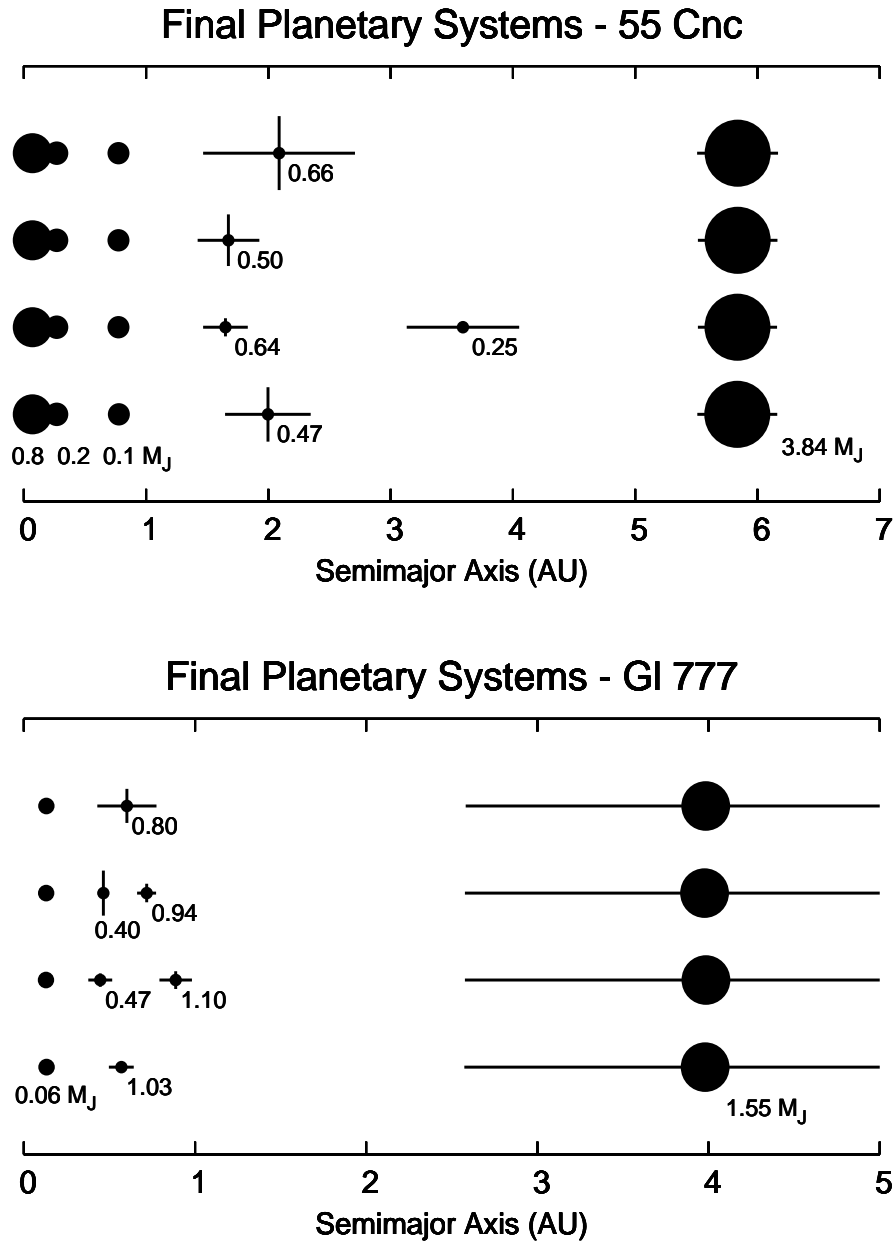


Fig. 7.— Schematic of the results of the dynamical simulations for 55Canceri (top panel) and Gl777 (bottom panel). Known giant planets are also shown with their masses in Jupiter masses (M_J). The horizontal lines indicate the range in distance from apastron to periastron. The vertical lines indicate variation in height above the midplane due to orbital inclination. Numerical values represent the mass of the planet in Earth masses.

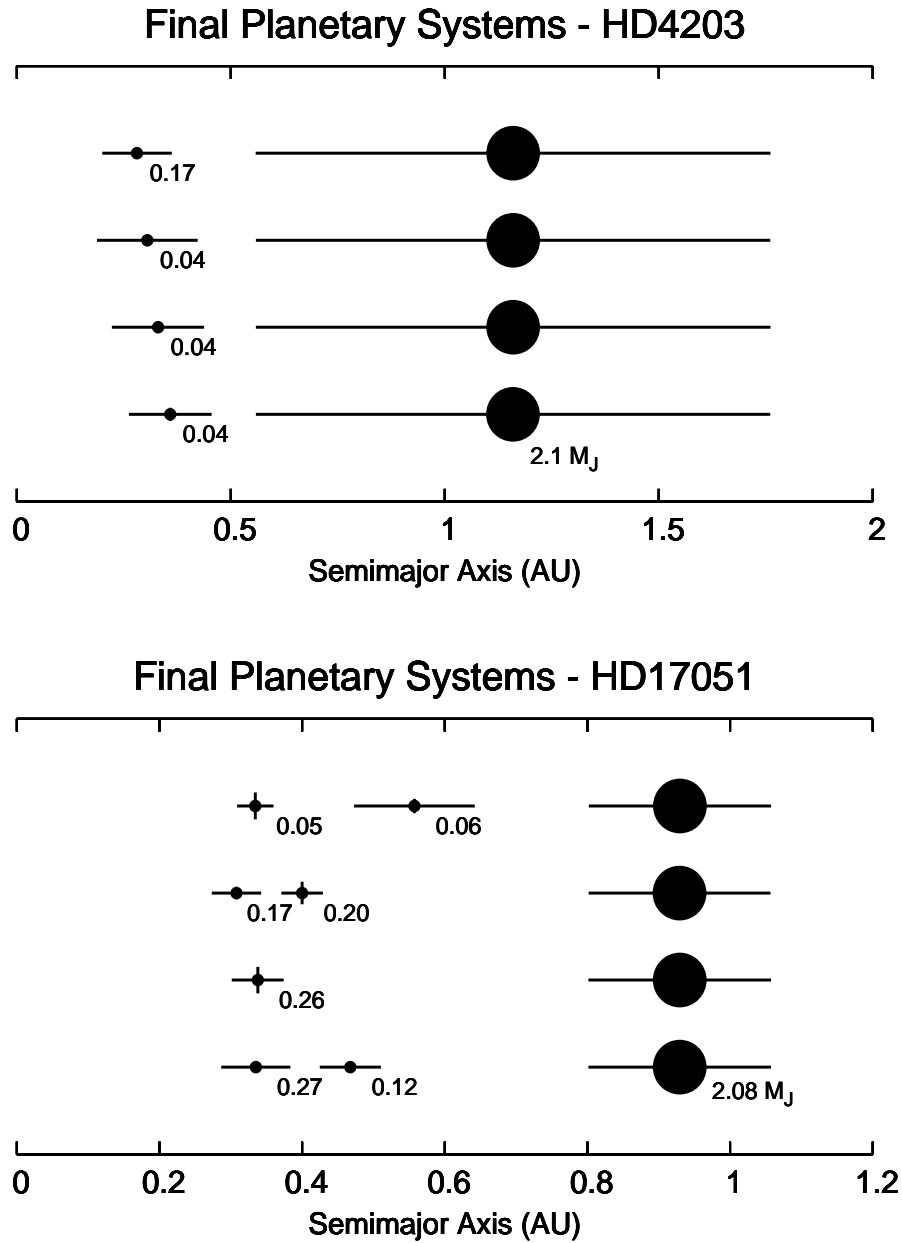


Fig. 8.— Schematic of the results of the dynamical simulations for HD4203 (top panel) and HD17051 (bottom panel). Known giant planets are also shown with their masses in Jupiter masses (M_J). The horizontal lines indicate the range in distance from apastron to periastron. The vertical lines indicate variation in height above the midplane due to orbital inclination. Numerical values represent the mass of the planet in Earth masses.

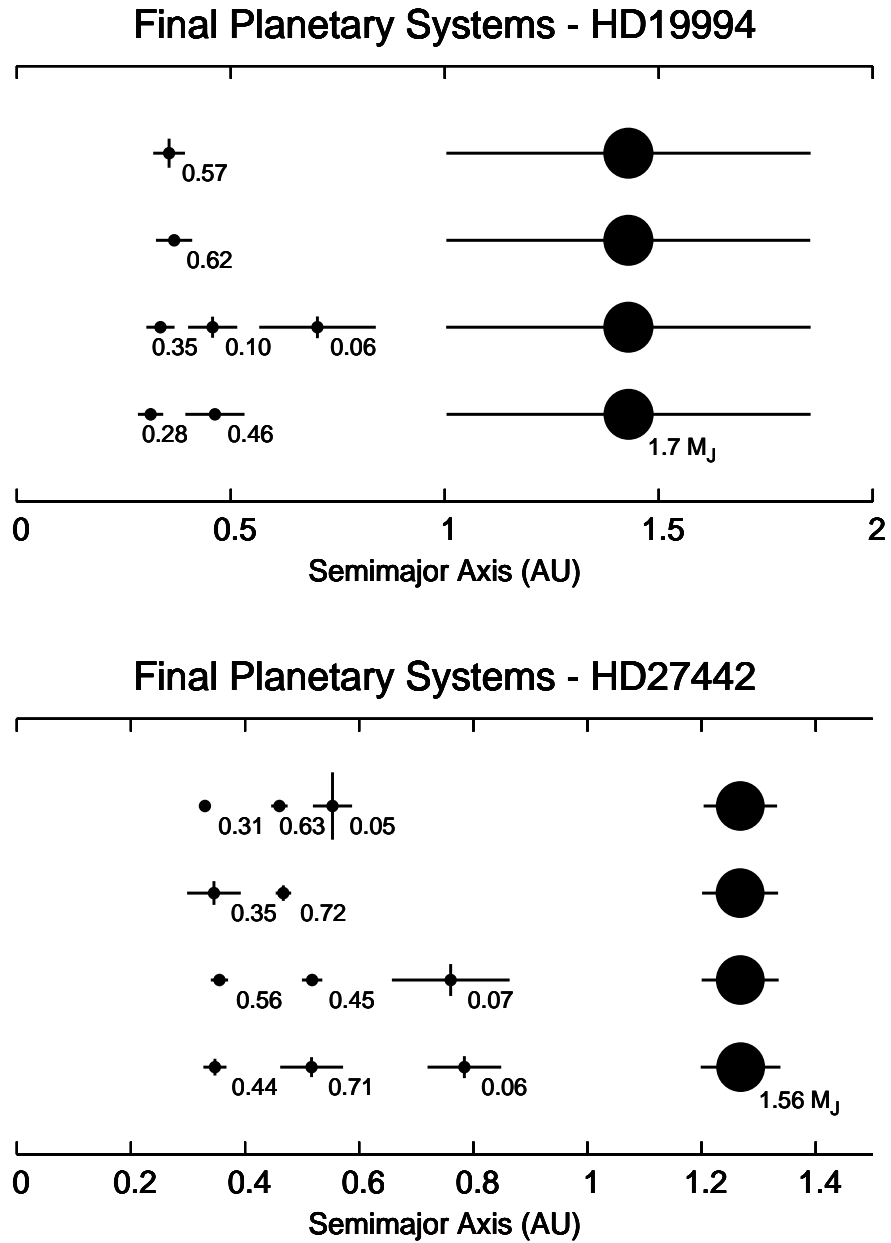


Fig. 9.— Schematic of the results of the dynamical simulations for HD19994 (top panel) and HD27442 (bottom panel). Known giant planets are also shown with their masses in Jupiter masses (M_J). The horizontal lines indicate the range in distance from apastron to periastron. The vertical lines indicate variation in height above the midplane due to orbital inclination. Numerical values represent the mass of the planet in Earth masses.

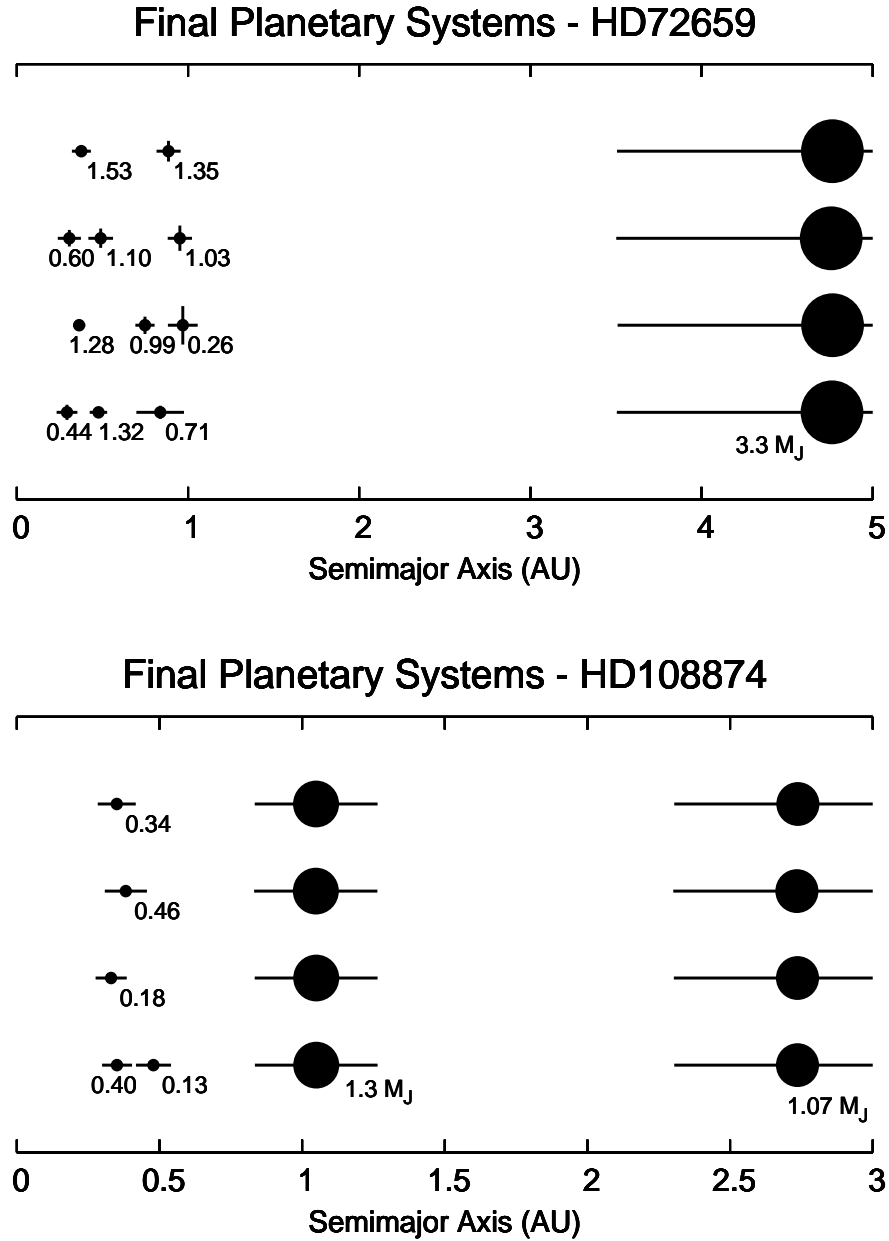


Fig. 10.— Schematic of the results of the dynamical simulations for HD72659 (top panel) and HD108874 (bottom panel). Known giant planets are also shown with their masses in Jupiter masses (M_J). The horizontal lines indicate the range in distance from apastron to periastron. The vertical lines indicate variation in height above the midplane due to orbital inclination. Numerical values represent the mass of the planet in Earth masses.

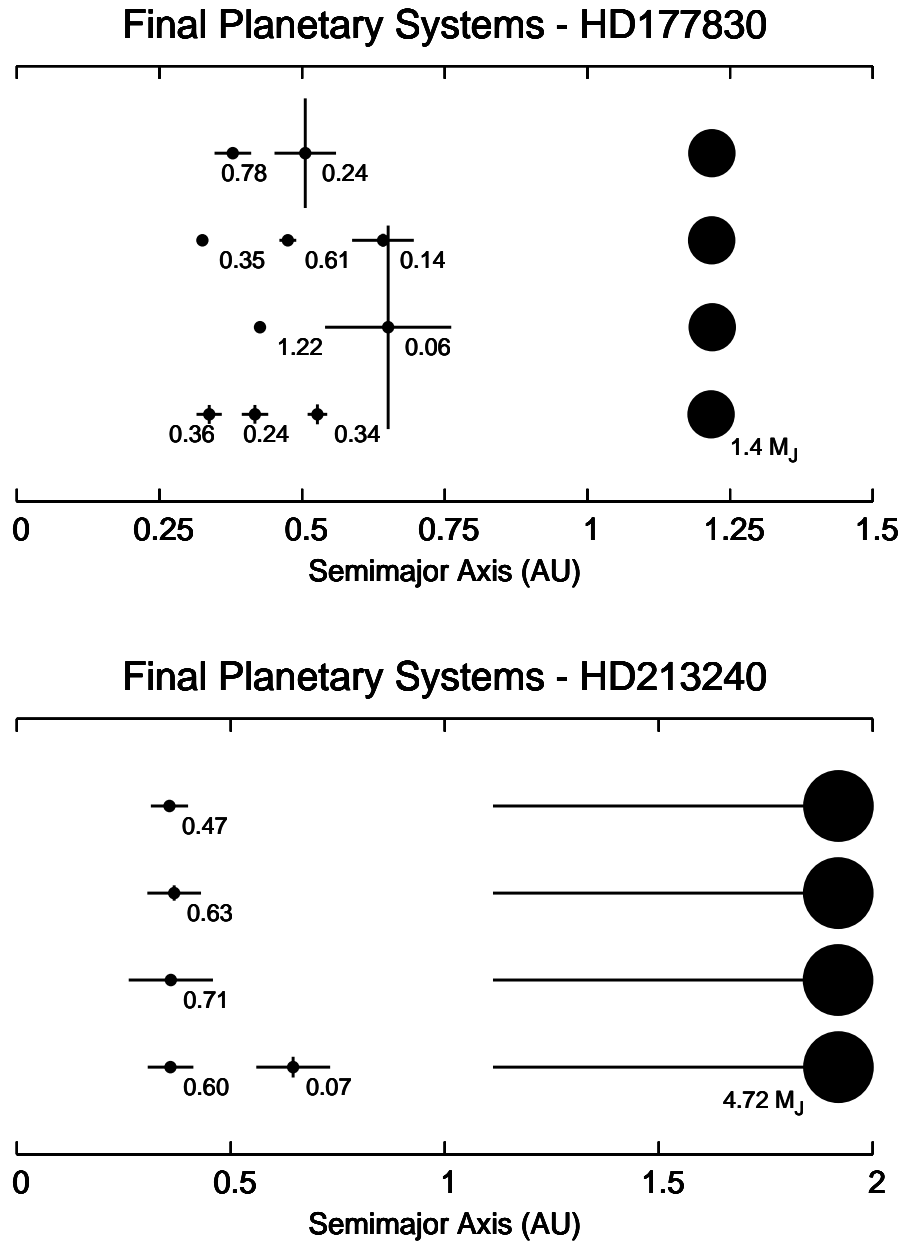


Fig. 11.— Schematic of the results of the dynamical simulations for HD177830 (top panel) and HD213240 (bottom panel). Known giant planets are also shown with their masses in Jupiter masses (M_J). The horizontal lines indicate the range in distance from apastron to periastron. The vertical lines indicate variation in height above the midplane due to orbital inclination. Numerical values represent the mass of the planet in Earth masses.

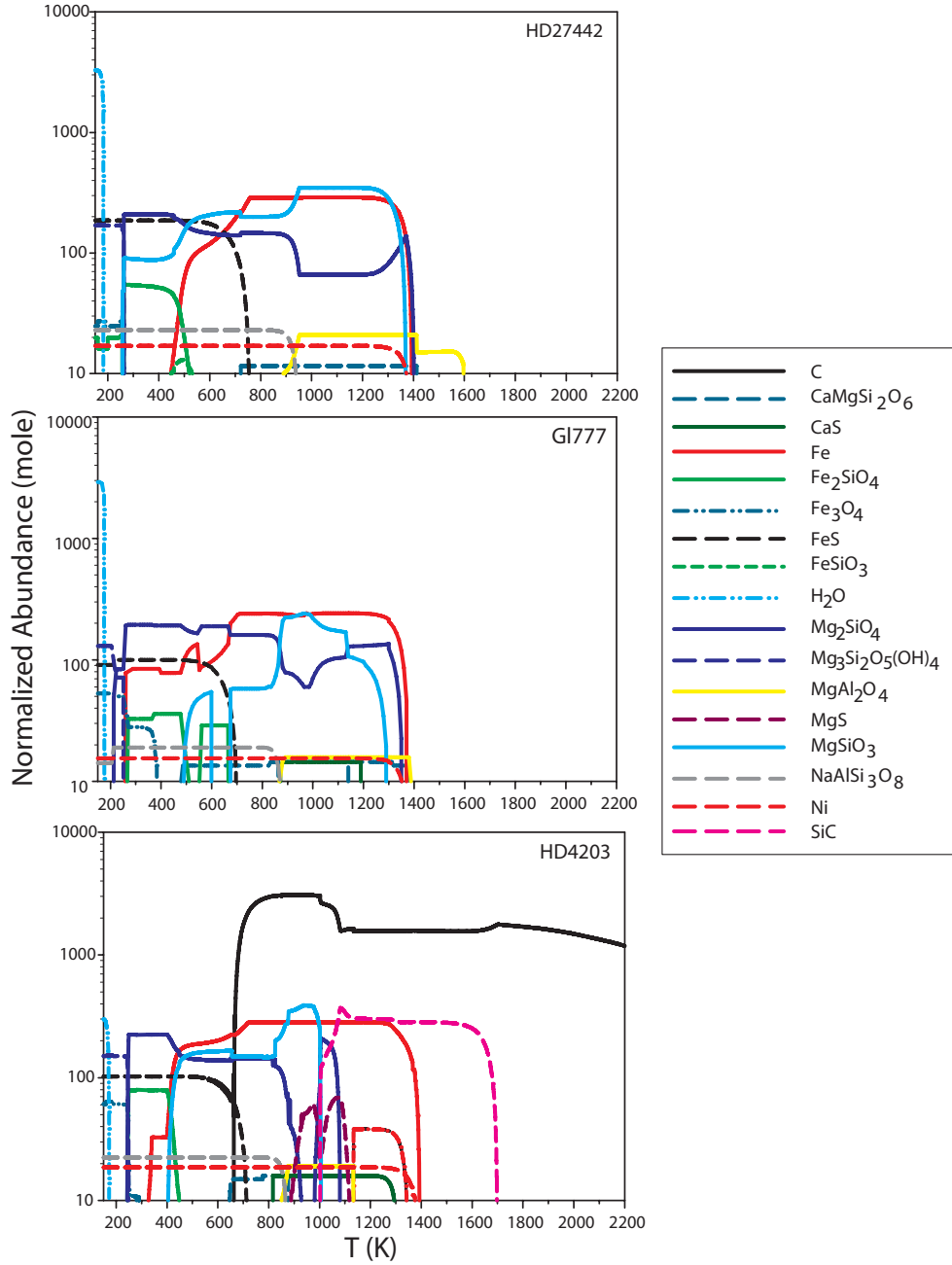


Fig. 12.— Schematic of the output obtained from HSC Chemistry for 3 representative systems: HD27442 (top), G1777 (middle) and HD4203 (bottom). All simulations were run with a system pressure of 10^{-4} bar. Only solid species present within the system are shown. All abundances are normalized to the least abundant species present. Input elemental abundances are shown in Table 7. Note that although G1777 is described as a low-C enriched systems, C and other carbide phases only appear for pressures at and below 10^{-5} bar and are thus absent from the current figure.

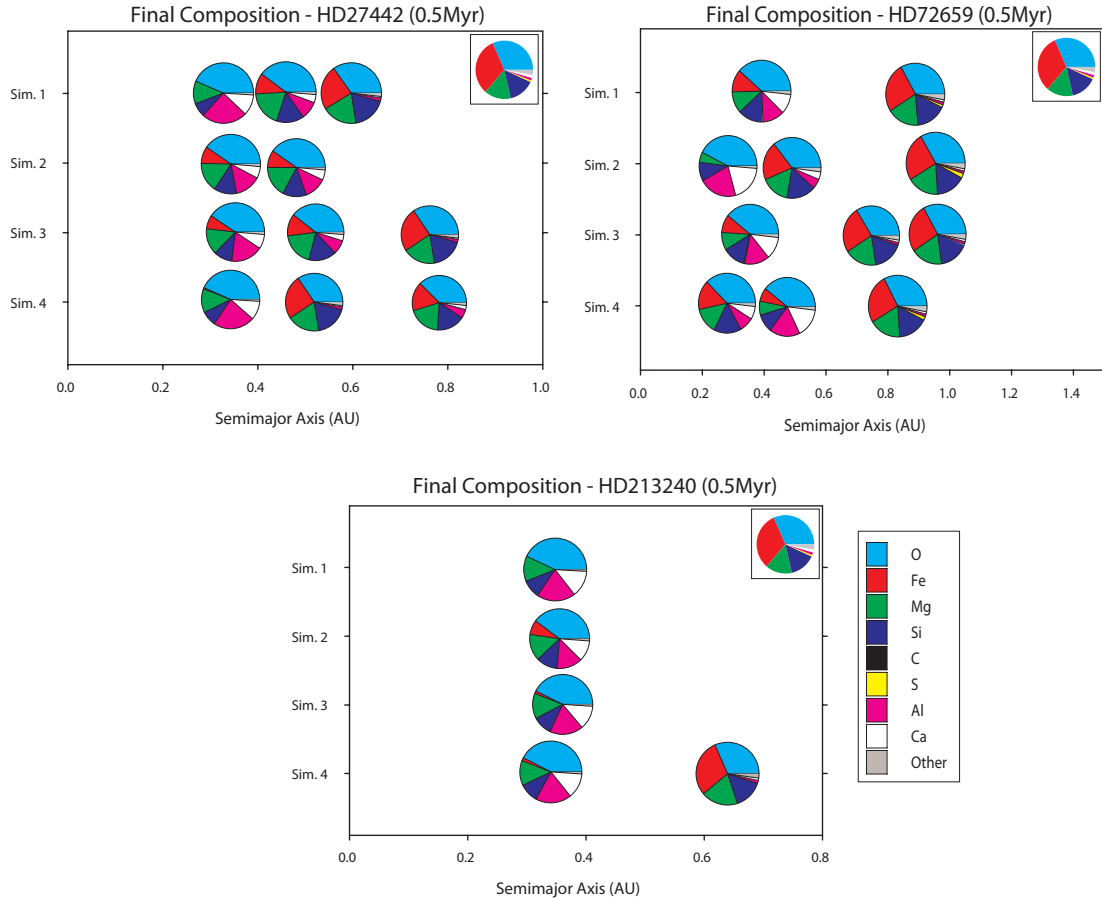


Fig. 13.— Schematic of the bulk elemental planetary composition for the Earth-like planetary systems HD27442 (top left), HD72659 (top right) and HD213240 (bottom). All values are wt% of the final simulated planet. Values are shown for the terrestrial planets produced in each of the four simulations run for the system. Size of bodies is not to scale. Earth values taken from Kargel & Lewis (1993) are shown in the upper right of each panel for comparison.

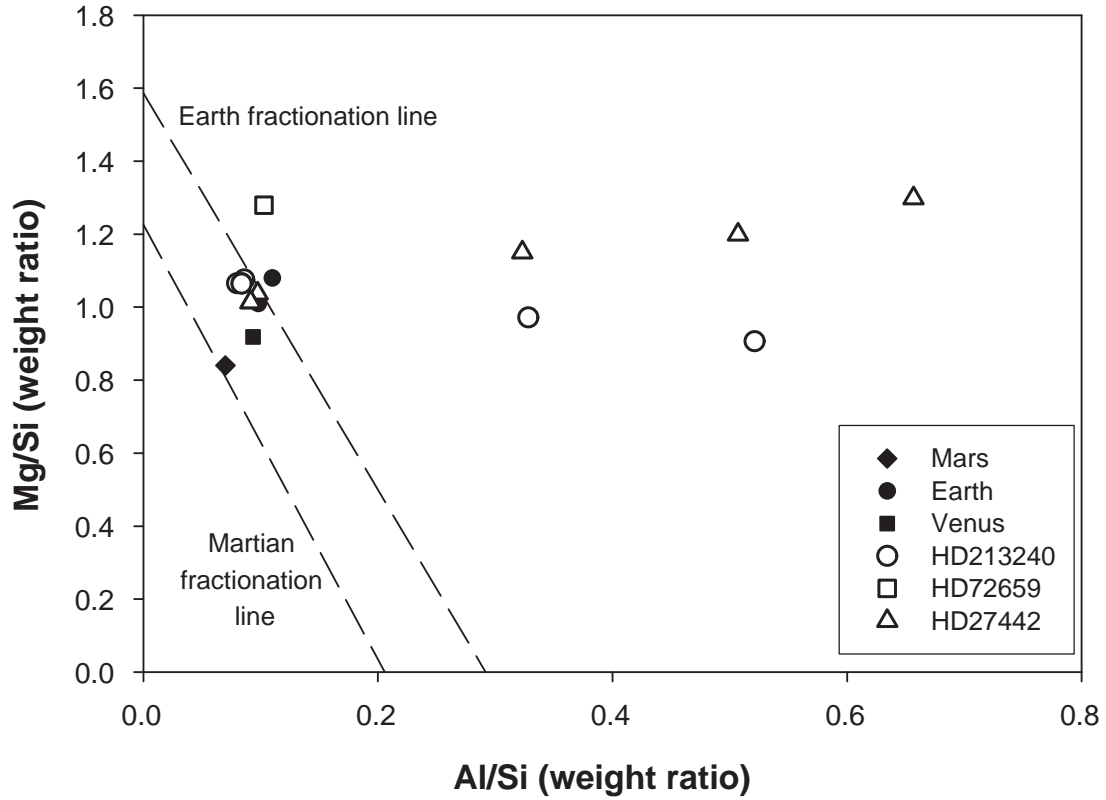


Fig. 14.— Al/Si v. Mg/Si for the planets of HD27442 (triangles), HD72659 (squares) and HD213240 (circles). Values are for disk conditions at 5×10^5 years. Earth values are shown as filled circles and are taken from Kargel & Lewis (1993) and McDonough & Sun (1995). Martian values are shown as filled diamonds and are taken from Lodders & Fegley (1997). Venus values are shown as filled squares and are taken from Morgan & Anders (1980). Note that the values for HD27442, HD72659 and HD213240 all extend off to the right, reaching Mg/Si values of up to 3.5.

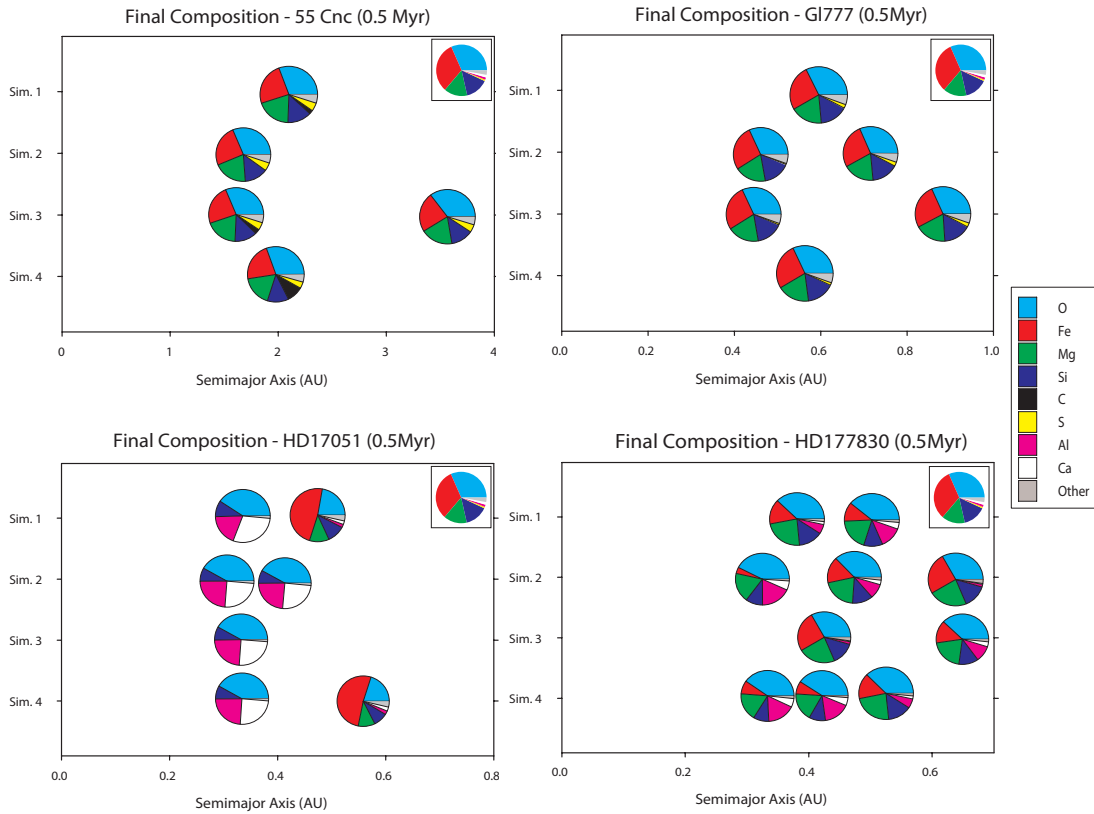


Fig. 15.— Schematic of the bulk elemental planetary composition for the low C-enrichment systems 55Cnc (top left), Gl777 (top right), HD17051 (bottom left) and HD177830 (bottom right). All values are wt% of the final simulated planet. Values are shown for the terrestrial planets produced in each of the four simulations run for the system. Size of bodies is not to scale. Earth values taken from Kargel & Lewis (1993) are shown in the upper right of each panel for comparison.

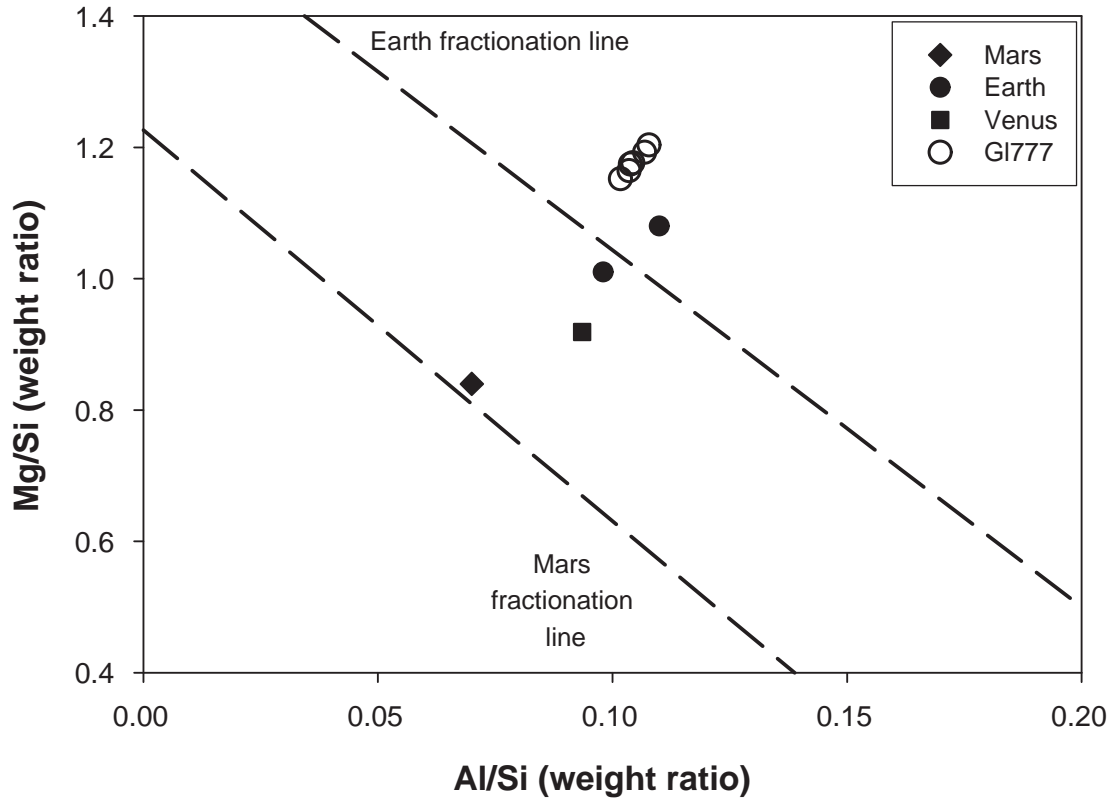


Fig. 16.— Al/Si v. Mg/Si for planets of Gl777. Open circles indicate values for simulated terrestrial planets produced with disk conditions at $t = 5 \times 10^5$ years. Values at all other times are concentrated at the 5×10^5 years values and omitted for clarity. Earth values are shown as filled circles and are taken from Kargel & Lewis (1993) and McDonough & Sun (1995). Martian values are shown as filled diamonds and are taken from Lodders & Fegley (1997). Venus values are shown as filled squares and are taken from Morgan & Anders (1980).

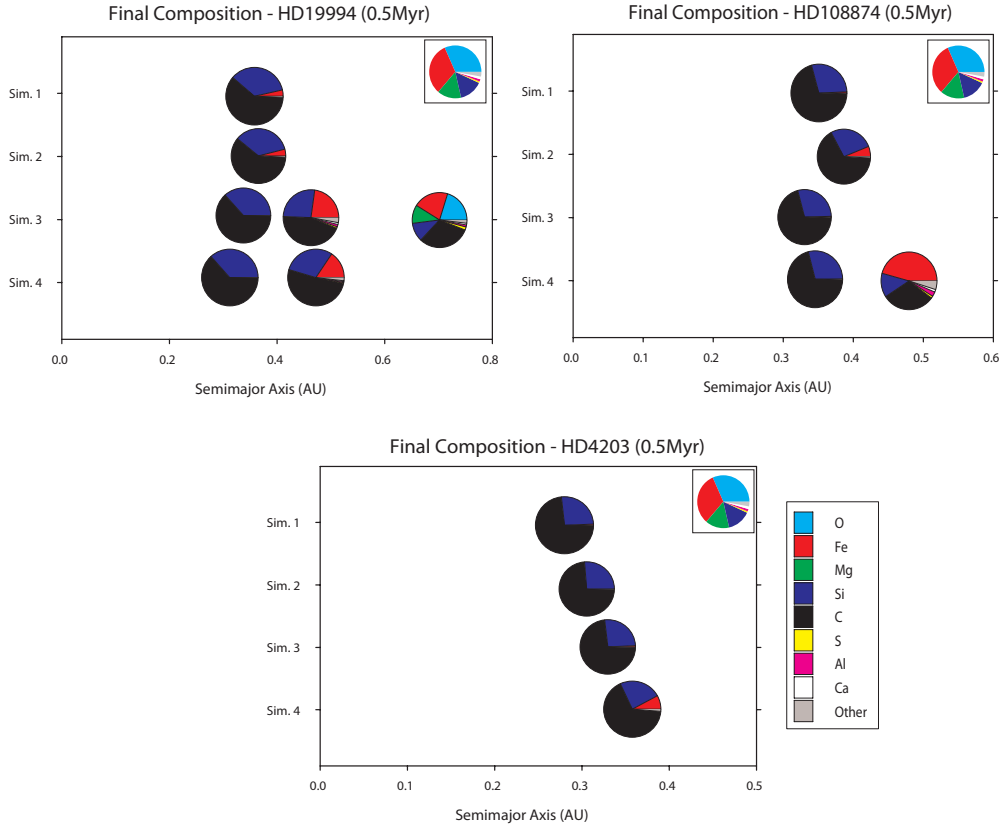


Fig. 17.— Schematic of the bulk elemental planetary composition for the high C-enrichment systems HD19994 (top left), HD108874 (top right) and HD4203 (bottom). All values are wt% of the final simulated planet. Values are shown for the terrestrial planets produced in each of the four simulations run for the system. Size of bodies is not to scale. Earth values taken from Kargel & Lewis (1993) are shown in the upper right of each panel for comparison.

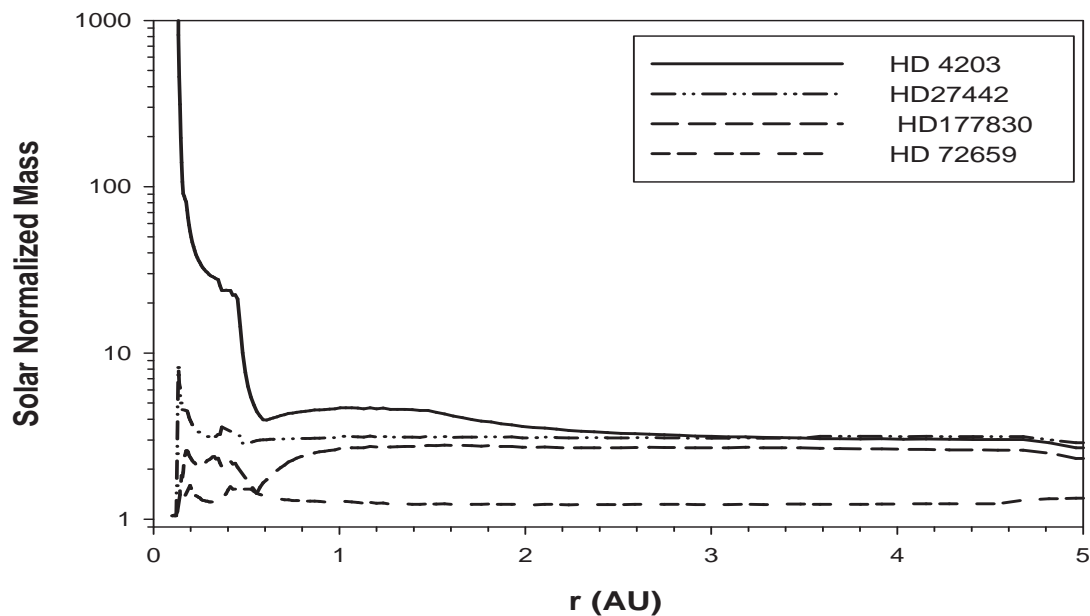


Fig. 18.— Solid mass distribution within the disk for four known extrasolar planetary systems. All distributions are normalized to the Solar distribution. Mass distributions are shown for HD4203 (solid) (Mg/Si= 1.29, C/O=1.86), HD27442 (dashed-dotted) (Mg/Si= 1.17, C/O=0.63), HD177830 (long dash) (Mg/Si= 1.91, C/O=0.83) and HD72659 (short dash) (Mg/Si= 1.23, C/O=0.40).

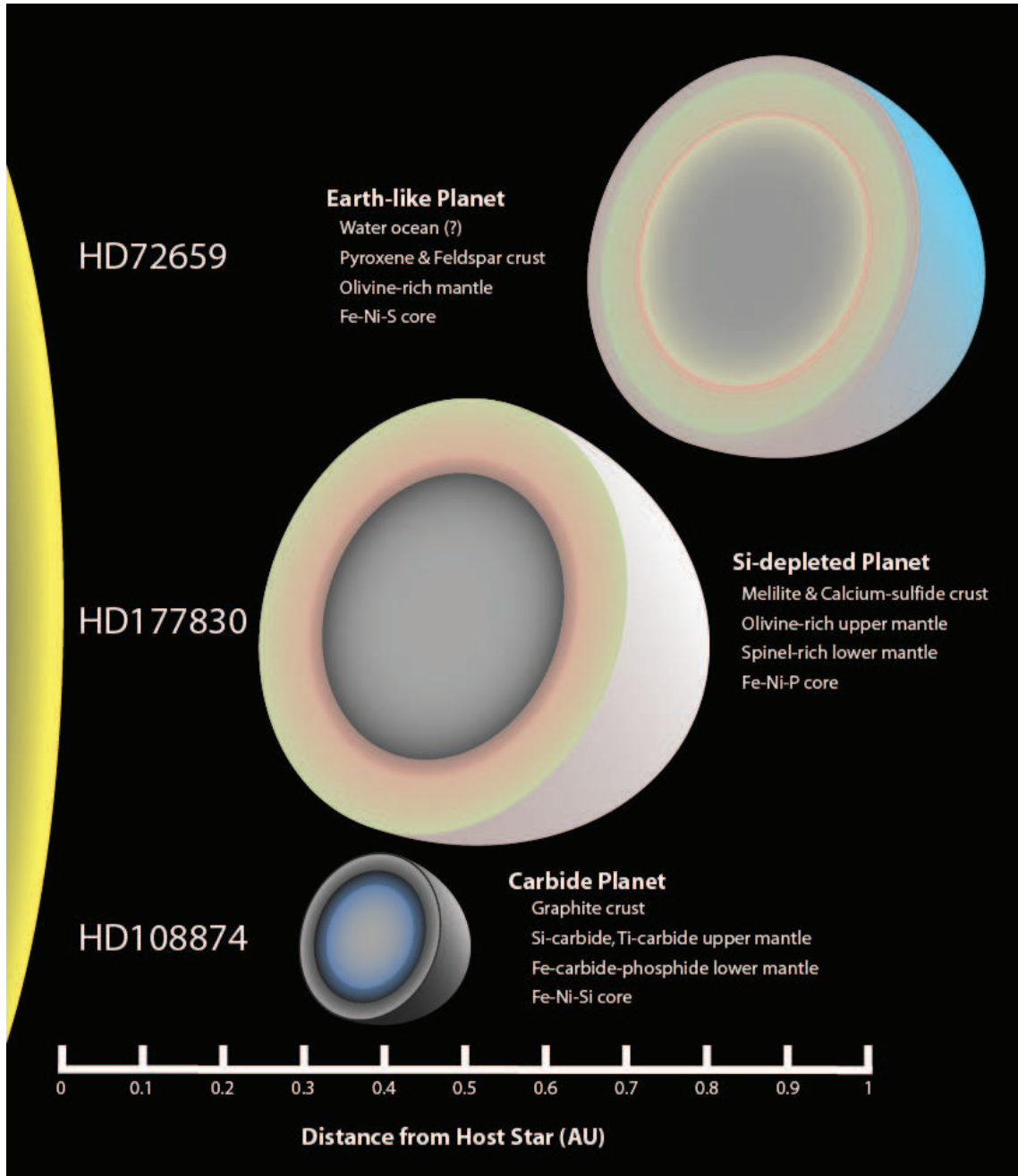


Fig. 19.— Schematic of notional interior models are based on calculations of bulk planetary compositions for disk conditions at $t = 5 \times 10^5$ years resulting from three different planetary systems: G1777 (HD190360) (top), HD177830 (middle) and HD108874 (bottom). Figures are to scale for planet and layer sizes and planet location.

Table 2: Statistical analysis of the host and non-host star distributions of Mg/Si and C/O. All values are based on the abundances determined in Bond et al. (2008). The quoted uncertainty is the standard error in the mean. All ratios are elemental number ratios, *not* solar normalized logarithmic values.

	Mean	Median	Standard Deviation
Mg/Si:			
Host Stars	0.83 ± 0.04	0.80	0.22
Non-Host Stars	0.80 ± 0.03	0.79	0.16
C/O:			
Host Stars	0.67 ± 0.03	0.68	0.23
Non-Host Stars	0.67 ± 0.03	0.69	0.23

Table 3: Orbital parameters of known extrasolar planets for the systems studied. Values taken from the University of California catalog located at www.exoplanets.org

Planet	M	a	e
	(M_{Jupiter})	(AU)	
55Cnc-b	0.82	0.11	0.02
55Cnc-c	0.17	0.24	0.05
55Cnc-d	3.84	5.84	0.08
55Cnc-e	0.02	0.04	0.09
55Cnc-f	0.14	0.70	0.20
Gl777-b	1.55	4.02	0.35
Gl777-c	0.06	0.13	0.07
HD4203-b	2.07	1.16	0.52
HD17051-b	2.08	0.93	0.14
HD19994-b	1.69	1.43	0.30
HD27442-b	1.56	1.27	0.06
HD72659-b	3.30	4.76	0.26
HD108874-b	1.30	1.05	0.21
HD108874-c	1.07	2.75	0.16
HD177830-b	1.43	1.22	0.03
HD213240-b	4.72	1.92	0.42

Table 4. Target star elemental abundances in standard logarithmic units, normalized to H and Solar values. A – indicates that a value was not available for a given element or star. See text for references.

	55Cnc	Gl777A	HD4203	HD17051	HD19994	HD27442	HD72659	HD108874	HD177830	HD213240
[Fe/H]	0.33	0.24	0.40	0.24	0.03	0.23	0.33	0.26	0.17	0.39
[C/H]	0.31	0.29	0.45	0.39	−0.11	0.21	0.48	0.28	0.17	0.34
[O/H]	0.13	0.22	0.00	0.11	0.11	−0.10	0.38	0.16	0.35	0.36
[Na/H]	0.26	0.26	0.42	0.48	0.07	0.13	0.37	0.24	0.22	0.41
[Mg/H]	0.48	0.33	0.48	0.21	0.11	0.27	0.56	0.19	0.23	0.51
[Al/H]	0.47	0.34	0.51	0.32	0.07	0.30	0.54	0.19	0.20	0.53
[Si/H]	0.29	0.24	0.44	0.23	0.05	0.14	0.31	0.19	0.09	0.47
[S/H]	0.12	0.10	0.20	−0.05	−0.23	–	–	0.00	−0.10	–
[Ca/H]	0.08	0.11	0.24	0.17	−0.03	0.01	−0.07	0.17	0.04	0.12
[Ti/H]	0.36	0.32	0.41	0.18	0.13	0.20	0.31	0.26	0.12	0.39
[Cr/H]	0.22	0.17	0.33	0.20	−0.01	0.15	0.13	0.16	0.05	0.21
[Ni/H]	0.31	0.25	0.42	0.27	0.01	0.18	0.39	0.19	0.13	0.36

Table 5. Target star elemental abundances as number of atoms and normalized to 10^6Si atoms. A – indicates that a value was not available for a given element or star. See text for references.

Element	Solar	55Cnc	G1777A	HD4203	HD17051	HD19994	HD27442	HD72659	HD108874	HD177830	HD213240
Fe	8.32×10^5	9.12×10^5	8.32×10^5	7.59×10^5	9.77×10^5	8.51×10^5	6.92×10^5	7.94×10^5	10.23×10^6	8.71×10^5	10.00×10^6
C	1.02×10^7	1.07×10^7	1.15×10^7	1.05×10^7	1.26×10^7	1.48×10^7	7.59×10^6	7.08×10^6	1.20×10^7	1.51×10^7	1.23×10^7
O	1.55×10^7	1.07×10^7	1.48×10^7	5.62×10^6	1.45×10^7	1.17×10^7	1.20×10^7	1.78×10^7	8.91×10^6	1.82×10^7	2.82×10^7
Na	6.03×10^4	5.62×10^4	6.31×10^4	5.75×10^4	6.76×10^4	1.07×10^5	5.25×10^4	6.31×10^4	5.89×10^4	6.92×10^4	8.13×10^4
Mg	1.07×10^6	1.66×10^6	1.32×10^6	1.17×10^6	1.07×10^6	1.02×10^6	1.17×10^6	1.23×10^6	1.45×10^6	1.91×10^6	1.48×10^6
Al	8.32×10^4	1.26×10^5	1.05×10^5	9.77×10^4	8.32×10^4	1.02×10^5	9.55×10^4	8.71×10^4	1.20×10^5	1.41×10^5	1.07×10^5
Si	1.00×10^6	1.00×10^6	1.00×10^6	1.00×10^6	1.00×10^6	1.00×10^6	1.00×10^6	1.00×10^6	1.00×10^6	1.00×10^6	1.00×10^6
S	4.57×10^5	3.09×10^5	3.31×10^5	2.63×10^5	2.95×10^5	2.40×10^5	–	–	4.57×10^5	4.57×10^5	–
Ca	6.46×10^4	3.98×10^4	4.79×10^4	4.07×10^4	6.17×10^4	5.62×10^4	2.88×10^4	5.37×10^4	4.79×10^4	2.69×10^4	5.75×10^4
Ti	2.75×10^3	3.24×10^3	3.31×10^3	2.57×10^3	3.24×10^3	2.45×10^3	2.29×10^3	3.31×10^3	3.16×10^3	2.75×10^3	2.95×10^3
Cr	1.32×10^4	1.12×10^4	1.12×10^4	1.02×10^4	1.23×10^4	1.23×10^4	7.24×10^3	1.15×10^4	1.35×10^4	0.87×10^3	1.20×10^4
Ni	5.01×10^4	5.25×10^4	5.13×10^4	4.79×10^4	5.01×10^4	5.50×10^4	3.89×10^4	4.57×10^4	5.50×10^4	6.03×10^4	5.50×10^4

Table 6. Chemical species included in the equilibrium calculations of HSC Chemistry.

Gaseous Species			
Al	CrO	MgOH	PN
AlH	CrOH	MgS	PO
AlO	CrS	N	PS
Al ₂ O	Fe	N ₂	S
AlOH	FeH	NH ₃	S ₂
AlS	FeO	NO	SN
C	FeOH	NS	SO
CH ₄	FeS	Na	SO ₂
CN	H	Na ₂	Si
CO	H ₂	NaH	SiC
CO ₂	HCN	NaO	SiH
CP	HCO	NaOH	SiN
CS	H ₂ O	Ni	SiO
Ca	HPO	NiH	SiP
CaH	HS	NiO	SiP ₂
CaO	H ₂ S	NiOH	SiS
CaOH	He	NiS	Ti
CaS	Mg	O	TiN
Cr	MgH	O ₂	TiO
CrH	MgN	P	TiO ₂
CrN	MgO	PH	TiS
Solid Species			
Al ₂ O ₃	FeSiO ₃	CaAl ₂ Si ₂ O ₈	C
CaAl ₁₂ O ₁₉	Fe ₃ P	NaAlSi ₃ O ₈	SiC

Table 6—Continued

Gaseous Species			
Ti_2O_3	Fe_3C	Cr_2FeO_4	TiC
CaTiO_3	Fe	$\text{Ca}_3(\text{PO}_4)_2$	TiN
$\text{Ca}_2\text{Al}_2\text{SiO}_7$	Ni	FeS	AlN
MgAl_2O_4	P	Fe_3O_4	CaS
Mg_2SiO_4	Si	$\text{Mg}_3\text{Si}_2\text{O}_5(\text{OH})_4$	MgS
MgSiO_3	Cr	H_2O	
Fe_2SiO_4	$\text{CaMgSi}_2\text{O}_6$		

Table 7. HSC Chemistry input values for the extrasolar planetary systems studied. All inputs are entered into the simulations of HSC Chemistry their elemental and gaseous state. All values are in moles and are based on the stellar abundance values listed in Tables 4 and 5.

Element	System									
	55Cnc	Gl777A	HD4203	HD17051	HD19994	HD27442	HD72659	HD108874	HD177830	HD213240
H	1.0×10^{12}	1.0×10^{12}	1.0×10^{12}	1.0×10^{12}	1.0×10^{12}	1.0×10^{12}	1.0×10^{12}	1.0×10^{12}	1.0×10^{12}	1.0×10^{12}
He	8.5×10^{10}	8.5×10^{10}	8.5×10^{10}	8.5×10^{10}	8.5×10^{10}	8.5×10^{10}	8.5×10^{10}	8.5×10^{10}	8.5×10^{10}	8.5×10^{10}
C	7.4×10^8	7.1×10^8	1.0×10^9	6.9×10^8	8.9×10^8	7.9×10^8	2.8×10^8	5.9×10^8	1.1×10^9	5.4×10^8
N	1.8×10^8	1.7×10^8	2.5×10^8	1.7×10^8	2.2×10^8	2.0×10^8	0.7×10^8	1.5×10^8	2.7×10^8	1.3×10^8
O	7.4×10^8	9.1×10^8	5.5×10^8	7.9×10^8	7.1×10^8	1.3×10^9	7.1×10^8	4.4×10^8	1.3×10^9	1.2×10^9
Na	3.9×10^6	3.9×10^6	5.6×10^6	3.7×10^6	6.5×10^6	5.5×10^6	2.5×10^6	2.9×10^6	5.0×10^6	3.6×10^6
Mg	1.2×10^8	8.1×10^7	1.2×10^8	5.9×10^7	6.2×10^7	1.2×10^8	4.9×10^7	7.1×10^7	1.4×10^8	6.5×10^7
Al	8.7×10^6	6.5×10^6	9.6×10^6	4.6×10^6	6.2×10^6	1.0×10^7	3.5×10^6	5.9×10^6	1.0×10^7	4.7×10^6
Si	6.9×10^7	6.2×10^7	9.8×10^7	5.5×10^7	6.0×10^7	1.1×10^8	4.0×10^7	4.9×10^7	7.2×10^7	4.4×10^7
P	8.5×10^5	6.3×10^5	9.3×10^5	4.5×10^5	6.0×10^5	9.8×10^5	3.4×10^5	5.8×10^5	1.0×10^6	4.6×10^5
S	2.1×10^7	2.0×10^7	2.6×10^7	1.6×10^7	1.4×10^7	4.5×10^7	1.0×10^7	2.2×10^7	3.3×10^7	1.3×10^7
Ca	2.8×10^6	3.0×10^6	4.0×10^6	3.4×10^6	3.4×10^6	3.0×10^6	2.1×10^6	2.3×10^6	1.9×10^6	2.5×10^6
Ti	2.2×10^5	2.0×10^5	2.5×10^5	1.8×10^5	1.5×10^5	2.4×10^5	1.3×10^5	1.6×10^5	2.0×10^5	1.3×10^5
Cr	7.8×10^5	6.9×10^5	1.0×10^6	6.8×10^5	7.4×10^5	7.6×10^5	4.6×10^5	6.6×10^5	6.3×10^5	5.2×10^5
Fe	6.3×10^7	5.1×10^7	7.4×10^7	5.4×10^7	5.1×10^7	7.2×10^7	3.2×10^7	5.0×10^7	6.3×10^7	4.4×10^7
Ni	3.6×10^6	3.2×10^6	4.7×10^6	2.8×10^6	3.3×10^6	4.1×10^6	1.8×10^6	2.7×10^6	4.4×10^6	2.4×10^6

Table 8: Stellar accretion rates for the extrasolar host stars studied. Stellar masses were obtained from the Simbad database. Solar values are the nominal model determined by Hersant et al. (2001). See text for details on the scaling relations applied.

System	Stellar Mass (M_{\odot})	\dot{M} (M_{\odot}/year)
Solar	1.00	5.00×10^{-6}
55Cnc	1.03	5.23×10^{-6}
G1777	1.04	5.30×10^{-6}
HD4203	1.06	5.46×10^{-6}
HD17051	1.11	5.50×10^{-6}
HD19994	1.35	7.84×10^{-6}
HD27442	1.20	6.00×10^{-6}
HD72659	0.95	4.63×10^{-6}
HD108874	1.00	5.00×10^{-6}
HD177830	1.48	9.00×10^{-6}
HD213240	1.22	6.10×10^{-6}

Table 9: Convective zone masses for each of the target stars. T_{eff} values taken from Santos et al. (2004). See text for details on the determination of M_{CZ} .

System	T_{eff} (K)	M_{CZ} (M_{\odot})
55Cnc	5279	0.0398
Gl777	5584	0.0316
HD4203	5636	0.0288
HD17051	6253	0.0035
HD19994	6190	0.0045
HD27442	4825	0.0562
HD72659	5995	0.0112
HD108874	5596	0.0321
HD177830	4804	0.0501
HD213240	5984	0.0100

Table 10. $T_{50\% \text{ condensation}}$, C/O and Mg/Si for extrasolar planetary systems studied in order of increasing C/O value. Solar values are also shown for comparison and are taken from Bond et al. (2009). Where less than 50% of an element condensed within a system, the maximum amount of condensation that occurred is shown in parentheses. All values are in K.

Element	System										
	HD72659	HD213240	HD27442	Solar	Gl777A	HD177830	HD17051	55Cnc	HD19994	HD108874	HD4203
Al	1665	1698	1688	1639	1636	1647	1551	1311	1320	1315	1333
C	<150	<150	<150	<150	<150	976 (6%)	955 (9%)	920 (34%)	954 (39%)	946	1049
Ca	1541	1562	1613	1527	1562	1556	1484	1248	1287	1289	1300
Cr	1297	1309	1327	1301	1314	1322	1316	1322	1313	1306	1324
Fe	1334	1346	1365	1339	1353	1361	1354	1361	1353	1352	1367
Mg	1359	1381	1377	1339	1328	1321	1224	1081	1075	1066	1074
Na	927	944	935	941	870	801	866	864	873	854	864
Ni	1346	1358	1377	1351	1364	1373	1365	1372	1364	1350	1378
O	180	183	183	180	181	184	180	207	180	331	1001
P	1312	1307	1327	1309	1346	1353	1359	1375	1392	1391	1407
S	625	641	709	658	664	691	652	667	646	669	677
Si	1349	1374	1360	1329	1306	1315	1125	1169	1626	1520	1645
Ti	1593	1610	1590	1580	1574	1567	1548	1754	1810	1810	1832
C/O	0.40	0.44	0.63	0.66	0.78	0.83	0.87	1.00	1.26	1.35	1.86
Mg/Si	1.23	1.48	1.17	1.07	1.32	1.91	1.07	1.66	1.02	1.45	1.29

Table 11. Predicted bulk elemental abundances for all simulated extrasolar terrestrial planets. All values are in wt% of the final predicted planet for all seven sets of disk conditions examined. Planet number increases with increasing distance from the host star.

System	H	Mg	O	S	Fe	Al	Ca	Na	Ni	Cr	P	Ti	Si	C	
55Cnc															
t=2.5×10 ⁵ years															
55Cnc 1-4	0.00	16.59	26.02	2.58	20.92	1.40	0.65	0.51	1.27	0.24	0.16	0.06	11.54	0.00	18.06
55Cnc 2-4	0.00	16.50	25.88	2.93	20.79	1.39	0.65	0.51	1.26	0.24	0.16	0.06	11.47	0.00	18.18
55Cnc 3-4	0.00	16.80	26.21	2.20	21.14	1.41	0.71	0.52	1.28	0.24	0.16	0.06	11.73	0.00	17.53
55Cnc 3-5	3.71	12.59	53.11	3.09	15.88	1.06	0.50	0.00	0.96	0.18	0.12	0.05	8.76	0.00	0.00
55Cnc 4-4	1.79	15.74	43.90	3.87	19.87	1.32	0.62	0.31	1.20	0.23	0.15	0.06	10.95	0.00	0.00

Note. — Table 11 is published in its entirety in the electronic edition of the *Astrophysical Journal*. A portion is shown here for guidance regarding its form and content.

Table 12. Average change in host star photospheric abundances produced by terrestrial planet formation. Values are based on the results of four separate simulations.

System	Mass Accreted (M_{\oplus})	Change in Abundance												
		Mg	O	S	Fe	Al	Ca	Na	Ni	Cr	P	Ti	Si	C
55Cnc	0.145	0.000	0.000	0.000	0.000	0.000	0.000	0.000	0.000	0.000	0.000	0.000	0.000	0.000
G1777	2.100	0.011	0.009	0.009	0.009	0.011	0.011	0.011	0.011	0.011	0.004	0.012	0.011	0.009
HD4203	0.631	0.000	0.000	0.000	0.000	0.000	0.000	0.000	0.000	0.000	0.000	0.002	0.001	0.001
HD17051	0.727	0.004	0.004	0.004	0.004	0.013	0.016	0.004	0.005	0.005	0.000	0.020	0.005	0.004
HD19994	0.898	0.004	0.003	0.003	0.003	0.005	0.005	0.003	0.005	0.005	0.000	0.006	0.006	0.005
HD27442	0.342	0.001	0.001	0.000	0.001	0.001	0.001	0.001	0.001	0.001	0.000	0.001	0.001	0.001
HD72659	2.640	0.021	0.017	0.001	0.016	0.020	0.030	0.023	0.021	0.025	0.007	0.026	0.023	0.016
HD108874	0.755	0.001	0.001	0.001	0.001	0.002	0.001	0.001	0.002	0.002	0.000	0.003	0.002	0.001
HD177830	0.237	0.001	0.001	0.001	0.001	0.001	0.001	0.001	0.001	0.001	0.000	0.001	0.001	0.001
HD213240	1.310	0.015	0.012	0.005	0.011	0.019	0.024	0.014	0.015	0.016	0.011	0.021	0.014	0.011